ROBUST CONTROLLER DESIGN FOR A FIXED WING UAV

A THESIS SUBMITTED TO
THE GRADUATE SCHOOL OF NATURAL AND APPLIED SCIENCES
OF
MIDDLE EAST TECHNICAL UNIVERSITY

BY

ANNA PRACH

IN PARTIAL FULFILLMENT OF THE REQUIREMENTS
FOR
THE DEGREE OF MASTER OF SCIENCE
IN
AEROSPACE ENGINEERING

SEPTEMBER 2009

Approval of the thesis:

ROBUST CONTROLLER DESIGN FOR A FIXED WING UAV

submitted by **ANNA PRACH** in partial fulfillment of the requirements for the degree of **Master of Science in Aerospace Engineering Department, Middle East Technical University** by,

Prof. Dr. Canan Özgen _____
Dean, Gradaute School of **Natural and Applied Sciences**

Prof. Dr. Ismail H. Tuncer _____
Head of Department, **Aerospace Engineering**

Prof. Dr. Nafiz Alemdaroğlu _____
Supervisor**, Aerospace Engineering Dept., METU**

Examining Committee Members:

Assoc. Prof. Dr. Serkan Özgen _____
Aerospace Engineering Dept., METU

Prof. Dr. Nafiz Alemdaroğlu _____
Aerospace Engineering Dept., METU

Assoc. Prof. Dr. Altan Kayran _____
Aerospace Engineering Dept., METU

Prof. Dr Kemal Leblebicioğlu _____
Electrical and Electronics Engineering Dept., METU

Dr. Volkan Nalbantoğlu _____
ASELSAN

Date: _____

I hereby declare that all information in this document has been obtained and presented in accordance with academic rules and ethical conduct. I also declare that, as required by these rules and conduct, I have fully cited and referenced all material and results that are not original to this work.

Name, Last name: Anna Prach

Signature :

ABSTRACT

ROBUST CONTROLLER DESIGN FOR A FIXED WING UAV

Prach, Anna
M.S., Department of Aerospace Engineering
Supervisor: Prof. Nafiz Alemdaroğlu

September 2009, 148 pages

This study describes the design and implementation of the pitch and roll autopilots for a fixed wing unmanned vehicle. A Tactical Unmanned Aerial Vehicle (TUAV), which is designed at the Middle East Technical University (METU), is used as a platform. This work combines development of the classical and robust controllers, which are used for the pitch and roll autopilots. One of the important steps in the thesis is development of the non-linear dynamic model of the UAV, which is developed in MATLAB/Simulink environment. Two different strategies of the controller design imply development of the PID and H_∞ controllers. Simulation results illustrate the performances of the designed controllers. Simulation is performed for the nominal model of the UAV and for the model that includes uncertainties and sensor noises.

Keywords: PID Controller, Robust Controller, Autopilot

ÖZ

SABİT KANATLI BİR İHA İÇİN GÜRBÜZ KONTROLCÜ TASARIMI

Prach, Anna
Yüksek Lisans, Havacılık ve Uzay Mühendisliği
Tez Yöneticisi: Prof.Dr.Nafiz Alemdaroğlu

Eylül 2009, 148 sayfa

Bu tez sabit kanatlı bir Insansız Hava Aracının (IHA) yunuslama ve yalpalama otopilotu tasarımının tasarım ve uygulanmasını anlatmaktadır. ODTU'de tasarlanan bir taktik İHA (TİHA) uygulama platformu olarak kullanılmaktadır. Bu çalışma yunuslama ve yalpalama harekteleri için klasik ve gürbüz kontrolcü tasarımlarını içermektedir. Bu tezde aynı zamanda IHA'nın doğrusal olmayan dinamik modeli MATLAB/SIMULINK ortamında geliştirilmiştir. Bu kapsamda PID ve H_∞ kontrolcüleri tasarlanmıştır. Benzetim sonuçları tasarlanan kontrolcülerin performansını göstermektedir. Benzetimler hem nominal IHA modeli hem de belirsizlik ve sensör gürültüsü içeren modeller üzerinde denenmiştir.

Anahtar Kelimeler: PID Kontrolü, Gürbüz Kontrol, Otopilot

In Living Memory of M. J. …

ACKNOWLEDGMENTS

I would like to express gratitude to my advisor, Prof. Dr. Nafiz Alemdaroğlu, for his valuable support and encouragement. Thanks to him I got an opportunity to start my master program at this university. I am very thankful to Dr. Volkan Nalbantoğlu, for his continuous guidance and supervision throughout this work. I want to express special gratitude to Dr. Ilkay Yavrucuk for his valuable suggestions and help that enabled me to complete my work successfully.

Lastly, I want to express my love and gratitude to my family for understanding and love through the duration of my studies.

TABLE OF CONTENTS

LIST OF TABLES

TABLES

LIST OF FIGURES

FIGURES

LIST OF SYMBOLS

	ROMAN SYMBOL
C_D	Drag coefficient
C_L	Lift coefficient
C_l	Rolling moment coefficient
C_m	Pitching moment coefficient
C_n	Yawing moment coefficient
C_p	Power coefficient
C_t	Thrust coefficient
FC	Fuel consumption
I	Inertia
J	Advanced ratio
m	Mass
n	Revolution per second
p	Body roll rate
q	Body pitch rate
r	Body yaw rate
u	Body velocity in x-direction
v	Body velocity in y-direction
w	Body velocity in z-direction
X	A/C position in north direction
Y	A/C position in east direction
Z	A/C altitude

	GREEK SYMBOLS
α	Angle of attack
β	Sideslip angle
φ	Roll angle
ψ	Yaw angle
ρ	Density
θ	Pitch angle
δ_a	Ailerons deflection angle
δ_e	Elevator deflection angle
δ_r	Rudder deflection angle
ω	Angular velocity

	ABBREVIATION DEFINITIONS
LFT	Linear Fractional Transformations
MIMO	Multi Input Multi Output
NP	Nominal Performance
NS	Nominal Stability
RP	Robust Performance
RS	Robust Stability
RC	Robust Controller
SISO	Single Input Single Output
PIDC	Proportional-Derivative- Integral Controller

CHAPTER 1

INTRODUCTION

Unmanned Aerial Vehicles (UAVs) are one of the fastest growing sectors of the world's aerospace industry. High demand for UAVs in the commercial industry arises by taking into account the advantages of UAVs over manned aircraft: low manufacturing and operational costs of the systems; elimination of the aircrew and related life support systems allows UAVs to be smaller than manned aircraft [1] and eliminates the risk of human lifes in difficult and dirty missions [2]. Removal of aircrew and their support systems means that UAVs are capable of flying longer, higher and faster without endangering lives. Furthermore, they promise better cost-effectiveness and greater utility than manned aircraft [3]. Some of the military and civil applications of UAVs are listed below [2].

Military applications: reconnaissance surveillance and target acquisition (RSTA), surveillance for peacetime and combat Synthetic Aperture Radar (SAR), deception operations, maritime operations (naval fire support, over the horizon targeting, anti ship missile defense, ship classification), UCAV (Unmanned combat air vehicle) applications, meteorology missions, route and landing reconnaissance support, electronic warfare (EW) and SIGINT (SIGnals INTelligence), radio and data relay.

Civil applications: security, search and rescue, wild fire suppression, topographical material and agriculture, communications relay, disaster and emergency management, industrial applications, etc.

Unmanned Aerial Vehicles rely on two basic approaches in implementing unmanned flight-autonomy and pilot-in-the-loop - which rely predominantly on microprocessor

and communication technologies, respectively. Both are used in differing levels in UAV's fields, together they compensate the absence of an onboard pilot and thus enable unmanned flight [4]. Autonomy of UAVs requires efficient and accurate control systems. One of the most important steps in control system design is the development of the aircraft model. The full model of an aircraft includes models of its subsystems such as: aerodynamics, propulsion, actuators. Development of the dynamic model of a UAV is of primary importance. For an accurate dynamic model it is necessary to have accurate data of UAVs' aerodynamics, which can be obtained by various means such as wind tunnel tests, CFD analyses or calculated by empirical formulas [5]. Physically an aircraft is a complicated system, which includes variation of its aerodynamic coefficients, sensor noise, and limited information of the system. Controllers designed with PID methods are unable to take into account errors in the system modeling and signal uncertainties. In cases, when it is impossible to obtain an accurate aerodynamic data for dynamical modeling of a UAV or there are simplifications used in the modelling (linearization of nonlinear dynamics), classical controller, implemented to the actual physical system, might not show the desired performance. Robust control theory provides methods for designing controllers that would produce accurate and fast response in the face of uncertainties or disturbances in the plant model.

The main objective of this thesis is the development, implementation and comparison of performances for pitch attitude and roll autopilots for the simulation of the METU TUAV, designed by means of classical and robust control theories. The problem for a controller design for the METU TUAV is the absence of an accurate data of the UAV's aerodynamics. In [6] aerodynamic coefficients and derivatives are obtained by empirical formulas. [7] provides the aerodynamic data obtained by wind tunnel test for a very similar UAV SCAUT, designed and developed at Politecnico Di Torino, which has similar geometrical properties to the METU TUAV. The purpose of this thesis is the comparison of performances of the PID controller and H_∞ robust controller. Simulations are performed for the nominal model of the UAV and the

models, which include uncertainties and sensor noise. Uncertainties are assumed to be present in the aerodynamic coefficients of the UAV.

In the literature, many different approaches can be seen related to the autonomous control of UAVs. In [8] Andrievsky B.R et.al. propose an algorithm of a combined adaptive controller, which uses both adaptation methods based on the parameter identification and variable-structure control technique. In [9] authors introduce flight control system is based on PID controller and uses gain scheduling algorithm based on the airspeed to improve performance of the controller. In [10] PID controller is used for autonomous landing for the METU TUAV. Model inversion is used in landing algorithm. S. Kurnaz et.al. [11] introduce fuzzy logic based control system for an autonomous UAV system. Robust nonlinear controller design is employed in [12] by M. Sadraey et.al. [13] by Etkin B. describes design of a robust flight control system for a mini-UAV using coupled stability derivatives.

This thesis is organized as follows: Chapter 2 includes the modelling of the UAV, its mass-inertia properties. Dynamic model is based on the 6-DOF equations of motion. Aerodynamic data is used from the reference [7]. Mass-inertia properties are taken from [6]. UAV model also includes models of actuators, gravity and atmosphere. Engine model is developed using the experimentally obtained data. Chapter 3 examines the basics of classical control theory, defines requirements to the control system. It also covers the design of PID controllers for the pitch and roll autopilots and simulation by a linear environment for a nominal model; command filter implementation to the control systems. Theoretical background to the robust control theory, definition of uncertainties, H_∞ design techniques are reviewed in Chapter 4. This chapter also contains the design of H_∞ robust controllers for pitch and roll autopilots, their simulation for a nominal model. Chapter 5 includes comparison of PID and robust controllers performances by a nonlinear simulation. Simulation is performed for both the nominal model and the model with uncertainties and sensor noise. In Chapter 6 conclusions and recommendations for future work are presented. The outline of the thesis can be expressed as follows:

- Development of the nonlinear dynamic model of the METU TUAV, its linearization and investigation of the open-loop response.
- Design and implementation of pitch and roll autopilots based on PID controllers.
- Design and implementation of pitch and roll autopilots, which use the controllers based on H_∞ robust technique.
- Performance comparison of PID and robust controllers.

CHAPTER 2

6-DOF MATHEMATICAL MODELING

In this chapter development of a 6-DOF nonlinear model of the METU TUAV is presented. The 6-DOF nonlinear model includes the aerodynamics, mass-inertia, propulsion, atmospheric and gravity models. The chapter covers linearization of the nonlinear model, decoupling of airplane dynamics into longitudinal and lateral dynamics, their state space representations as well as the analysis of the open-loop responses.

2.1 Platform

The platform used in this thesis is the METU tactical UAV system which is developed with the initial funding provided from the State Planning Office (DPT) in 2004. The UAV is designed and manufactured in the Aerospace Engineering Department of Middle East Technical University and is practically near its completion. The first flight is foreseen within 2009 or early 2010. The UAV is completely manufactured from composite materials, using fiber glass, carbon fiber and Kevlar clothes as composite materials. The aircraft has a fuselage and a high wing configuration and a twin boom T tail configuration. The booms are also manufactured from composite material using filament winding technique. The basic geometrical dimensions and the technical characteristics of the tactical UAV is given in the following Table 2.1. The maximum take off weight of the UAV is estimated as 120 kg. However, this may be slightly less than this predicted value. The final weight will be definite when the aircraft is fully completed. The total payload capacity of the

UAV is about 30 kg and is sufficient to carry a daylight and an IR camera mounted in a gimbal system. Besides these Electro Optical (EO) payload system envisaged at this stage other useful payload systems can easily be integrated into the UAV since there is enough payload volume within the fuselage. The aerodynamical control surfaces of the aircraft includes left and right ailerons, left and right flaps, left and right rudders and an elevator. All these control surfaces are actuated by means of servomotors with sufficient torque capacity. The take off and landing of the UAV is foreseen to be conventional at this stage. However, in the near future this capability will be augmented by incorporating catapult launch and parachute recovery systems into the UAV. The UAV is equipped with steerable front and fixed main landing gears having hydraulic breaking capability. All of the landing wheels are flight qualified. The aircraft is a pusher configuration with the engine mounted at the rear of the fuselage in between the tail booms. The engine used is gasoline powered Limbach L 275 E engine producing 21 HP of output. It is a two stroke cycle opposed twin cylinder engine (boxer engine) where each cylinder is operated by separate carburators. Due to this fact each cylinder operates individually and in case of failure of one of the cylinders the other cylinder produces enough power to propel the aircraft. The preliminary ground tests of the engine and the propeller system shows that a total thrust of about 40 kg is obtained from the engine at normal ground level operations. This much thrust is more than enough for flying the UAV. The aircraft can be operated remotely line of sight by radio control or by auto pilot.

Characteristics of the METU TUAV system are the following:

- Conventional take off and landing from runway
- Autonomous Flight
- 2 stroke cycle, 2 opposed cylinders, dual carburator IC engine delivering 21 HP
- Electro-optical and infrared camera inside a Gimbal system
- Real time video downlink to ground station
- Fully composite structure

Figure 2.1 METU Tactical UAV

Table 2.1 Technical Specifications of the METU Tactical UAV System

Wing Span:	4.3 m
Length:	3 m
Width of Fuselage:	0.3 m
Empty Weight:	90 kg
Maximum Take-off Weight:	120 kg
Maximum Payload Weight:	30 kg
Maximum Speed:	300 km/h
Stall Speed:	65 km/h
Cruise Speed:	145 km/h
Range:	600 km
Maximum Endurance:	5 hr
Operation Altitude:	3000 m
Payload:	FLIR Camera
Propulsion:	21HP Two Cylinder Gasoline Engine

2.2. Reference Frames and Coordinate systems

The following frames and systems are of primary importance for the modeling of the vehicle dynamics.

Inertial reference frame is fixed or in uniform rectilinear translation, relative to the distant stars; in it Newton's second law is valid for the motion of a particle [13]. If the rotation of the Earth is neglected and the surface is assumed to be flat an Earth-surface reference frame is considered as an inertial frame, with origin near the vehicle if possible and with Oz axis directed vertically down. x- and y-axis is the local horizontal plane, x-axis points north and y-axis points east. Vehicle's position is calculated with respect to the inertial frame.

Navigation frame (north-east-down frame), also called as vehicle-carried frame, is used the reference frame in which the origin is attached to the vehicle (usually at the center of gravity), z-axis points down along the local gravity vector, x-axis is directed north and y-axis is directed east.

If the aircraft is considered as a rigid body, it is represented by a frame, the so-called body frame. Although this frame is not used as a reference, it is nevertheless important [14]. The body coordinate system is used for deriving the equations of motion of the vehicle. The origin of this coordinate system is at the center of gravity of the airplane, x-axis points through the nose of the vehicle and lies with the downward pointing z-axis in the plane of symmetry, y-axis, out the right wing, completes the coordinate system.

Transformation from navigation frame to the body frame is composed of three transformations, which are represented by so-called Euler angles: yaw, pitch and roll, or ψ, θ and ϕ. The first rotation is around the z-axis of the navigation frame by angle ψ, second rotation is around the y-axis of an intermediate frame, obtained after the first rotation by the pitch angle θ and the last rotation is around the x-axis of the coordinate system obtained after second rotation by angle ϕ. This transformation is also called the direction cosine matrix.

The transformation matrix:

$$L_{bn} = \begin{bmatrix} \cos\psi\cos\theta & \sin\psi\cos\theta & -\sin\theta \\ \cos\psi\sin\theta\sin\phi - \sin\psi\cos\phi & \sin\psi\sin\theta\sin\phi + \cos\psi\cos\phi & \cos\theta\sin\phi \\ \cos\psi\sin\theta\cos\phi - \sin\psi\sin\phi & \sin\psi\sin\theta\cos\phi - \cos\psi\sin\phi & \cos\theta\cos\phi \end{bmatrix}$$

Wind coordinate system is frequently used for defining aerodynamic forces and moments acting on the aircraft. x-axis is parallel to the free-stream velocity vector. Transformation from the wind axis to body is composed of two rotations: by angle $-\beta$ around the z-axis of the wind coordinate system and rotation by angle α around y-axis such that it coincides with the body axis. Angles α and β are called angle of attack and sideslip angle. The transformation matrix from the wind axis to body:

$$L_{bw} = \begin{bmatrix} \cos\alpha\cos\beta & -\cos\alpha\sin\beta & -\sin\alpha \\ \sin\beta & \cos\beta & 0 \\ \sin\alpha\cos\beta & \sin\alpha\sin\beta & \cos\alpha \end{bmatrix}$$

2.3 6-DOF Equations of Motion

The airplane nonlinear equations of motion are developed by applying Newton's second law and law of conservation of linear momentum. The equations are written in a body-fixed axis system, $X_b Y_b Z_b$ which moves with the airplane and which has its origin at the airplane center of mass. The vehicle is assumed to be a rigid body with six degrees of freedom. Three translational degrees describe the motion of the center of mass and three attitude degrees describe the orientation of the vehicle. Plane XZ is a plane of symmetry of the airplane, therefore $I_{xy} = I_{yz} = 0$.

The scalar force equations of motion in the airplane body-fixed axis system [15]:

Force along *X*:

$$m(\dot{u} - rv + qw) = -mg\sin\theta + X \tag{2.1a}$$

Force along *Y*:

$$m(\dot{v} + ru - pw) = mg\cos\theta\sin\phi + Y \tag{2.1b}$$

Force along Z:

$$m(\dot{w} - qu + pv) = mg\cos\varphi\cos\theta + Z \tag{2.1c}$$

The scalar moment equations in the airplane body-fixed axis system:

Rolling moment about X_b:

$$I_{xx}\dot{p} - I_{xz}\dot{r} - I_{xz}pq + (I_{zz} - I_{yy})qr = L \tag{2.2a}$$

Pitching moment about Y_b:

$$I_{yy}\dot{q} + (I_{xx} - I_{zz})pr + I_{xz}(p^2 - r^2) = M \tag{2.2b}$$

Yawing moment about Z_b:

$$I_{zz}\dot{r} - I_{xz}\dot{p} + (I_{yy} - I_{xx})pq + I_{xz}qr = N \tag{2.2c}$$

Kinematic equations:

Roll rate about X_b:

$$p = \dot{\varphi} - \dot{\psi}\sin\theta \tag{2.3a}$$

Pitch rate about Y_b:

$$q = \dot{\theta}\cos\phi + \dot{\psi}\cos\theta\sin\phi \tag{2.3b}$$

Yaw rate about Z_b:

$$r = \dot{\psi}\cos\theta\cos\phi - \dot{\theta}\sin\phi \tag{2.3c}$$

In scalar force equations of motion forces X, Y and Z include aerodynamic forces and propulsion forces.

2.4 Aerodynamic Forces and Moments

Aerodynamic forces and moments can be determined in two ways: by experimental methods (flight test or wind tunnel test), by computational and/or empirical methods.

Experimental methods have a great advantage of allowing rather accurate predictions of full-scale airplane aerodynamic behavior over a wide range of flight conditions, including nonlinear effects. A disadvantage of experimental methods is that their cost is very high, both in time and in money. Therefore, in most preliminary design and parametric design studies theoretical and empirical methods are used [15].

The main emphasis is on the so-called build-up method for modeling aerodynamic and thrust forces and moments. In this method, the airplane is assumed to be built up from a number of components. The total forces and moments, which act on the airplane, are then assumed to follow from summing the forces and moments, which act on these components. In these terms, aerodynamic coefficients can be expressed as follows:

$$F_{AA/C} = F_{Aw.b.} + F_{Ah.tail} + F_{Av.tail} + \ldots \tag{2.4}$$

The number of components, which should be used, depends on the airplane configuration and on the level of accuracy desired. The stability axis system is used for modeling aerodynamic forces and moments.

2.4.1 Longitudinal Aerodynamic Forces and Moments

Figure 2.2 illustrates the longitudinal aerodynamic forces and moments that act on the airplane in a steady state flight condition. In the stability axis system, these forces and moments are written as:

Longitudinal force in x-direction:

$$F_{Axs} = -D \tag{2.5}$$

Longitudinal force in z-direction:

$$F_{Azs} = -L \tag{2.6}$$

Airplane pitching moment:

$$M_{As} = M_A \tag{2.7}$$

Aerodynamic longitudinal forces and moment are non-dimensionalized in the following way:

$$D = C_D \bar{q} S \tag{2.8}$$

$$L = C_L \bar{q} S \tag{2.9}$$

$$M_A = C_m \bar{q} S \bar{c} \tag{2.10}$$

where: C_D is the total airplane drag coefficient; C_L is the total airplane lift coefficient. Total airplane drag and lift coefficients are the functions of the angle of attack, α, pitching rate, q, elevator and flap deflections, δ_e, δ_f, Mach number and Reynolds number. C_m is the total airplane aerodynamic pitching moment coefficient which in the steady state flight depends on the angle of attack (α), dynamic pressure($\bar{q}$), control surface deflections (δ_e, δ_f), Mach number and Reynolds number, and moment reference center (usually the center of gravity) location.

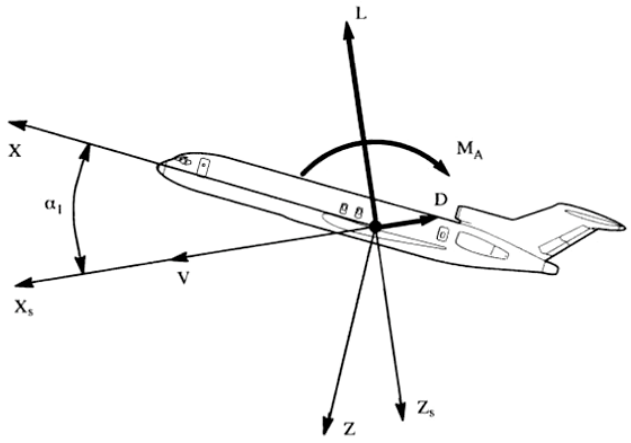

Figure 2.2 Longitudinal Forces and Moment in Stability Axes

For an airplane equipped with an elevator and flaps, the drag coefficient is expressed in terms of the first order Taylor series [15]:

$$C_D = C_{D0} + C_{D_\alpha}\alpha + C_{D_{\delta e}}\delta_e + C_{D_{\delta f}}\delta_f \tag{2.11}$$

where C_{D_0} - the value of airplane drag coefficient for zero angle of attack, zero deflections of control surfaces.

$C_{D_\alpha} = \partial C_D / \partial \alpha$ - the change of airplane drag due to change in airplane angle of attack, α.

$C_{D_{\delta e}} = \partial C_D / \partial \delta_e$ - the change in airplane drag due to elevator deflection δ_e.

$C_{D_{\delta f}} = \partial C_D / \partial \delta_f$ - the change in airplane drag due to flap deflection δ_f.

Similarly, the lift coefficient, C_L, can be expressed in terms of a first order Taylor series as follows:

$$C_L = C_{L_0} + C_{L_\alpha}\alpha + C_{L_{\delta e}}\delta_e + C_{L_{\delta f}}\delta_f \tag{2.12}$$

where:

C_{L_0} - the value of airplane lift coefficient for zero angle of attack, zero control surfaces deflections.

$C_{L_\alpha} = \partial C_L / \partial \alpha$ - the change of airplane lift due to a change in airplane angle of attack, α.

$C_{L_{\delta_e}} = \partial C_L / \partial \delta_e$ - the change in airplane lift due to change in elevator angle.

$C_{L_{\delta f}} = \partial C_L / \partial \delta f$ - the change in airplane lift due to change in flap angle.

The aerodynamic pitching moment coefficient C_m is expressed in the form of the first order Taylor series as:

$$C_m = C_{m\alpha}\alpha + C_{m\dot{\alpha}}\dot{\alpha} + C_{mq}q + C_{m\delta e}\delta_e + C_{m\delta f}\delta_f \tag{2.13}$$

$C_{m\delta e}$ and $C_{m\delta f}$ denote change in airplane pitching moment due to change in deflection of control surfaces.

The derivative $C_{m\alpha}$ is the change in airplane aerodynamic pitching moment coefficient due to a change in angle of attack, it is also called the static longitudinal

stability derivative. It is of major importance to airplane stability and controls [15]. Another important derivative, which effects airplane stability is C_{mq}, also called the pitch-damping derivative.

The steady state model for the aerodynamic force in the stability x-axis direction is:

$$F_{Axs} = -D = -C_D \bar{q} S = -(C_{D_0} + C_{D_\alpha}\alpha + C_{D_{\delta e}}\delta_e + C_{D_{\delta f}}\delta_f)\bar{q}S \qquad (2.14)$$

The steady state model for the aerodynamic force in the stability z-axis direction is:

$$F_{Fxs} = -L = -C_L \bar{q} S = -(C_{L_0} + C_{L_\alpha}\alpha + C_{L_{\delta e}}\delta_e + C_{L_{\delta f}}\delta_f)\bar{q}S \qquad (2.15)$$

The steady state model of the aerodynamic pitching moment in stability axes is:

$$M_{As} = C_m \bar{q} Sc = (C_{m\alpha}\alpha + C_{m\dot{\alpha}}\dot{\alpha} + C_{mq}q + C_{m\delta e}\delta_e + C_{m\delta f}\delta_f)\bar{q}Sc \qquad 2.16)$$

It should be noted that the stability y-axis coincide with the body-fixed y-axis, therefore $M_{As} = M_A$.

2.4.2 Lateral-Directional Aerodynamic Forces and Moments

Lateral-directional force and moments that act on the airplane are shown in Figure 2.3.

In stability axis system, aerodynamic lateral-directional force and moments are written as follows:

Aerodynamic rolling moment:

$$L_{As} = L_A \qquad (2.17)$$

Aerodynamic side force:

$$F_{Ays} = Y_A \qquad (2.18)$$

Aerodynamic yawing moment:

$$N_{As} = N_A \qquad (2.19)$$

For steady state flight conditions these force and moments are non-dimensionalized as:

$$L_A = C_l \bar{q} Sb \qquad (2.20)$$

$$Y_A = C_Y \bar{q} S \tag{2.21}$$

$$N_A = C_n \bar{q} S b \tag{2.22}$$

where C_l is aerodynamic rolling moment coefficient of an airplane; C_y is airplane aerodynamic side-force coefficient; C_n is the airplane aerodynamic yawing coefficient, which in a steady state depends on:

- angle of sideslip, β
- angle of attack, α
- dynamic pressure, $\bar{q}$
- moment reference center (usually the center of gravity) location
- deflection of lateral control surfaces
- deflection of directional control surfaces
- Mach number and Reynolds number

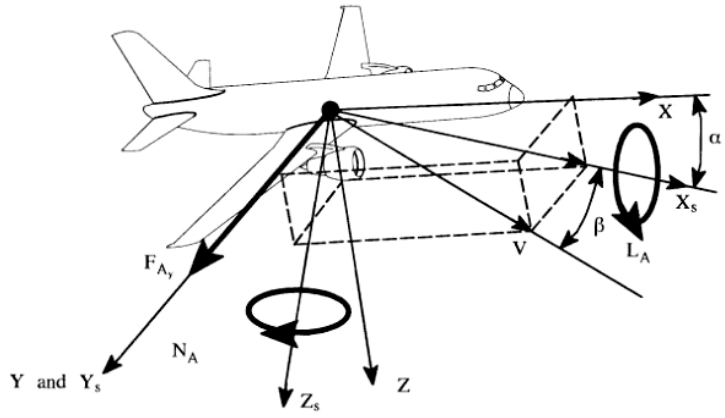

Figure 2.3 Lateral-Directional Force and Moments in Stability Axes

In terms of the first order Taylor series, these coefficients can be expressed as follows:

$$C_l = C_{l_0} + C_{l_\beta}\beta + C_{lp}p + C_{lr}r + C_{l_{\delta_a}}\delta_a + C_{l_{\delta_r}}\delta_r \quad (2.23)$$

$$C_y = C_{y_0} + C_{y_\beta}\beta + C_{yp}p + C_{yr}r + C_{y_{\delta_a}}\delta_a + C_{y_{\delta_r}}\delta_r \quad (2.24)$$

$$C_n = C_{n_0} + C_{n_\beta}\beta + C_{np}p + C_{nr}r + C_{n_{\delta_a}}\delta_a + C_{n_{\delta_r}}\delta_r \quad (2.25)$$

The coefficients and derivatives are defined in a similar way as for the longitudinal stability coefficients and derivatives.

The derivative C_{l_β} is called the airplane effective dihedral; this derivative plays a major role in determining airplane stability. The control power derivative $C_{l_{\delta_a}}$ is a dominant factor on the bank angle maneuverability of airplanes. The magnitude of a cross-control derivative $C_{l\delta r}$ should preferably be close to zero.

The coefficient C_{y_0} tends to be zero for symmetrical airplanes. The derivative C_{y_p} is an important derivative in dutch-roll dynamics. It is also important in flight path control. The control derivative $C_{y_{\delta_a}}$ is normally negligible.

For symmetrical airplanes coefficient C_{n_0} tends to be equal to zero. The derivative C_{n_β} is an important derivative in dutch-roll and spiral dynamics, it is referred to as a static directional stability derivative [15].

The steady state models for airplane aerodynamic rolling moment, side force and yawing moment are:

$$L_{As} = L_A = C_l \bar{q} Sb = (C_{l_0} + C_{l_\beta}\beta + C_{lp}p + C_{lr}r + C_{l_{\delta_a}}\delta_a + C_{l_{\delta_r}}\delta)\bar{q}Sb \quad (2.26)$$

$$F_{As} = Y_A = C_y \bar{q} S = (C_{y_0} + C_{y_\beta}\beta + C_{yp}p + C_{yr}r + C_{y_{\delta_a}}\delta_a + C_{y_{\delta_r}}\delta_r)\bar{q}S \quad 2.27)$$

$$N_{As} = N_A = C_n \bar{q} Sb = (C_{n_0} + C_{n_\beta}\beta + C_{np}p + C_{nr}r + C_{n_{\delta_a}}\delta_a + C_{n_{\delta_r}}\delta_r)\bar{q}Sb \quad (2.28)$$

The values of the aerodynamics coefficients and derivatives are taken from the reference [7], which contains wind tunnel test data, performed for analog airplane

SCAUT at Politecnico di Torino, Italy. Gaphs for the aerodynamic coefficients and derivatives may be found in the Appendix A.

2.5 Mass- Inertia model

The mass inertia model contains the mass of the airplane and its tensor of inertia.
The mass is lumped and concentrated at the center of gravity (c.g.) location and the inertia tensor is calculated with respect to the c.g.
Table 2.2. includes maximum take-off gross weight, fuel weight and moments of inertia of the MTUAV [6].

Table 2.2. Mass and Inertia Properties of the METU TUAV

$m_{MTOW}\ (kg)$	$m_{fuel}(kg)$	$I_{xx}\ (kgm^2)$	$I_{yy}\ (kgm^2)$	$I_{zz}\ (kgm^2)$	$I_{xz}\ (kgm^2)$
105	15	37.58	34.12	67.04	-6.91

The change of the gross weight and c.g. location of the MTUAV is neglected for simulation purposes. Change in the c.g. location is very small, and its position moves towards the nose of the airplane during the flight, increasing longitudinal stability of the aircraft. Moments of inertia are considered to be constant for all time of simulation.

2. 6 Propulsion Model

The propulsion model of the METU TUAV is represented by the engine model and propeller model. METU TUAV uses two-cylinder engine Limbach L275 E shown in the Figure 2.4

Characteristics of the engine are obtained from [16] and presented in the Figure 2.5. Characteristics include required power (P), torque and specific fuel consumption (SFC) dependence on RPM. The data are shown for RPM variation from 4000 to 7200. It is assumed that the dependence of required power and SFC on RPM for RPM is less than 4000 is linear. Fuel consumption (FC) can be found as follows:

$$FC = SFC \cdot P \tag{2.29}$$

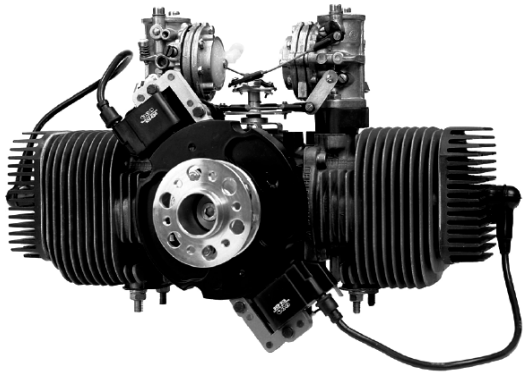

Figure 2.4 Limbach L 275 E

Propeller is represented by the following characteristics:

the thrust coefficient given by

$$C_t = \frac{T}{\rho n^2 D^4} \tag{2.30}$$

where T is the thrust of the propeller;

power coefficient

$$C_p = \frac{P}{\rho n^3 D^5} \tag{2.31}$$

advanced ratio

$$J = \frac{V_\infty}{nD} \tag{2.32}$$

Thrust and power coefficients and geometric properties of METU TUAV propeller sections can be found in [6].

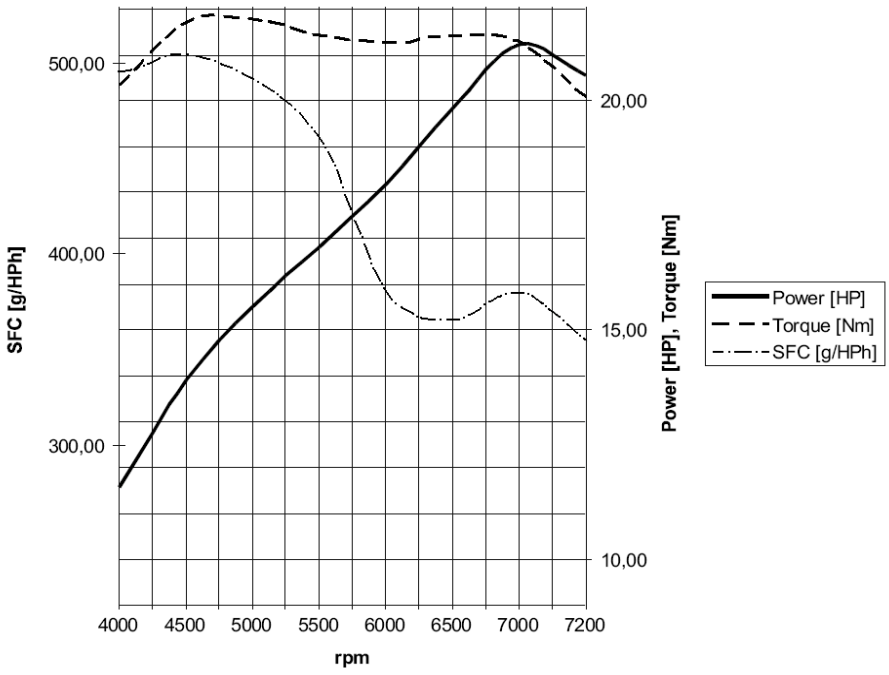

Figure 2.5 Power, Torque and SFC vs. RPM of Limbach L 275 E

2.7 Actuator Models

The actuators servo are assumed to be a first order servo with a transfer function

$$Gact = \frac{T}{s+T} \tag{2.33}$$

Dynamics of control surfaces (elevator, ailerons and rudder) is assumed faster than dynamics of a UAV, the bandwidth T has been chosen equal to 30 rad/s. The inputs to the actuators are subjected to the strict limits on the range of variations that can be achieved. These limitations include physical limitations on the actuators themselves and also ensure the system of being damaged [55]. Elevator deflection is constrained up to $\pm 30\,\text{deg}$, rudder and ailerons deflection is limited to $\pm 25\,\text{deg}$.

2.8 Atmosphere model

Atmosphere model is used for developing more accurate aerodynamic model of the vehicle. The main parameter that has an influence on the aerodynamic and thrust forces and moments is air density ρ, which depends on altitude. The altitude range for MTUAV is 10 km. Change in air temperature, pressure and viscosity has a secondary effect upon the aerodynamic and thrust forces and moments.

For simulating atmosphere effects Aerospace blockset of MATLAB/Simulink provides a COESA Atmosphere Model block. The COESA Atmosphere Model block implements the mathematical representation of the 1976 Committee on Extension to the Standard Atmosphere (COESA) United States standard lower atmospheric values for absolute temperature, pressure, density, and speed of sound for the input geopotential altitude. Below the geopotential altitude of 0 m and above the geopotential altitude of 84852 m temperature values are extrapolated linearly and pressure values are extrapolated logarithmically. Density and speed of sound are calculated using a perfect gas relationship. More information can be found in [17].

2.9 Gravity Model

The Earth model blocks available in the Aerospace Blockset. WGS84 Gravity Model block implements the mathematical representation of the geocentric equipotential ellipsoid of the World Geodetic System (WGS84). The block output is the Earth's gravity at a specific location.

Use of the WGS84 Close Approximation model should be limited to a geodetic height of 20000 m. Below this height, it gives results with high precision. More specific information about the Earth gravity model is present in [20].

2.10 Non-Linear Simulation

6-DoF nonlinear model of METU TUAV is developed in MATLAB/Simulink, its Simulink block diagram is illustrated in the Figure 2.6. The model consists of several blocks:

- The 6DoF (Euler Angles) block implements an Euler angle representation of six-degrees-of-freedom equations of motion of a vehicle
- Block which contains aerodynamic coefficients and derivatives of the METU TUAV
- Environment model block, which contains blocks with atmosphere model and gravity model
- Block, which computes the aerodynamic forces and moments using the aerodynamic coefficients, dynamic pressure, center of gravity, and center of pressure.
- Block that is used to calculate angle of attack, sideslip angle, and Mach number.

For the 6DoF equations of motion block, it is assumed that the applied forces are acting at the center of gravity of the body, and that the mass and inertia are constant. Aerodynamic coefficients and derivatives were taken from [6] and [7]. Atmospheric model provides data for atmospheric values for absolute temperature, pressure,

density, and speed of sound for the given altitude. Gravity model provides the Earth's gravity information.

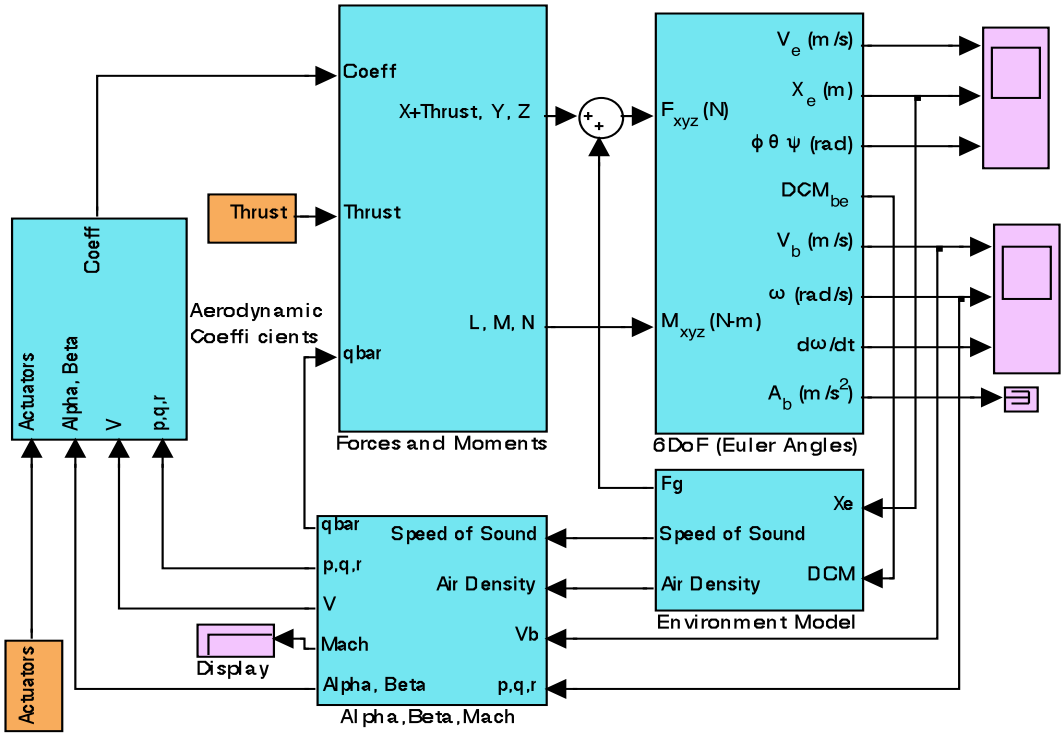

Figure 2.6 Simulink Block Diagram of the Nonlinear System

2.11 Linearization of Equations of Motion and State Space Representation

Using the small disturbance theory, the nonlinear equations of motion of the airplane are linearized for small disturbances around an equilibrium point of the airplane.

The steady-level-flight condition is chosen for the trim analysis. Under certain assumptions, equations of motion can be uncoupled and airplane longitudinal and lateral dynamics can be analyzed separately. Existence of pure longitudinal motion requires three approximations and assumptions: the flat-Earth approximation, existence of a plane of symmetry and absence of rotor gyroscopic effects. Existence of the uncoupled lateral motions besides the restrictions above also requires neglecting all aerodynamic cross-coupling terms (which may not be strictly equal to zero) [14].

Linearization of the nonlinear model of the METU TUAV has been done using the Simulink Control Design tools. Linearization is the approximation of a nonlinear system as a linear system, based on the assumption that the system is almost linear within a certain range of operation. Linearization is performed around certain equilibrium point (or trim condition) of the nonlinear system.

Trim condition used for linearization task is given below:

velocity in x-direction in body axis $u_0 = 36\ m/s$, velocity in z-direction in body axis $w_0 = 1.81\ m/s$, pitch angle $\theta_0 = 4.4\ deg$, $Thrust = 100\ H$.

2.11.1 Longitudinal Dynamics

Consider the state space representation of the longitudinal dynamics. The states are $\lfloor \Delta u, w, q, \Delta\theta \rfloor$, the input is elevator deflection $\lfloor \Delta\delta_e \rfloor$ and the outputs are $\lfloor \Delta u, w, q, \Delta\theta \rfloor$. Expression for a state matrix and input matrix are the following:

$$A_{long} = \begin{bmatrix} \frac{X_u}{m} & \frac{X_w}{m} & 0 & -g\cos\theta_e \\ \frac{Z_u}{m - Z_{\dot{w}}} & \frac{Z_w}{m - Z_{\dot{w}}} & \frac{Z_q + mu_0}{m - Z_{\dot{w}}} & -\frac{mg\sin\theta_e}{m - Z_{\dot{w}}} \\ \frac{1}{I_y}\left[M_u + \frac{M_{\dot{w}} Z_u}{m - Z_{\dot{w}}}\right] & \frac{1}{I_y}\left[M_w + \frac{M_{\dot{w}} Z_u}{m - Z_{\dot{w}}}\right] & \frac{1}{I_y}\left[M_q + \frac{M_{\dot{w}}(Z_q + mu_0)}{m - Z_{\dot{w}}}\right] & -\frac{M_{\dot{\alpha}} mg\sin\theta_e}{I_y(m - Z_{\dot{w}})} \\ 0 & 0 & 1 & 0 \end{bmatrix}$$

$$B_{long} = \begin{bmatrix} \frac{X_{\delta e}}{m} \\ \frac{Z_{\delta e}}{m - Z_{\dot{w}}} \\ \frac{1}{I_y}\left[M_{\delta e} + \frac{M_{\dot{w}} Z_{\delta e}}{m - Z_{\dot{w}}}\right] \\ 0 \end{bmatrix}$$

For a trim condition described above, longitudinal state matrix A_{long} and input matrix B_{long} are given below:

$$A_{long} = \begin{bmatrix} -0.0304 & 0.3784 & -1.7860 & -9.7514 \\ -0.4208 & -2.5015 & 35.5219 & -0.751 \\ 0.1264 & -2.5188 & -2.96 & 0 \\ 0 & 0 & 1.0 & 0 \end{bmatrix} \quad B_{long} = \begin{bmatrix} -0.8761 \\ -7.181 \\ -48.67 \\ 0 \end{bmatrix}$$

Roots of the characteristic equation of the airplane (eigenvalues) are equal to:

$s_{1,2} = -2.7317 \pm 9.4696i$

$s_{3,4} = -0.0142 \pm 0.3711i$

The pair of roots of the characteristic equation that are located more far away from the imaginary axis and have a greater absolute value is referred to as a short period mode. The other pair of roots of the characteristic equation, with a smaller imaginary part that are located closer to the imaginary axis, defines a phugoid mode [18]. The phugoid or long-period mode is the one in which there is a large-amplitude variation of air-speed, pitch angle, and altitude, but almost no angle-of-attack variation. In practice airplane is always under the action of disturbances caused by different factors (pilot, control system etc.). The phugoid oscillation is really a slow interchange of kinetic energy (velocity) and potential energy (height) about some

equilibrium energy level as the aircraft attempts to re-establish the equilibrium level-flight condition from which it had been disturbed. The short-period mode is a very fast, usually heavily damped, oscillation with a period of a few seconds. This motion might be, for example, a rapid pitching of the aircraft about the center of gravity. The period is so short that the speed does not have time to change, so the oscillation is essentially an angle-of-attack variation [15]. Characteristics of the longitudinal modes are given in Table 2.3.

Table 2.3 Longitudinal Modes Characteristics

Mode Name	Root Location	Natural Frequency ω_n (rad/s)	Period (s)	Damping ratio ξ	Time to Half Amplitude t_{half} (s)
Short Period	$-2.7317 \pm 9.4696i$	9.855	0.637	0.288	0.252
Phugoid	$-0.02 \pm 0.2615i$	0.262	23.981	0.076	34.65

2.11.2 Lateral Dynamics

States, which correspond to the lateral dynamics of an aircraft, are: side velocity in body axis (v), roll rate (p), yaw rate (r) and roll angle (ϕ). To control the lateral motion ailerons and rudder are used. State and control matrices, which describe lateral motion of an aircraft are as given below:

$$A_{lat} = \begin{bmatrix} \frac{Y_v}{m} & \frac{Y_p}{m} & \frac{Y_r}{m} - u_0 & g\cos\theta_0 \\ \frac{Y_v}{J_x} + J_{zx}N_v & \frac{Y_p}{J_x} + J_{zx}N_p & \frac{Y_r}{J_x} + J_{zx}N_r & 0 \\ J_{zx}L_v + \frac{N_v}{J_z} & J_{zx}L_p + \frac{N_p}{J_z} & J_{zx}L_r + \frac{N_r}{J_z} & 0 \\ 0 & 1 & \tan\theta_0 & 0 \end{bmatrix}$$

$$B_{lat} = \begin{bmatrix} \frac{Y_{\delta_a}}{m} & \frac{Y_{\delta_r}}{m} \\ \frac{L_{\delta_a}}{J_x} + J_{zx}N_{\delta_a} & \frac{L_{\delta_r}}{J_x} + J_{zx}N_{\delta_r} \\ J_{zx}L_{\delta_a} + \frac{N_{\delta_a}}{J_z} & J_{zx}L_{\delta r} + \frac{N_{\delta_r}}{J_z} \\ 0 & 0 \end{bmatrix}$$

where

$$J_x = (I_x I_z - I_{zx}^2)/I_z$$

$$J_z = (I_x I_z - I_{zx}^2)/I_x$$

$$J_{zx} = I_{zx}/(I_x I_z - I_{zx}^2)$$

For a trim condition, lateral state and input matrices A_{lat} and B_{lat} are obtained as follows:

$$A_{lat} = \begin{bmatrix} -0.173 & 1.78 & -35.79 & 9.751 \\ -0.54 & -5.764 & 0.7258 & 0 \\ 0.2023 & -0.7669 & -0.6072 & 0 \\ 0 & 1.0 & 0.07705 & 0 \end{bmatrix} \quad B_{lat} = \begin{bmatrix} 0 & 1.834 \\ 52.09 & 19.36 \\ 3.861 & -3.636 \\ 0 & 0 \end{bmatrix}$$

The eigenvalues of the lateral state matrix A_{lat} are equal to:

$s_{1,2} = -0.2441 \pm 3.2075i$;

$s_3 = -6.0467$;

$s_4 = -0.0092$.

The lateral motion of aircraft is described by 3 dynamic modes: roll mode, dutch-roll mode and spiral mode.

The first two roots of the characteristic equation is a complex conjugate pair. This pair is referred to as a dutch-roll mode, which is a coupled roll and yaw motion. This mode is usually poorly damped.

The real root with a larger magnitude defines the roll mode. The roll mode consists of almost pure rolling motion and is generally well damped. The real root which is closer to the origin corresponds to the spiral mode, which is usually slow and unstable. In order to reduce the impact of the spiral mode aircraft should have sufficiently large wing dihedral, which increases roll stability. The lateral modes characteristics are shown in the Table 2.4 and 2.5.

Table 2.4 Dutch-roll Mode Characteristics

Mode Name	Root Location	Natural Frequency ω_n (rad/s)	Period (s)	Damping ratio ξ	Time to Half Amplitude t_{half} (s)
Dutch-roll	$-0.2441 \pm 3.2075i$	3.216	1.953	0.076	2.826

Table 2.5 Roll and Spiral Mode Characteristics

Mode Name	Root Location	Time Constant (s)	Time to Half Amplitude t_{half} (s)
Roll	-6.0467	0.165	0.114
Spiral	-0.0092	108.695	75.0

2.12 Open-Loop Simulation

Open-loop simulation shows response of the system to the deflection of control surfaces. As it has been mentioned before, elevator is used as a control to longitudinal dynamics, ailerons and rudder are used as controls to lateral motion of an aircraft. Open-loop response simulation is performed for both linearized and nonlinear models of the UAV in comparison purposes.

Giving the elevator input of 5 degrees for the time interval between 10 and 15 seconds system's open-loop response represented by body x and z velocities, pitch angle and pitch angular rate is shown in Figures 2.7 – 2.10. System's response to the ailerons deflection of 1 degree for five seconds starting at 10th second in terms of body y velocity, roll angle, roll and yaw angular rates is shown in Figures 2.11 – 2.14. Change of the UAV position in time for the aileron one degree step input at 5th second, simulated for a nonlinear model is shown in the Figure 2.15.

As it is seen from the plots on the figures below, that the open-loop response characteristics are not satisfactory: it takes more than 200 seconds for a system to reach its longitudinal trim condition with quite large overshoot. From the response of the system to change in ailerons position, it is seen that though analysis of the linear model shows that the spiral mode is stable (because the eigenvalue, which corresponds to the spiral mode, is negative), nonlinear simulation shows that the spiral mode is unstable. This difference may occur because of the numerical algorithm, which was used for the linearization.

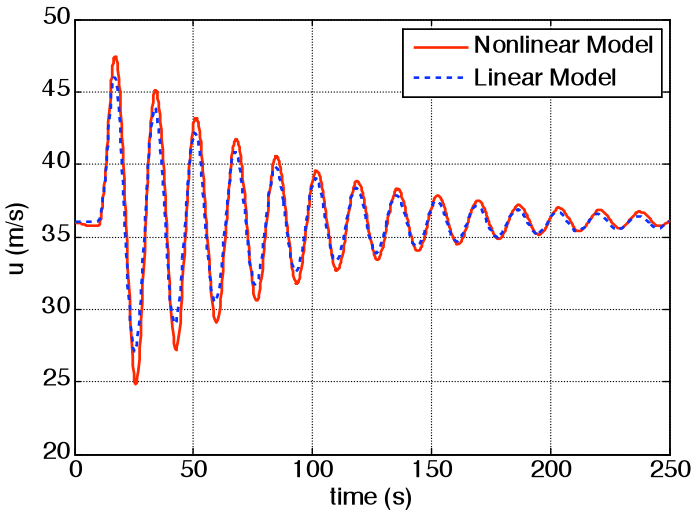

Figure 2.7 System Response to Elevator Input: x-body Velocity

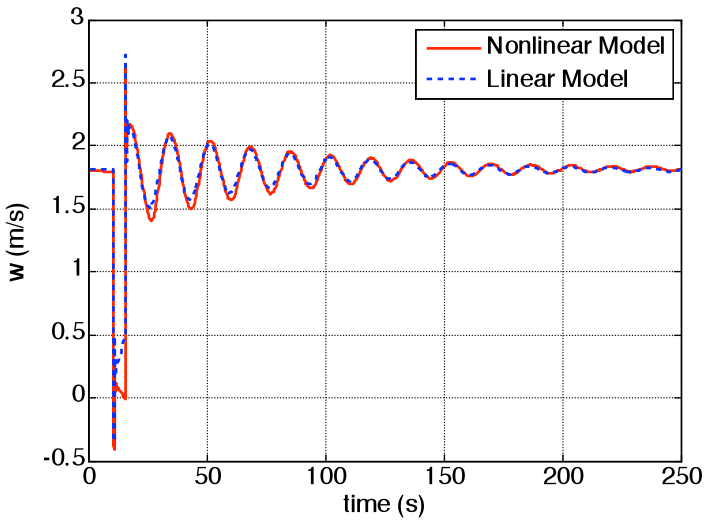

Figure 2.8 System Response to Elevator Input: z-body Velocity

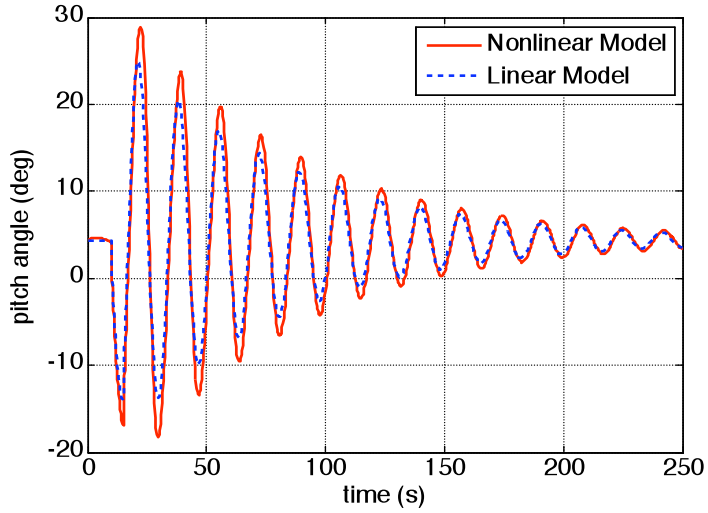

Figure 2.9 System Response to Elevator Input: Pitch Angle

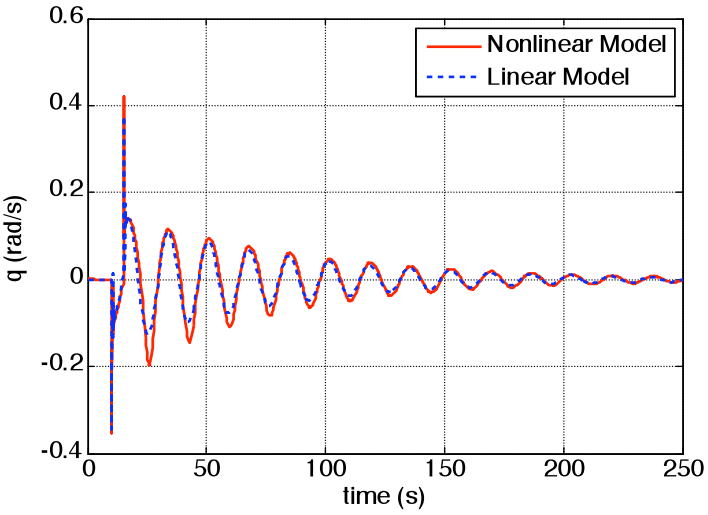

Figure 2.10 System Response to Elevator Input: Pitch Rate

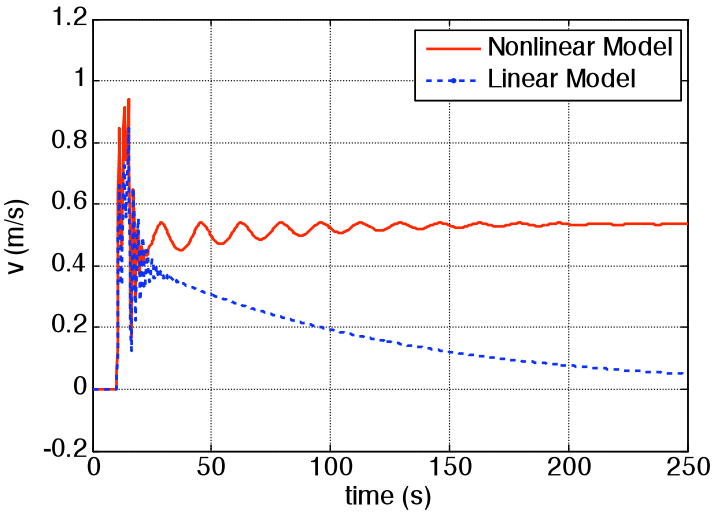

Figure 2.11 System Response to Ailerons Input: y-body Velocity

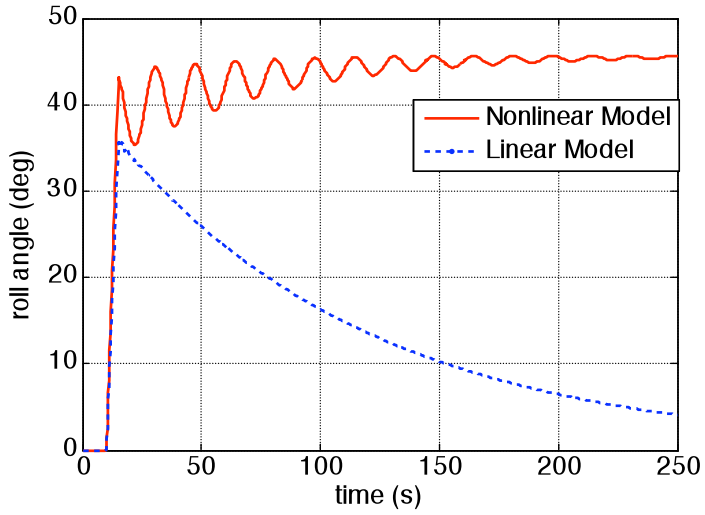

Figure 2.12 System Response to Ailerons Input: Roll Angle

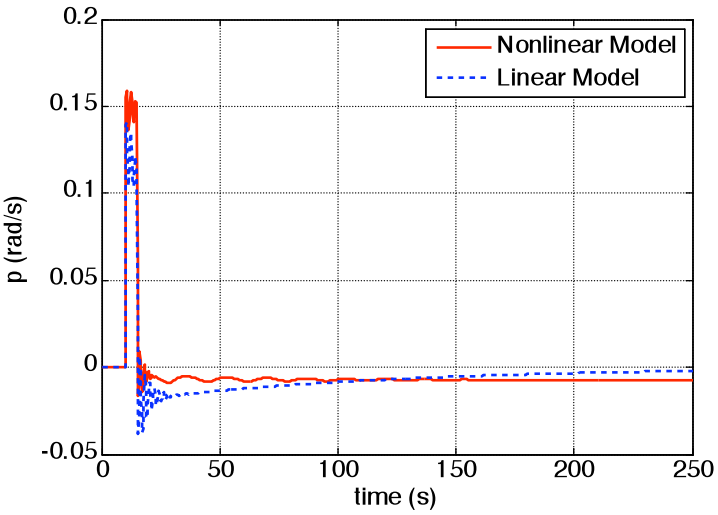

Figure 2.13 System Response to Ailerons Input: Roll Rate

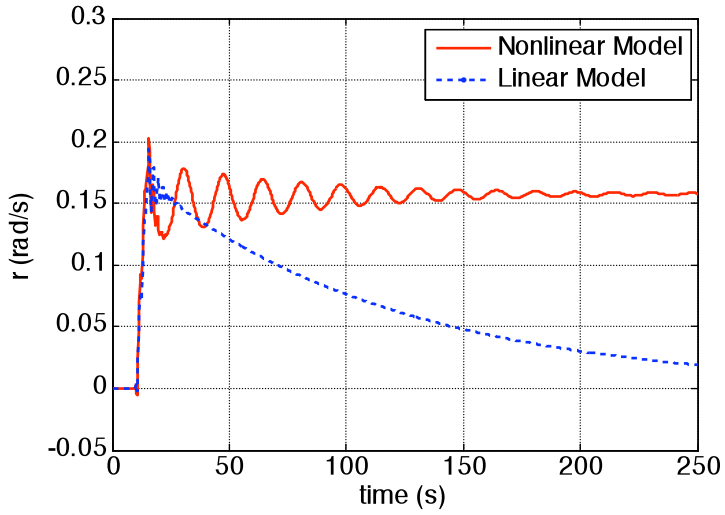

Figure 2.14 System Response to Ailerons Input: Yaw Rate

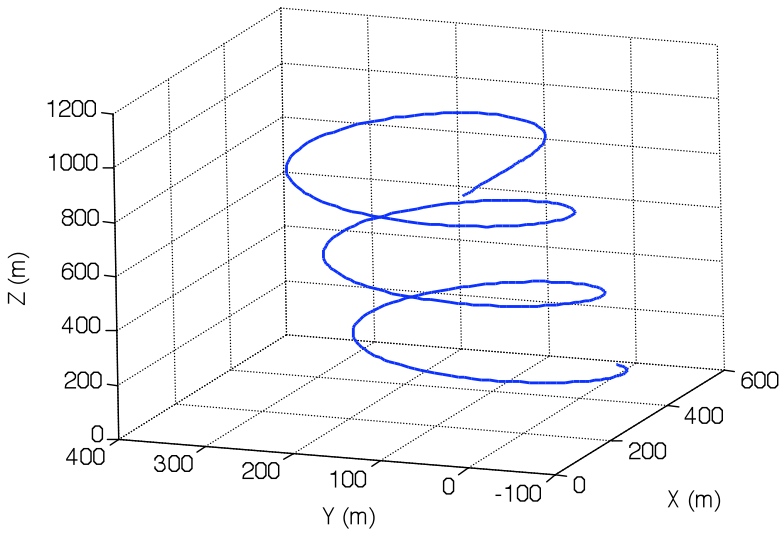

Figure 2.15 System Response to Ailerons Step Input

CHAPTER 3

CLASSICAL CONTROLLER DESIGN

In this chapter, classical approach to controller design is presented. Pitch attitude controller and roll autopilot design for METU TUAV using a PID controller is performed.

3.1 PID Controller Background

Classical controller design techniques are based on a frequency domain analysis of system dynamics. A closed-loop controller uses feedback to control states or outputs of a dynamical system.

Feedback control system, in general, consists of system to be controlled, which includes actuators, sensors to measure system's output, and a controller (see Figure 3.1).

The main reason to use feedback is to minimize the effect of "uncertainty" [21]. The term "uncertainty" includes the uncertainties of system modeling, disturbances and noise. More detailed description of uncertainty and its sources will be given further.

Feedback controllers have many advantages over the open-loop controllers:

- improve system response characteristics
- show good performance in the presence of model uncertainties
- noise and disturbance rejection
- unstable processes can be stabilized

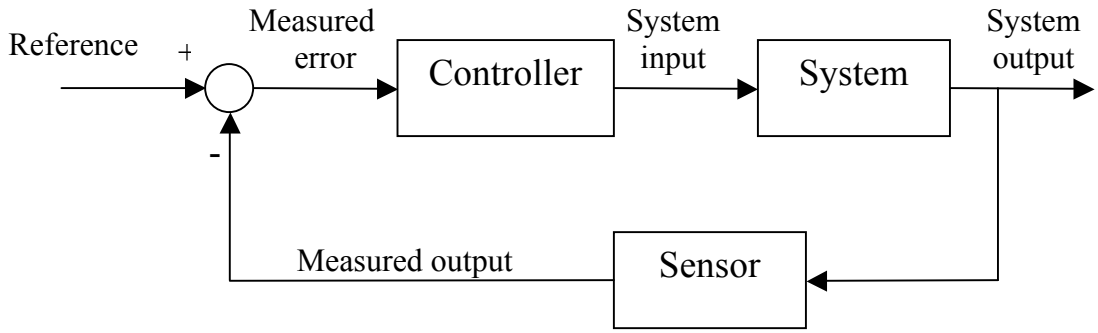

Figure 3.1 Standard Feedback Configuration

A common closed-loop controller architecture is the PID controller. PID controller includes three terms in parallel: proportional (P), integral (I) and derivative (D). Because of the simple design, PID controllers are widely used in industry. Transfer function of a PID controller is the following [22]:

$$G_{PID}(s) = K_p + \frac{K_i}{s} + K_d s \tag{3.1}$$

where K_p, K_i and K_d are controller gains.

Block diagram of a PID controller is shown in the Figure 3.2 .

Some authors (for example, in references [23], [36], [37]) use representation of a PID controller in terms of proportional gain K_p, integral time T_i, and derivative time T_d. In these terms, the PID algorithm can be described as:

$$u(t) = K_p \left(e(t) + \frac{1}{T_i} \int_0^t e(\tau) d\tau + T_d \frac{de(t)}{dt} \right) \tag{3.2}$$

where *u* is the control signal and *e* is the control error (difference between the set-point and output).

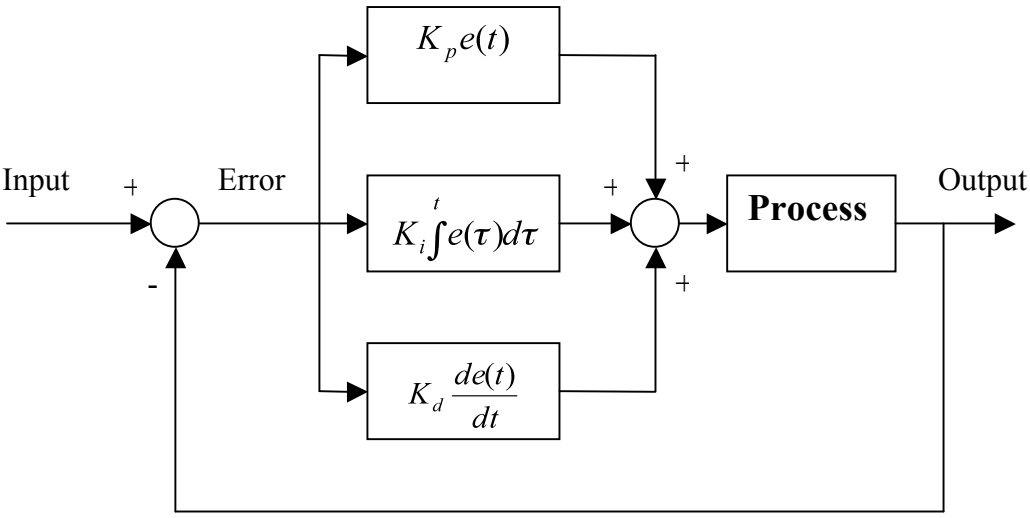

Figure 3.2 Block Diagram of a PID Controller

Thus, controller parameters that must be determined are K_p, T_i, and T_d. PID controller combines both PI and PD controllers and therefore includes the advantages of both. Since PI controller performs its action in a low-frequency region and PD controller – in a high-frequency region, PID controller can be used for design of control systems in which it is required to improve characteristics of both transient and steady state response [23].

Proportional term reduces the rise time and steady-state error (but never eliminates it); it also attenuates noise at high frequencies. However, increasing the controller gain makes system unstable. Adding an integral term adds a zero at the origin, which makes the controller to have an infinite gain at zero frequency. The presence of a pole at the origin of the complex plane allows the reduction to zero of the steady-state error when a step reference signal is applied or a step load disturbance occurs. Derivative term improves the closed-loop stability: reduces overshoot and settling time of the system response, it has no effect on the steady-state error. Disadvantage

of a derivative term is its sensitivity to noise in the error term, so if noise amplitude and the derivative gain are large system becomes unstable. More detailed information about PID controllers is introduces in [25], [26], [27].

Considering representation of a PID controller as it is shown in (3.1), if $e(t)$ denotes the input to PID controller, then its output $u(t)$ is a linear combination of $e(t)$, its integral, and its derivative.

Presence of pure derivation action makes the controller transfer function not proper and therefore it cannot be implemented in practice. The difficulty in designing PID controller is in physical implementation of a derivative term. Very often, in practice, proper approximation of a derivative term is used:

$$G_{PID}(s) \cong K_p + \frac{K_i}{s} + \frac{K_d s}{1 + \varepsilon s} \tag{3.3}$$

where ε is a small positive number [21].

Usually it is sufficient to use only PI controller, which is done in many industrial controllers. PI controller shows sufficient performance for all processes where the dynamics are essentially of the first order or if the process requirements are not too high. PID controllers are used for systems with dynamics of second order or when a tight control of a high-order system is required. [36] and [37] cover principles of PID controllers, implementation details, when to use PID controllers, design of PID controllers, etc.

3.1.1 PID Controller Tuning Rules

There are different techniques for determining gains of PID (proportional–integral–derivative) controllers. Tuning the gains of a PID controller can be done using a design experience or by various design techniques for determining parameters for the controller. [23] gives Ziegler-Nichols rules for tuning PID controllers. [32] presents Ziegler-Nichols Types of Tuning Rule for PID controllers. An Internal Model Control method (IMC) is described in [28]. This method is used for defining the

structure of a controller and it introduces a tuning technique for tuning of the controller's gains, so-called IMC-PID tunings. [30] provides the most comprehensive summary of PID controller tuning rules to date. Tuning of the controller's parameters is performed after specifying the structure of the controller as well as the form of the model used to represent the dynamic response of the controlled variables. Although tuning rules that provide the best performance often vary from case to case, modern rules such as IMC and direct synthesis tend to provide better results than traditional techniques such as Ziegler Nichols or Cohen-Coon tuning. [31] covers PID controller design for various systems, evaluates several existing PID tuning rules from the robustness and fragility point of view. The range of system parameters is given for each tuning rule such that the system remains stable when the PID parameters deviate from the nominal value within the given range. This reference also provides several examples to illustrate the design of PID control to satisfy time domain performance specifications. [32] gives basics and fundamentals of PID control, online model-free methods, with emphasis on the iterative feedback tuning (IFT) method, nonparametric methods for PID tuning through the concept of relay feedback, a well-known technique that experimentally locates critical points in the frequency response that can then be used for controller tuning, it also covers the topics of using of relay feedback for multivariable systems, parametric design methods that assume that a transfer function model is available at the onset of the design procedure. [36] and [37] include Ziegler-Nichols classical methods of PID controllers design and their extensions; pole placement and other methods; auto-tuning techniques. Reference [36] provides some adoptive techniques, which include auto-tuning, gain scheduling and adaptation.

3.2 Control Problem Definition

Solving the control problem generally involves:

- Choosing sensors to measure the plant outputs

- Choosing actuators to drive the plant
- Developing mathematical models for plant, actuators and sensors
- Define control criteria
- Designing the controller, which is based on the developed models and control criteria
- Check controller performance by simulation.

Control criteria usually include (see reference [22]):

- Reducing the effects of the disturbance of the output
- Steady-state errors
- Transient response characteristics
- Sensitivity to parameter changes in the plant.

Mathematical models of plant and actuators has been given in a previous chapter. The following section describes sensors required for a controller synthesis and give definition to a command filter.

The following requirements for the system response must be considered and satisfied pending the controller design for METU TUAV:

- overshoot: < 10%
- settling time: < 3 sec
- rise time: < 1 sec
- steady state error: < 2%

3.3 Sensors

Onboard sensors are necessary to measure the states of the aircraft. The measurements are performed with respect to certain reference frames (inertial frame, Earth frame, body frame, etc.). Dynamics of inertial sensors, like accelerometers and gyros, with a high bandwidth is usually neglected. These sensors are modeled as simple gains [24].

The following sensors are available on the board of METU TUAV:

- Inertial Navigation System (INS) is used to obtain the position and orientation of a vehicle. INS is an autonomous system. Inertial measurement unit (IMU) typically includes three orthogonal accelerometers, and three orthogonal gyros (usually rate-gyros). Inertial measurement unit gives the information about linear accelerations and angular turning rates about the airplane's body axis. Euler angles are obtained by integrating body angular rates. Position of the vehicle is calculated by integrating linear accelerations. INS outputs also provide "steering commands to the autopilot to steer the airplane through predetermined waypoints". However, output of INS tends to drift during the integration process: small errors in the measurement of acceleration and angular velocity grow in time with integration. This leads to significantly larger errors in position and orientation. This problem can be eliminated by fusing INS with GPS. More detailed information about characteristics and basic principles of INS can be obtained from [29].
- Global Positioning System (GPS), which gives accurate three-dimensional position and velocity information. However, GPS is not autonomous system; it is subjected to jamming. Integrating INS and GPS combines advantages of both systems and eliminates the disadvantages. Therefore, data, obtained in such a way, are reliable for navigation purposes.
- Airspeed indicator. The airspeed indicator or airspeed gauge is used in an aircraft to display the aircraft's airspeed.
- Altimeter is an instrument used to measure the altitude of an aircraft with respect to a fixed level. Barometric altimeter (or pressure altimeter) uses an aneroid barometer measures the atmospheric pressure from a static port outside the aircraft.

3.4 Classical Controller Design for METU TUAV: Pitch Attitude Controller

The purpose of the pitch attitude autopilot is to follow the desired reference input and maintain the pitch orientation of the aircraft after it has reached desired value. For design purposes, linearized longitudinal dynamic equations are used for the controller synthesis and simulation. Later performance of the controller is checked for the 6-DoF nonlinear model of the airplane. Response of the control system through the nonlinear simulation with comparisons to a robust controller response is given in Chapter 5.

3.4.1 Controller Configuration

The basic block diagram for the closed-loop system of the pitch autopilot is shown in Figure 3.3. Command input θ_c is first introduced into the closed-loop. A pitch angle error is the input to the controller. It represents the difference between the system output (measured pitch angle θ) and the commanded pitch angle θ_c.

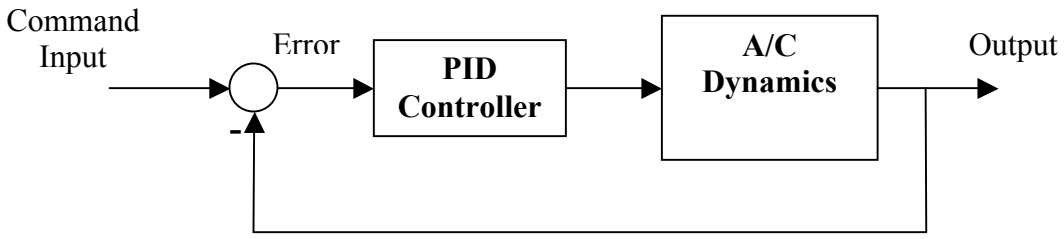

Figure 3.3 Basic Controller Configuration

Aircraft dynamics includes linearized longitudinal dynamics of the METU TUAV and actuator model. Elevator deflection is used as a control surface.

Pitch angle to elevator deflection transfer function is obtained as:

$$W_{\theta/\delta e} = -\frac{48.7s^2 + 105.3s + 12.5}{s^4 + 5.4919s^3 + 97.428s^2 + 3.5150s + 13.3973} \tag{3.4}$$

The transfer function of a PID controller:

$$G_c = -K_p\left(1 + \frac{1}{sT_i} + sT_d\right) \tag{3.5}$$

where controller parameters (proportional gain, integral time and derivative time) must be determined.

Negative sign indicates that a positive deflection of a control surface creates a negative pitching moment therefore, negative pitch angle.

3.4.2 Determining Controller Parameters and Controller Performance

For determining the parameters of a PID controller, which is used in pitch attitude control system, Ziegler-Nichols rule, based on step response of the plant, presented in [3] is used. This method can be applied in case if its response to the unit step looks like S-shaped curve, which is shown in the Figure 3.4.

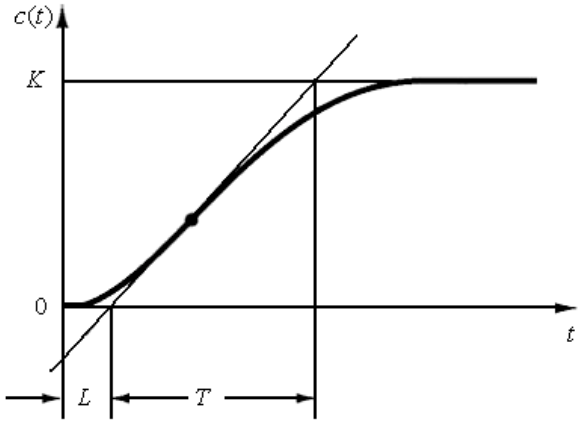

Figure 3.4 S-shaped Response Curve

The response curve can be characterized by two parameters: delay time *L* and time constant *T*, which are obtained by drawing a tangent line at the inflection point and defining cross points as it is shown in Figure 3.4. Reference [3] gives formulas for calculating K_p, T_i and T_d based on values for *L* and *T*. It should be noted, that a PID controller tuned by Ziegler-Nichols rules will have a response with 10%-60% maximum overshoot. However, by experimental tuning it is possible to adjust parameters of the controller such that it would exhibit desired responses. Therefore, Ziegler- Nichols tuning rules are very useful in order to find an initial point to start tuning of a PID controller.

The plant is described by the transfer function (3.4). Applying the method explained above, define the parameters of the S-shaped step response as: $L = 0.25$, $T = 2$, the following values of the controller parameters are obtained: $K_p = 9.6$, $T_i = 0.5$, $T_d = 0.125$. However, the simulation does not show the desired response to the pitch command. Having knowledge of how each parameter effects the response of the closed-loop system, by manual tuning it is possible to adjust the values of the

parameters of the PID controller such, that the response curve would have a desired shape. The following values of the parameters were obtained: $K_p = 3$, $T_i = 0.46$, $T_d = 0.073$.

Then the controller transfer function can be written as:

$$G_c = -3\left(1 + \frac{1}{0.46s} + 0.073s\right) = -\frac{0.22s^2 + 3s + 6.5}{s} \tag{3.6}$$

It should be noted, that tuning of the PID controller's coefficients is performed for the nominal plant, however presence of a sensor noise is also taken into account in simulation.

Phase and gain margins are illustrated in the Bode plot of the open-loop system in Figure 3.5.

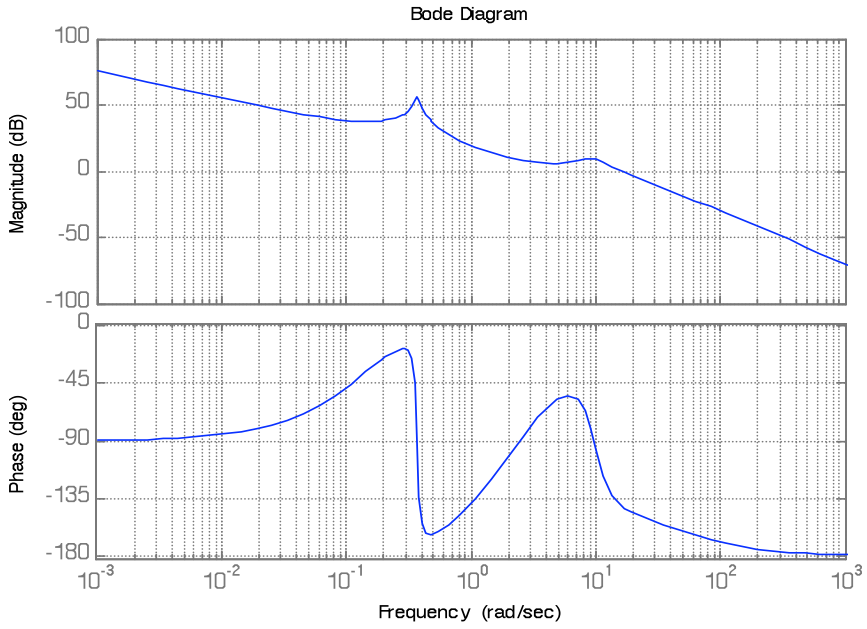

Figure 3.5 Bode Plot of the Open-Loop System

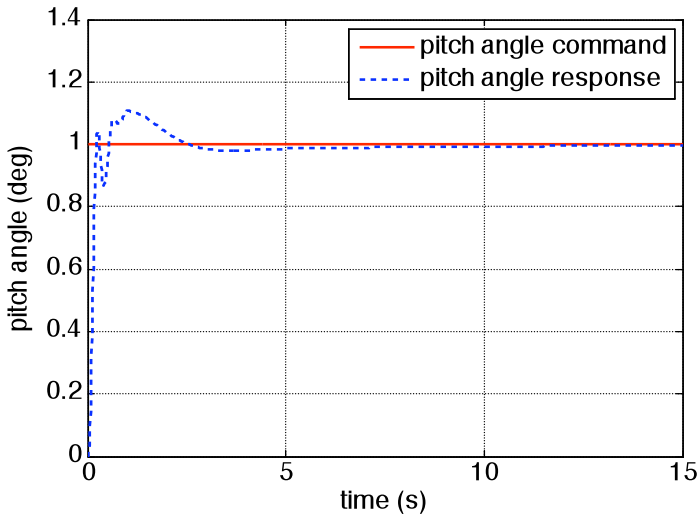

Figure 3.6 System Response to a Unit Step Input: Pitch Angle

Response of a closed-loop system to a unit step input is illustrated in Figure 3.6 and has the following characteristics:

- overshoot: 10%
- settling time: < 3 sec
- rise time: < 1 sec
- steady state error: < 0.2%.

Elevator deflection and deflection rate for a unit step input is shown in Figures 3.7, 3.8.

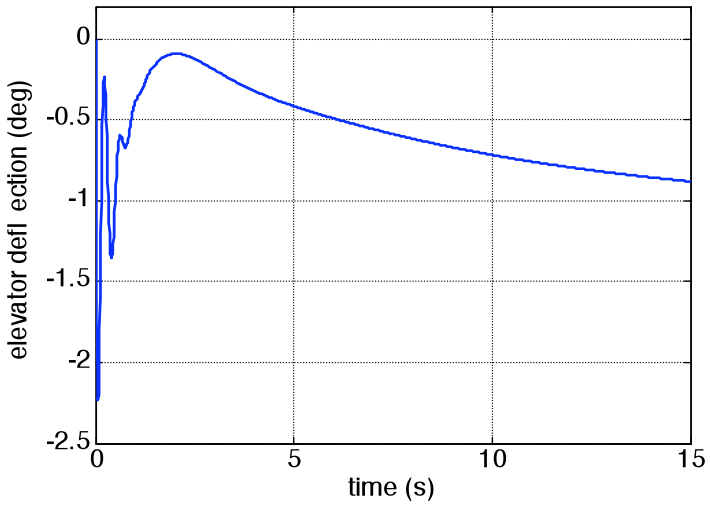

Figure 3.7 Elevator Deflection for a Unit Step Input

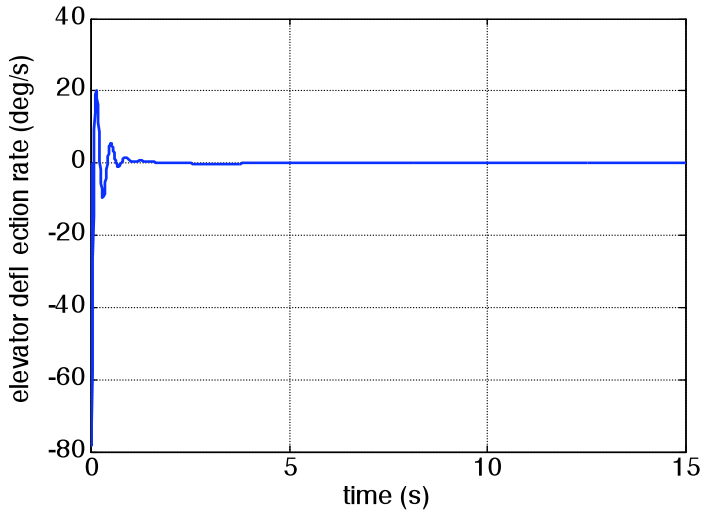

Figure 3.8 Elevator Deflection Rate for a Unit Step Input

From Figure 3.8 it is seen that the rate of elevator deflection is high at initial time of the input, which is not desired in the physical system. This problem is solved by using a command filter. Architecture of the command filter and its implementation are described in section 3.6.

3.5 Classical Controller Design for METU TUAV: Roll Autopilot

The basic function of the roll autopilot is to bring the airplane to a desired roll orientation. Ailerons are used as a control surfaces. Design of the PID controller and simulation is done using a linearized lateral dynamics of the METU TUAV. In Chapter 5 performance of the PID controller is given on the nonlinear model in comparison with nonlinear simulation of Robust controller.

3.5.1 Controller Configuration

Configuration of a controller, which is used for roll autopilot, is chosen to be similar to those used in pitch attitude control, as it is given in Figure 3.3.

Roll angle command is used as an input to the system. Similarly, to the pitch attitude controller, the error, which represents difference between the command roll angle ϕ_c and system response ϕ, is given to the input of a PID controller. Ailerons deflection signal is an output of the controller. Aircraft dynamics is represented by the lateral linearized dynamics of the METU TUAV and actuator model. Lateral linearized dynamics of the MTU TUAV is given as a transfer function from ailerons deflection to roll angle of the airplane:

$$W_{\phi/\delta a} = \frac{52.4s^3 + 42.1s^2 + 458.3s}{s^4 + 6.544s^3 + 13.36s^2 + 62.69s + 0.5783} \tag{3.7}$$

The transfer function of a PID controller is given by:

$$G_c = K_p\left(1 + \frac{1}{sT_i} + sT_d\right) \tag{3.8}$$

Controller parameters are subjected to be determined such that response of a closed-loop system would satisfy specified requirements.

3.5.2 Determining Controller Parameters and Controller Performance

The same method as it is described in section 3.4.2 is used to determine parameters of the PID controller used for roll autopilot. Consider the same S-shape of the desired step response as for the pitch controller. PID parameters, which correspond to this response are: $K_p = 9.6$, $T_i = 0.5$, $T_d = 0.125$. As simulation shows, the response of the closed-loop system is not satisfactory. Using these values as a start point, manual tuning is performed to make a step response's characteristics correspond to the desired ones; noise attenuation is taken into account while tuning. The following values of controller parameters are chosen: $K_p = 2.5$, $T_i = 1.66$, $T_d = 0.12$.

Transfer function of the PID controller:

$$G_c = 2.5\left(1 + \frac{1}{1.66s} + 0.12s\right) = \frac{0.3s^2 + 2.5s + 1.5}{s} \tag{3.9}$$

Figure 3.9 shows the Bode plot of the open-loop system, which provides information about phase and gain margins and stability of the closed loop system.

Response of a closed-loop system in terms of roll angle, position and rate of ailerons is illustrated in the Figures 3.10, 3.11, 3.12.

Response of the closed-loop system has characteristics listed below:

- overshoot: 7%
- settling time: < 3 sec
- rise time: < 1 sec
- no steady state error

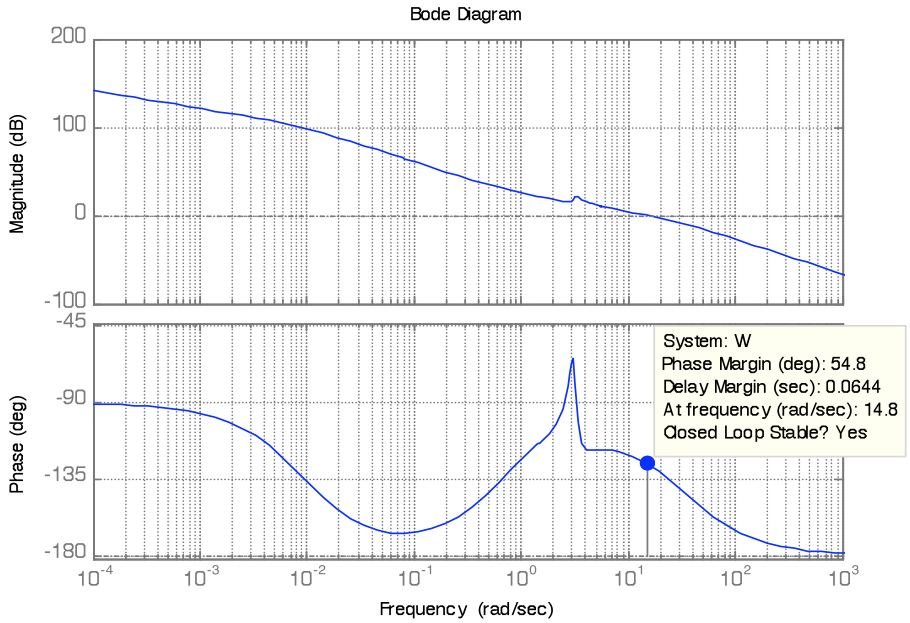

Figure 3.9 Bode Plot of the Open-Loop System

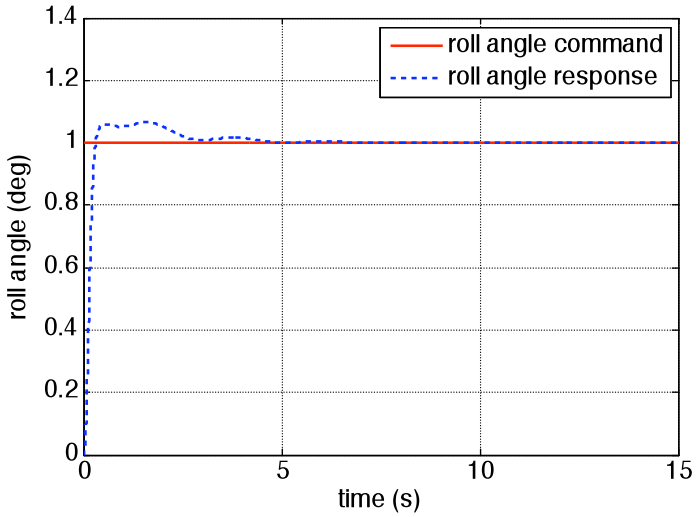

Figure 3.10 System Response to a Unit Step Input Roll Angle

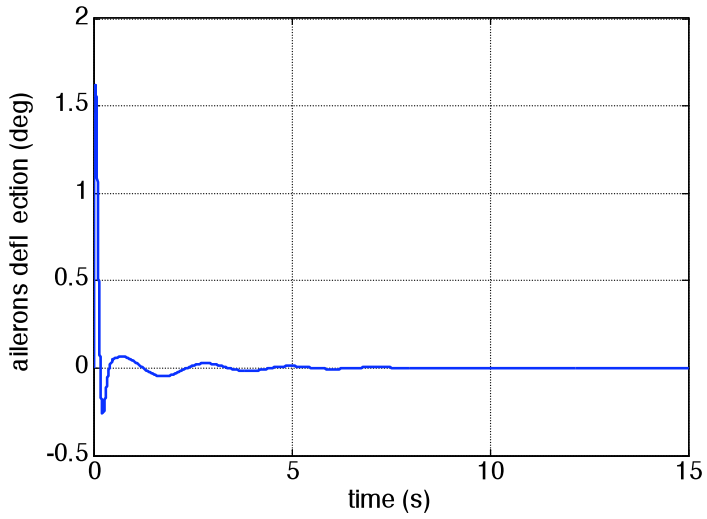

Figure 3.11 Ailerons Deflection for a Unit Step Input

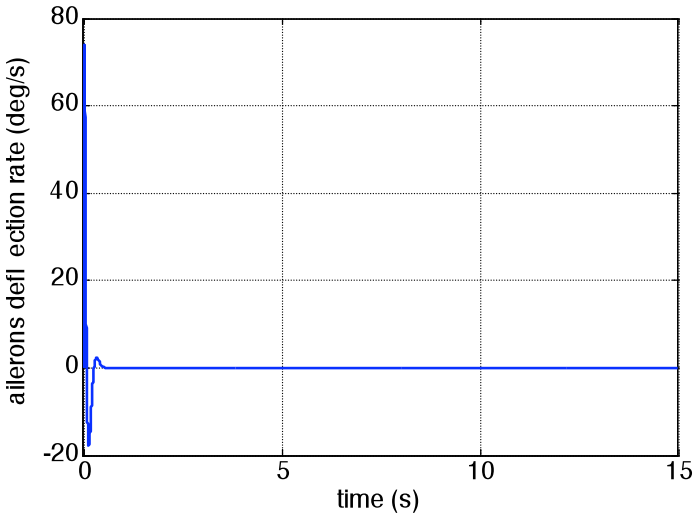

Figure 3.12 Ailerons Deflection Rate for a Unit Step Input

3.6 Command Filter Implementation for a Control System

3.6.1 Command Filter

Command filters are used in order to shape the command signal so its dynamics matches the dynamics of the vehicle. If the command input is a step function (for example pitch angle for a pitch attitude autopilot), this means that the rate of change of the input (pitch rate) will be infinite. This might cause saturation of control surfaces. The purpose of command filter is to smooth the input signal such an airplane would be able to follow it (see Figure 3.13).

Figure 3.13 Command Filter

Command filters are low-pass filters. For the purposes of this thesis, second order command filter is used. The transfer function for a second order low pass filter is

$$\frac{\omega_n^2}{s^2 + 2s\xi\omega_n + \omega_n^2} \tag{3.11}$$

Command filters are frequently used in control systems and are well described in literature. In [33] a time varying bandwidth (TVB) command shaping filter, which is

used to improve the tracking transient performance, is introduced. TVB filter limits the actuator deflection rate to achievable values. Reference [34] explaines the usage of a command filter in order to improve a system's step response: command filter removes high frequency components from a command input, therefore reducing the overshoot of the response. Command filter does not cause a destabilizing action upon a control system as it is located outside of the loop. [35] shows the way of using a pre-filter in order to eliminate the effect of the zero of a closed-loop transfer function on the step response. In reference [10] 2nd order command filter is employed to the autolanding control system designed for the METU TUAV.
Figure 3.14 gives a block diagram of a closed-loop control system with a command filter implemented.

3.6.2 Pitch Autopilot Performance with a Command Filter Implementation

Consider the block diagram of the control system as it is shown in Figure 3.14. Aircraft dynamics includes a state space representation of the linearized longitudinal dynamics of the UAV. Command input to a closed-loop system is given in Figure 3.15.

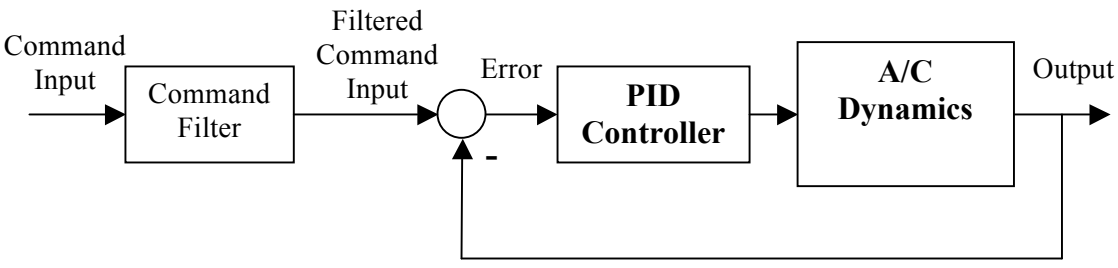

Figure 3.14 Basic Controller Configuration with Command Filter

Nominal command for angle of attack is shaped by passing through a command filter. Filtered command represents the desired change in pitch angle, which should be provided by a PID controller in a closed-loop configuration. Response of the closed-loop system that includes linear dynamics of the UAV to a given input is shown in Figure 3.16. Control surface deflection and its rate are presented in Figure 3.17 and Figure 3.18 respectively. From the plots above it is seen that implementing a command filter to the control system improves its response. Shaping the input command decreases the control surface efforts required to bring an airplane to a desired pitch attitude.

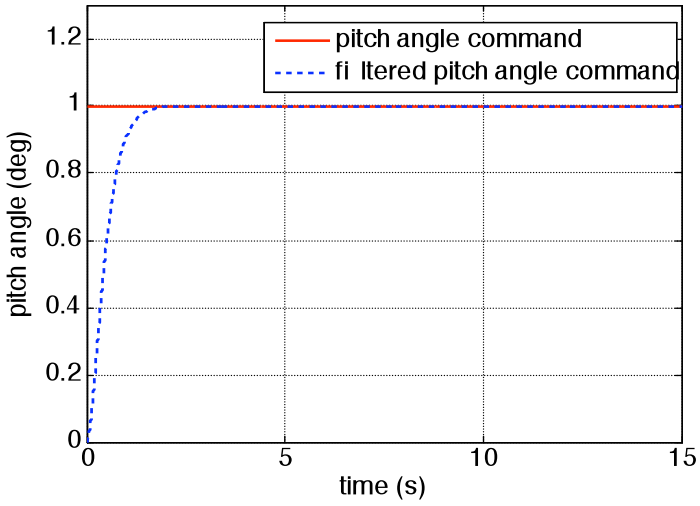

Figure 3.15 Pitch Angle Command: Nominal vs. Filtered

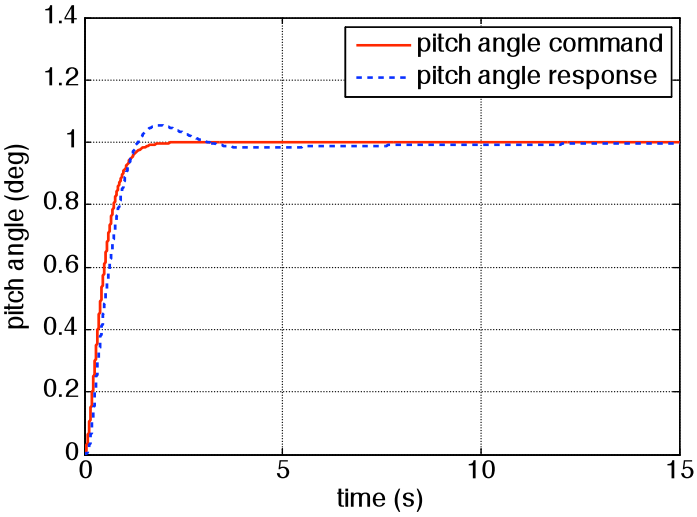

Figure 3.16 System Response to Pitch Angle Command

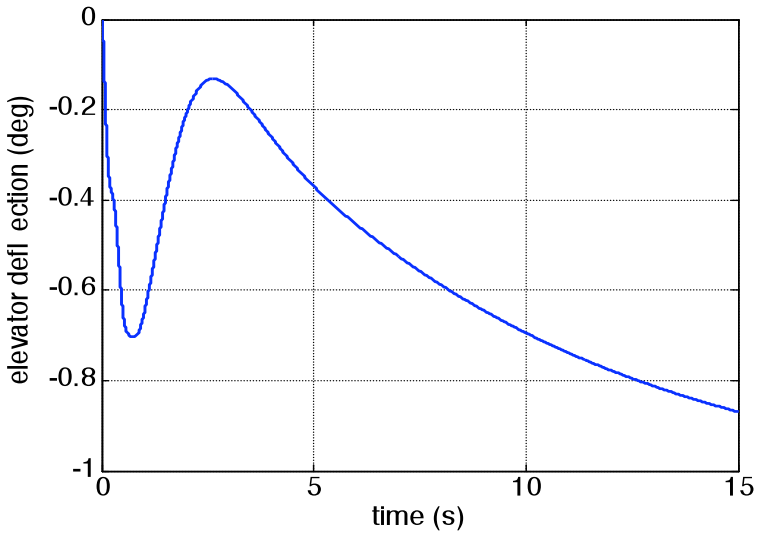

Figure 3.17 Elevator Deflection

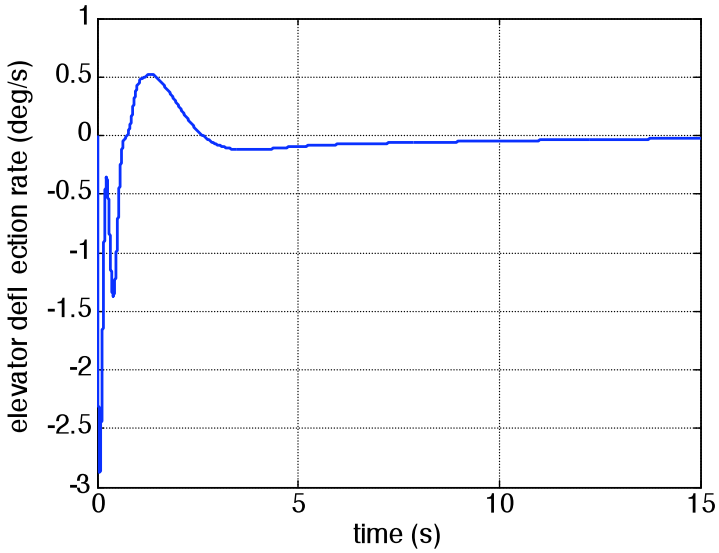

Figure 3.18 Elevator Deflection Rate

3.6.3 Roll Autopilot Performance with a Command Filter Implementation

Control system configuration is given in Figure 3.11. Aircraft dynamics consists of the state space model of the linearized lateral dynamics of the METU TUAV. In order to analyze performance of the roll autopilot with an implemented command filter, consider the roll angle input command as it is given in the Figure 3.19. Actual command to the control system is a filtered output of the command filter.

Performance of the PID controller, represented by a roll angle response, is given in Figure 3.20. Deflection of the control surfaces is shown in Figure 3.21. Figure 3.22 shows rate of the ailerons deflection.

From the simulation results, it is seen that adding a command filter to the control system sufficiently reduces angle of ailerons deflection and the rate of deflection making it correspond to the UAV's physical capabilities.

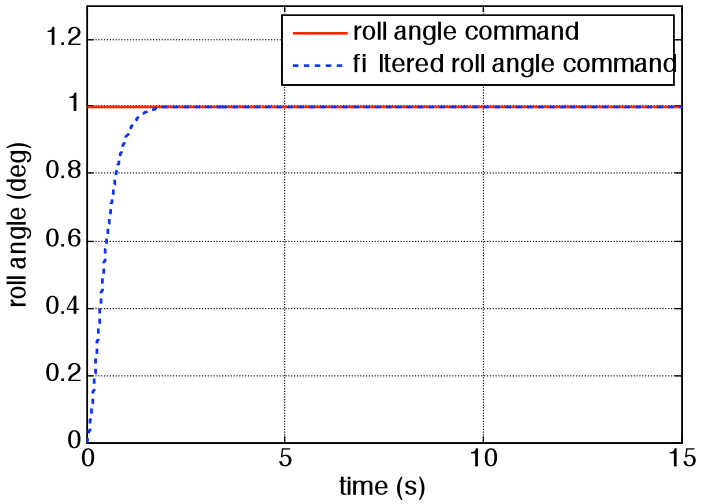

Figure 3.19 Roll Angle Command: Nominal vs. Filtered

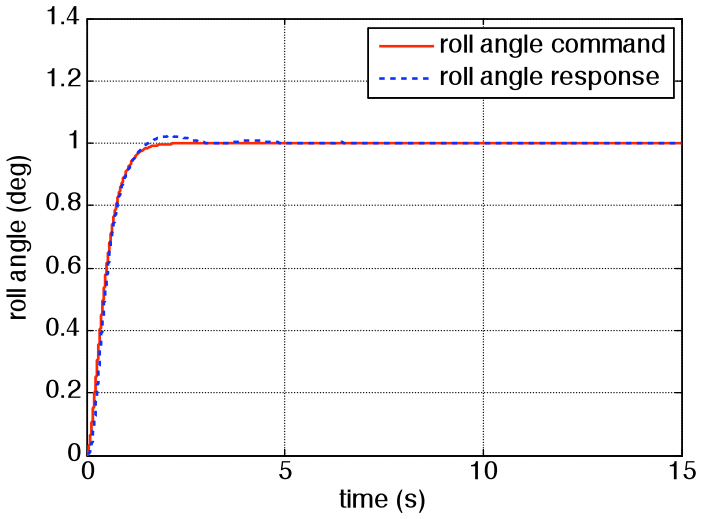

Figure 3.20 System Response to a Command Roll Angle

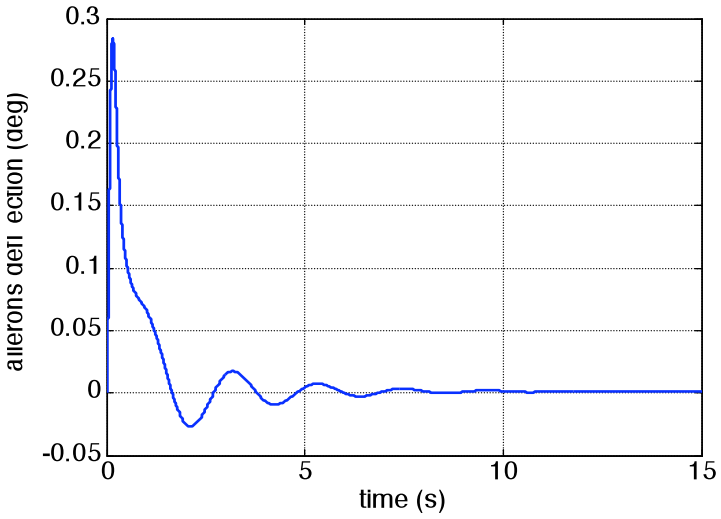

Figure 3.21 Ailerons Deflection

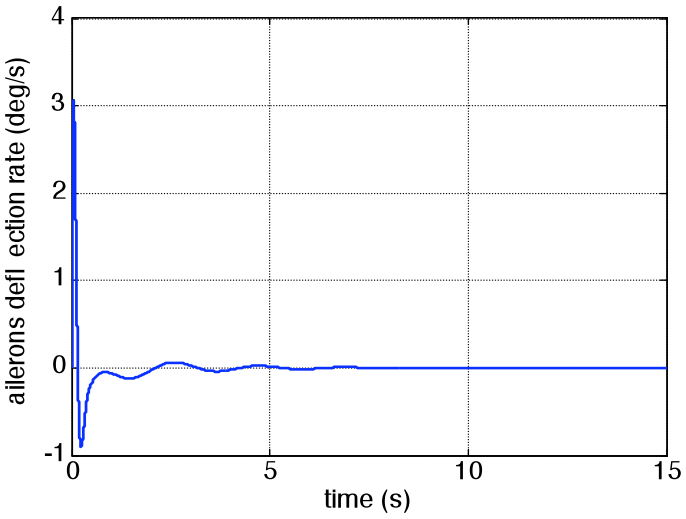

Figure 3.22 Ailerons Deflection Rate

CHAPTER 4

ROBUST CONTROLLER DESIGN

Robust control design focuses on the implications of model uncertainty. The controller should provide stability of the system in the face of uncertainties.

This chapter gives brief historical and theoretical backgrounds of the robust control theory. Techniques of robust control, such as H_∞ design and μ-analysis, are described.

4.1 Historical Review

Research in robust control theory has been one of the most active areas of modern control theory since the late 70s. The first important works were made by Zames [38] and Zames and Francis [39] in the late 1970s and early 1980s. Later this theory became known as H_∞ optimal control theory. The main idea was to find design techniques that would provide stability of a closed-loop system under the system uncertainties. Zames formulated three fundamental problems in robust control:

1) the uncertain disturbance attenuation problem, know as the standard H_∞ problem;

2) a plant and disturbance attenuation problem, known as the optimal robust disturbance attenuation problem;

3) and a filtering of plant uncertainty problem in which he posed the question of how much feedback can reduce uncertainty, when the plant lies in some set of uncertainty.

The works of Athans [40], Safanov [41], Grimble [42] and others show how uncertainty can be modelled and give the concept of the H_∞ norm and μ-synthesis theory. In 1987 B. A. Francis and John C. Doyle gave a modified solution to the general rational MIMO H_∞ optimal problem but suffered from the high order of the Riccati equations [43], [44]. State space methods for solving the H_∞ problem for MIMO systems were firstly introduced in [45]. The connection between H_∞ control problem and classical control was made in [46], in which H_∞ loop shaping design techniques were introduced. More detail and different perspectives can be found in the books by Zhou, Doyle, and Glover (see references [47] ,[48]).

4.2 Theoretical Background

This section introduces brief theoretical information about systems uncertainties, their modeling, stability and performance specifications, and robust controller design tools.

4.2.1 Problem Formulation

Consider a control system, block diagram of which is given in the Figure 4.1
In the Fig. 4.1 P is a generalized plant derived from the nominal plant but includes weighting functions. P is also assumed Finite Dimensional Linear Time Invariant (FDLTI) system; K is a controller; w is an external input signal, which includes the reference signal, disturbances and noise; u represents control signal; y is a signal that contains measured variables, and z represents the error signals. It is assumed that state space models of P and K are available and that their realizations are assumed stabilizable and detectable [47]. The goal of robust control design is to minimize the H_∞ norm of the transfer function from w to z under the constraint of internal stability. The definition of internal stability will be given in further section.

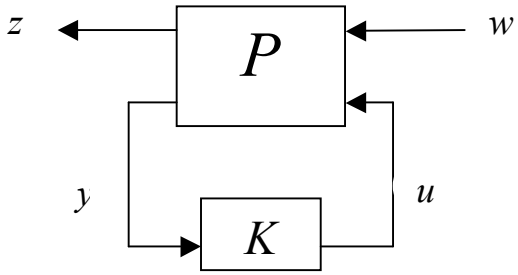

Figure 4.1 Block Diagram

4.2.2 Signals and Systems norms

Norms are used to characterize the size of signals or systems. The main purpose of system norms computation is to get proper measures to compare the performance of a control system, which can be based on the measure of the error signals, system gains, etc.

Consider the block diagram of an LTI system in the Figure 4.2.

Figure 4.2 Schematic Block Diagram of an LTI System

Following norms can be defined for scalar signals:

L_1 norm: $\|u\|_{L_1} = \int_0^\infty |u(t)|dt$ (4.1)

L_2 norm: $\|u\|_{L_2} = \left(\int_0^\infty |u(t)|^2 dt \right)^{1/2}$ (4.2)

L_p norm: $\|u\|_{L_p} = \left(\int_0^\infty |u(t)|^p dt \right)^{1/p}$ (4.3)

L_∞ norm: $\|u\|_\infty = \sup_{t \in [0;\infty]} |u(t)|$ (4.4)

Another important measure for signals is root mean square value (RMS). It reflects a signal's eventual average size:

$$\|u\|_{RMS} = \left(\lim_{T \to \infty} \frac{1}{T} \int_0^\infty |u(t)|^2 dt \right)^{1/2} \quad (4.5)$$

Norms of systems are usually determined in terms of norms of input and output signals (induced norms). For a stable SISO linear system the H_2 norm:

$$\|G\|_2 = \left(\frac{1}{2\pi} \int_0^\infty |G(j\omega)|^2 d\omega \right)^{1/2} \quad (4.6)$$

Physical interpretation of H_2 norm: H_2-norm of a transfer function measures the RMS response of its output when it is driven by a white noise input.

H_∞ norm of the system provides a measure of a worst-case system gain. H_∞ norm of a stable SISO system is defined as:

$$\|G\|_\infty = \sup_\omega |G(j\omega)| \quad (4.7)$$

H_∞ norm is a peak value in the Bode magnitude plot of the system. It provides a bound on the system gain.

For a MIMO system $G(s)$ is a rational $n \times m$ transfer function matrix $G(s) = [g_{kl}(s)]$. H_2 norm is defined as:

$$\|G\|_2 = \left(\sum_{kl} \|g_{kl}\|_2^2 \right)^{1/2} = \left(\frac{1}{2\pi} \int_{-\infty}^{\infty} \sum_{kl} |g_{kl}(j\omega)|^2 d\omega \right)^{1/2} = \left(\frac{1}{2\pi} \int_{-\infty}^{\infty} \sum_{kl} g_{kl}(-j\omega) g_{kl}(j\omega) d\omega \right)^{1/2}$$

$$= \left(\frac{1}{2\pi} \int_{-\infty}^{\infty} tr\left[G(-j\omega)^T G(j\omega) \right] d\omega \right)^{1/2}$$

H_∞ norm:

$$\|G\|_\infty = \sup_\omega \|G(j\omega)\| = \sup_\omega \bar{\sigma}(G(j\omega)) \tag{4.8}$$

where $\bar{\sigma}(G(j\omega))$ is the maximum singular value of the matrix $G(j\omega)$.

H_∞ norm of the system describes the maximum energy gain and is computed by the peak value of the largest singular value of the frequency response matrix over the whole frequency range [49].

4.2.3 Modeling Uncertainty

The term "uncertainty" means that the mathematical model of the plant differs from the actual physical model. It can be caused by few reasons: disturbance signals and dynamic perturbations. Disturbance signals usually include input and output disturbances (gust on the A/C), sensor noise, actuators noise. Dynamic perturbations include the differences between the mathematical model and the actual system: missing high frequency dynamics, system parameters errors or their variation in time, etc.

Taking into account the model uncertainty it is assumed that the dynamic behaviour of the plant is described by a set of possible LTI models π is a set of all perturbed plants. Consider the following notation for plant models:

$G(s) \in \pi$: nominal plant model with no uncertainties;

$G_p(s) \in \pi$: particular perturbed plant.

Assume that all the uncertainties (such as missing high frequency dynamics), that may occur in different parts of the system, are lumped into one block Δ, which is represented by any stable transfer function with H_∞ norm less than unity.

4.2.3.1 Additive Uncertainties

A block diagram that represents an additive uncertainty configuration is shown in Figure 4.3 below.

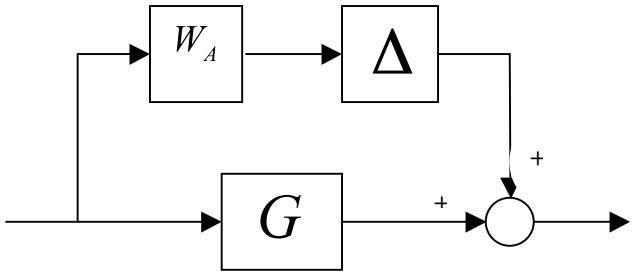

Figure 4.3 Additive Uncertainty Configuration

Perturbed plant is defined as:

$$G_p(s) = G(s) + \Delta W_A(s) \tag{4.9}$$

is a stable transfer function, which defines the magnitude of the uncertainty in all frequency range. Δ block represents a stable transfer function, which satisfies $\|\Delta\|_\infty \leq 1$.

4.2.3.2 Multiplicative Uncertainties

A block diagram that represents a multiplicative uncertainty configuration is given as in the Figure 4.4.

Perturbed plant with a multiplicative uncertainty can be defined as:

$$G_p(s) = G(s)\left[1 + \Delta W_m(s)\right] \tag{4.10}$$

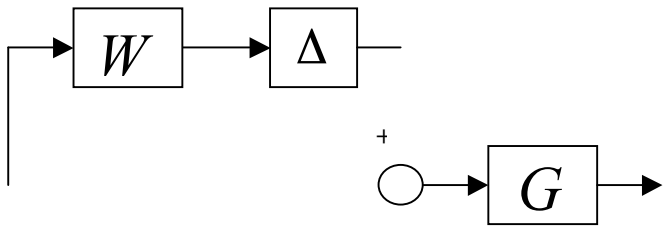

Figure 4.4 Multiplicative Uncertainty Configuration

As for an additive uncertainty, $W_m(s)$ for multiplicative uncertainty is a stable weighting transfer function, which defines the uncertainty magnitude at each frequency:

$$\left|W_m(j\omega)\right| > \max_{G_p \in \tau} \left| \frac{G_p(j\omega) - G(j\omega)}{G(j\omega)} \right| \tag{4.11}$$

Weighting function for a multiplicative uncertainty typically has the properties illustrated in Figure 4.5 (see reference [47]).

4.2.3.3 Parametric Uncertainties

For parametric representation of uncertainty it is assumed that the structure of the plant is known but some of the parameters are uncertain. Parameters of a physical system, which is modeled, determine the coefficients of the nominal plant $G(s)$. The

structure of the perturbed plant $G_p(s)$ is known: the whole set of possible perturbed plants have the same structure as the nominal plant $G(s)$, but some of the parameters are uncertain [21]. These uncertainties will affect the closed-loop system performance at low frequencies.

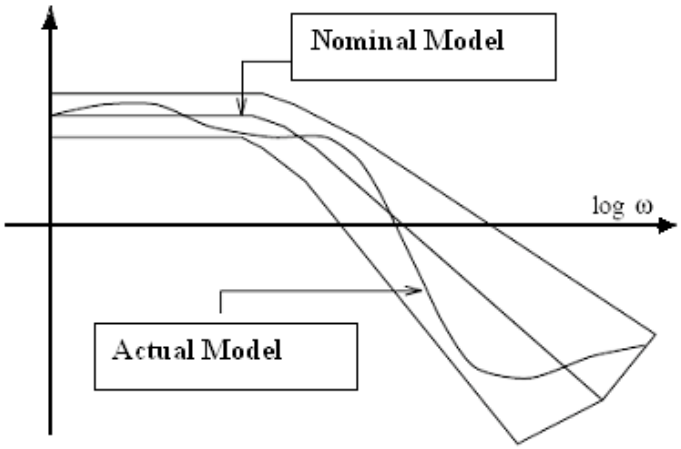

Figure 4.5 Typical Behavior of Multiplicative Uncertainty

4.2.4 Linear Fractional Transformations

Consider the general framework of a control problem as shown in Figure 4.6.

Suppose, that that plant $P = \left[\begin{array}{c|c} A & B \\ \hline C & D \end{array}\right]$ is partitioned as follows:

$$P(s) = \begin{bmatrix} P_{11}(s) & P_{12}(s) \\ P_{21}(s) & P_{22}(s) \end{bmatrix} \tag{4.12}$$

$$z = P_{11}w + P_{12}u$$
$$y = P_{21}w + P_{22}u \tag{4.13}$$

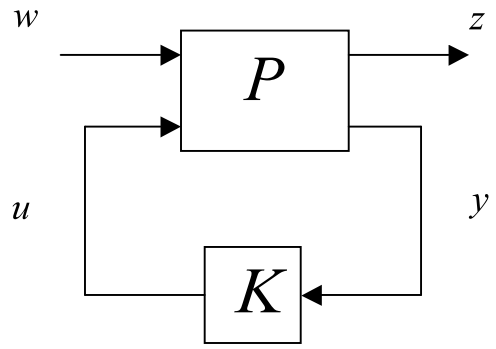

Figure 4.6 Lower Linear Fractional Transformation

Using $u = Ky$ it is possible to eliminate u and y:

$$y = (I - P_{22}K)^{-1}P_{21}w$$

$$z = [P_{11} + P_{12}(I - P_{22}K)^{-1}P_{21}]w \text{ , if } (I - P_{22}K) \text{ is invertible.}$$

When the inverse exists, then

$$F_l(P,K) = P_{11} + P_{12}(I - P_{22}K)^{-1}P_{21} \tag{4.14}$$

$F_l(P,K)$ is called a lower linear fractional transformation (LLFT), which is used to indicate the incorporation of a controller K into a system.

In a similar way, consider a $P - \Delta$ configuration shown in the Figure 4.7.

Upper linear fractional transformation of P and Δ can be defined as:

$$F_u(P,\Delta) = P_{22} + P_{21}(I - P_{11}K)^{-1}P_{12} \tag{4.15}$$

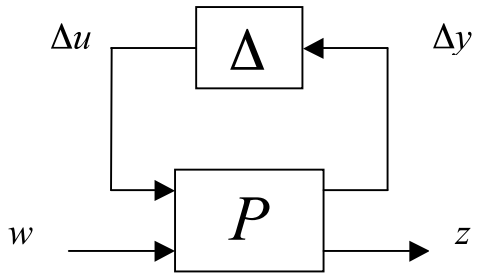

Figure 4.7 Upper Linear Fractional Transformation

4.2.5 Transfer Functions of a Closed Loop System

Consider the following feedback configuration as it is shown in Figure 4.8.

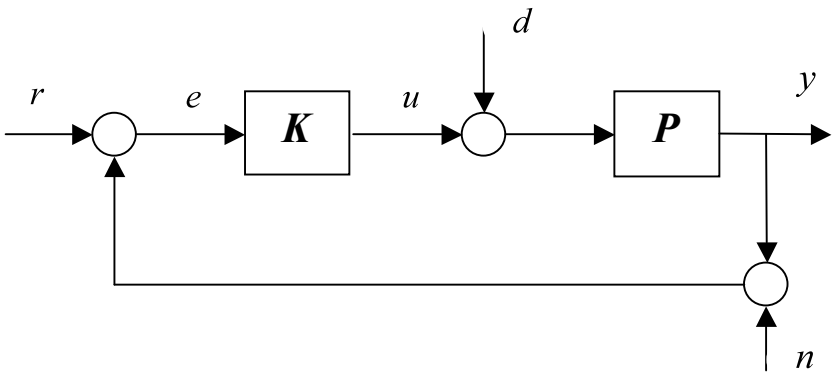

Figure 4.8 Feedback Configuration

P represents the plant to be controlled, K block represents a controller, r represents a reference command, e represents the error signal, u represents controller's output, d and n represents disturbances and noise, and y represents system's output.

Transfer function of a closed-loop system for a given feedback configuration is defined as:

$$y = P\left[K(r - y - n) + d\right]$$

By easy manipulations, it can be derived that

$$y = \underbrace{\left(I + PK\right)^{-1} PK}_{T} r + \underbrace{\left(I + PK\right)^{-1} P}_{S} d + \underbrace{\left(I + PK\right)^{-1} PK}_{T} n \tag{4.16}$$

S is so-called Sensitivity Function, T is a Complementary Sensitivity Function.

T is a transfer function from the reference command input to system's output, S is a transfer function from disturbances to the output. It should be emphasized that $S + T = 1$.

From the relation (4.16) above it is obvious, that for a good reference tracking ($y \approx r$) complementary sensitivity function should be as much closer to unity. For a good disturbance rejection sensitivity function S has to be zero. Noise rejection requires T being zero, which contradicts to $S + T = 1$. Therefore, it is impossible to have a good tracking and disturbance/noise rejection at the same time. However, this problem can be solved by frequency analysis of a reference signal and noise. Usually command inputs are signals with a low frequency and noise is assumed as a high frequency signal. Therefore, for a low frequency range T should be large for a good tracking and S small for disturbances attenuation. At high frequencies the main purpose is noise rejection, therefore T is small.

Using the definition of a complementary sensitivity function:

$$T = \left(I + PK\right)^{-1} PK = \left(I + L\right)^{-1} L \tag{4.17}$$

From relation (4.17) it is obvious that for a good tracking system gain has to be very large.

4.2.6 Stabilization and Performance Requirements (SISO Systems)

This section provides stabilization and performance requirements in robust design and introduces a 'small-gain theorem', which is of the great importance in H_∞ optimization techniques. The system to be considered is shown in the Figure 4.9.

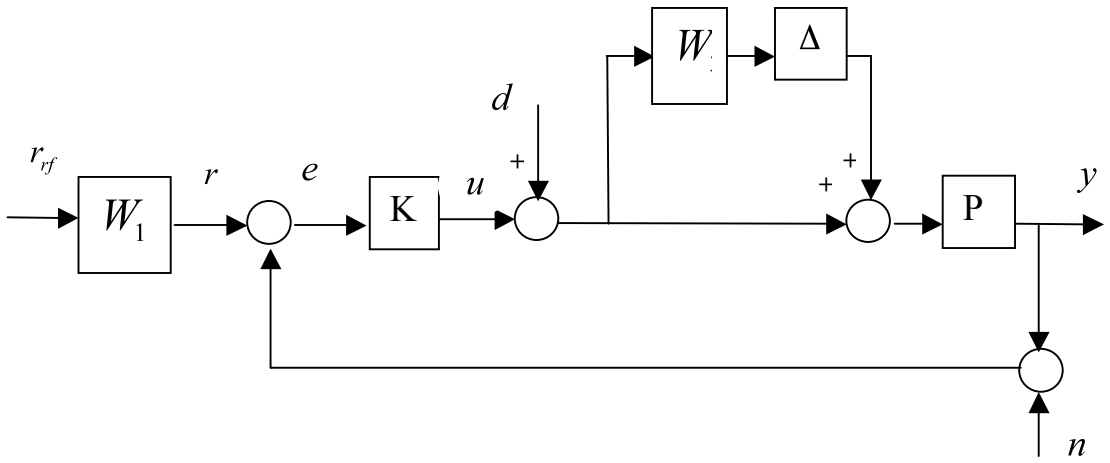

Figure 4.9 System Block Diagram

4.2.6.1 Nominal Stability (NS)

NS implies that the system is stable with no model uncertainty. An interconnected system is internally stable if the subsystems of all input-output pairs are asymptotically stable [12]. To guarantee NS of a system its closed-loop transfer function T should have all the poles in LHP and no unstable zero/pole cancellation. More detailed explanation of internal stability can be found in [48], [49].

4.2.6.2 Nominal Performance (NP)

NP means that the system satisfies the performance specifications with no model uncertainty. NP implies that the norm of a transfer function from disturbances to error must be small. For H_∞ norm notation:

$$\|W_1 S\|_\infty < 1 \tag{4.18}$$

where W_1 is any stable transfer function which defines the magnitude of uncertainty. S is a transfer function from disturbances to errors.

4.2.6.3 Robust Stability (RS)

The definition of RS is the following: the system is stable for all perturbed plants about the nominal model up to the worst case of uncertainty. So if the controller K internally stabilizes each of the perturbed plant including the nominal, robust stability is guaranteed.

If the H_∞ norm is used, condition for robust stability is the following:

$$\|W_2 T\|_\infty < 1,\ \forall \|\Delta\|_\infty < 1 \tag{4.19}$$

Small gain theorem is the basis for derivation of a robust stability test. Consider the block diagram from the Figure 4.9 in a modified form. By isolating the Δ block and re-drawing the feedback connection, the block diagram of a feedback configuration is obtained as shown in Figure 4.10.

Theorem: if M and Δ are stable linear systems, the closed-loop system is internally stable if and only if $\|M\Delta\|_\infty < 1$ for all ω.

Consider the transfer function from disturbances to errors: $TF_{d\to e} = M = \dfrac{W_2 PK}{1+PK} = W_2 T$.

Applying Nyquist stability criteria: $M\Delta$ should not encircle the -1 point on a complex plane for all Δ:

$|1 + M\Delta| > 0, \quad \forall\omega, \quad \forall|\Delta| \le 1.$

The worst case for the condition above is when $\Delta = -1$. Then the condition for RS can be written in the form: $|M(j\omega)| < 1$.

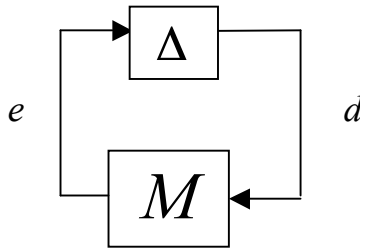

Figure 4.10 $M - \Delta$ Structure

In terms of H_∞ norm: if $\|\Delta\|_\infty \le \gamma$ (γ is a small positive number) the condition for RS is:

$$\|M\|_\infty = \|W_2 T\|_\infty \le \frac{1}{\gamma} \tag{4.20}$$

4.2.6.4 Robust Performance (RP)

RP implies that the performance specifications are satisfied for every perturbed plant about the nominal model up to the worst case uncertainty. In other words RR requires the NP condition to be satisfied for all possible perturbed plants.

For internally stable nominal feedback system NP condition is $\|W_2T\|_\infty < 1$. Considering the case with multiplicative uncertainty. The perturbed plant $P_p = (1 + \Delta W_2)P$, then S is perturbed to $\frac{1}{1 + (1 + \Delta W_2)L} = \frac{S}{1 + \Delta W_2 T}$.

The RP condition becomes

$$\|W_2T\|_\infty < 1 \text{ and } \left\| \frac{W_1 S}{1 + \Delta W_2 T} \right\|_\infty < 1, \ \forall \Delta, \ \|\Delta\|_\infty < 1.$$

The theorem below gives a test for a RP:

"A necessary and sufficient condition for robust performance is

$$\| |W_1 S| + |W_2 T| \|_\infty < 1" \tag{4.21}$$

Proof of (4.21) can be found in [50].

4.2.7 Stabilization and Performance Requirements (MIMO Systems)

Similar approach as for SISO systems is used for MIMO case. Conception of LFT is used to derive stability and performance requirements for MIMO system.

For a general case hence both uncertainties and disturbances act upon the system the following configuration as shown in Figure 4.11 is considered.

In the Figure 4.11, plant P and controller K are combined into block M, which represents the lower linear fractional transformation: $M = F_l(P, K)$.

The transfer function from disturbances to errors: $e(s) = F_u(M, \Delta)d(s)$.

$F_u(M, \Delta)$ represents the upper linear fractional transformation of M with Δ:

$$F_u(M, \Delta) = M_{22} + M_{21}\Delta(I - M_{11}\Delta)^{-1} M_{12} \tag{4.22}$$

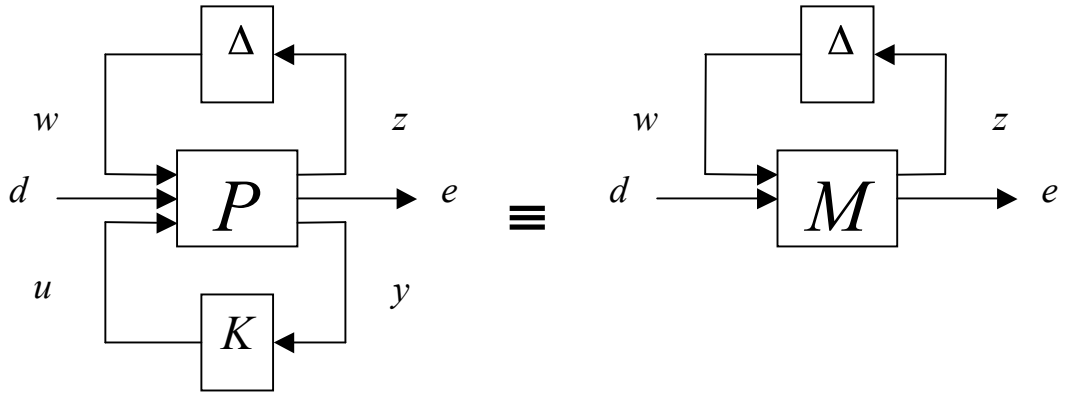

Figure 4.11 Plant Controller Configuration Set Up

4.2.7.1 Nominal Stability (NS)

Condition for NS for a MMO system comes from the criterion for SISO system. Transfer functions from all inputs to all outputs must satisfy NS conditions for SISO case.

4.2.7.2 Nominal Performance (NP)

NP requires minimization of a transfer function from disturbances to errors with no system uncertainties. Therefore, from relation (4.22) in terms of H_∞ norm condition for NP is:

$$\left\| M_{22} \right\|_\infty < 1 \tag{4.23}$$

4.2.7.3 Robust Stability (RS)

A criterion for RS is derived using the small gain theorem: if $\|\Delta\|_\infty \le \gamma$ then

$$\|M_{11}\|_\infty < 1/\gamma \tag{4.24}$$

(4.24) gives a condition for RS in terms of H_∞ norm.

4.2.7.4 Robust Performance (RP)

RP requires that the $TF_{d\to e}$ must be small even in the presence of Δ. Minimizing of the norm:

$$\min_{K(s)} \max_{\Delta} \|F_u(F_l(P,K)\Delta)\|_\infty$$

if $\|F_u(F_l(P,K)\Delta)\|_\infty = \|F_u(M,\Delta)\|_\infty < 1$ for all Δ with $\|\Delta\|_\infty < 1$, then the closed-loop system satisfies RP criterion.

Using the small gain theorem, the "sufficient condition" for RP is to have

$$\|M\|_\infty < 1 \tag{4.25}$$

4.3 H_∞ Design

The main aim of robust design is to find a controller for the system, such that the closed-loop system is robust.

Optimal H_∞ control problem statement is the following: "find all the admissible controllers $K(s)$ such that $\|T_{zw}\|_\infty$ is minimized". However, for MIMO systems, the procedure of finding the optimal H_∞ controller is very complicated andthere is no closed form solution. Therefore, instead of the problem statement given above, another definition of H_∞ control problem is used: "Given $\gamma > 0$, find all admissible controllers $K(s)$, if there is any, such that $\|T_{zw}\|_\infty < \gamma$". This problem is called suboptimal H_∞ control problem.

Consider the system block diagram of which is shown in Fig. 4-1, where controller *K* and plant *G* are assumed real rational and proper.

Consider the following realization of the transfer function matrix:

$$\begin{bmatrix} z \\ y \end{bmatrix} = G(s)\begin{bmatrix} w \\ u \end{bmatrix} = \begin{bmatrix} G_{11}(s) & G_{12}(s) \\ G_{21}(s) & G_{22}(s) \end{bmatrix}\begin{bmatrix} w \\ u \end{bmatrix} \tag{4.26}$$

$$u(s) = K(s)y(s)$$

$$G = \left[\begin{array}{c|cc} A & B_1 & B_2 \\ \hline C_1 & D_{11} & D_{12} \\ C_2 & D_{21} & D_{122} \end{array}\right] \tag{4.27}$$

According to (4.26) system equations can be written in the form:

$$\begin{aligned} \dot{x} &= Ax + B_1 w + B_2 u \\ z &= C_1 x + D_{12} u \\ y &= C_2 x + D_{21} w \end{aligned} \tag{4.28}$$

Theorem above gives necessary and sufficient conditions for existence of a controller $K(s)$.

According to the theorem, if three conditions are satisfied there exist a controller such that $\|T_{zw}\|_\infty < \gamma$.

The required conditions are:

i) there exists $X_\infty > 0$ - a solution to ARE

$$X_\infty A + A^* X_\infty + X_\infty (\frac{1}{\gamma^2} B_1 B_1^* - B_2 B_2^*) X_\infty + C_1^* C_1 = 0 \tag{4.29}$$

ii) there exists $Y_\infty > 0$ - a solution to ARE

$$AY_\infty + Y_\infty A^* + Y_\infty (\frac{1}{\gamma^2} C_1^* C_1 - C_2^* C_2) Y_\infty + B_1 B_1^* = 0 \tag{4.30}$$

iii) $\rho(X_\infty, Y_\infty) < \gamma^2$ (4.31)

When these conditions are satisfied, the controller is given by:

$$K(s) = \left[\begin{array}{c|c} A_\infty & -Z_\infty L_\infty \\ \hline F_\infty & 0 \end{array}\right] \tag{4.32}$$

where

$$A_\infty = A + \frac{1}{\gamma^2} B_1 B_1^* X_\infty + B_2 F_\infty + Z_\infty L_\infty C_2;$$

$$F_\infty = -B_2^* X_\infty;$$

$$L_\infty = -Y_\infty C_2^*;$$

The following assumptions should be made for the derivation of the results of the theorem:

1) (A, B_2) is stabilizable

2) (A, C_2) is detectable

3) $D_{12}^*[C_1 \quad D_{12}] = [0 \quad I]$

4) $\begin{bmatrix} B_1 \\ D_{21} \end{bmatrix} D_{21}^* = \begin{bmatrix} 0 \\ I \end{bmatrix}$.

More detailed description of the solution of H_∞ problem for a general case can be found in [45], another approach for H_∞ solution derivation is present in [51].

4.4 μ Analysis

4.4.1 Definition and Properties of Structured Singular Value (μ)

Consider the block diagram as it is shown in the Figure 4.12. The uncertainty block in the $M - \Delta$ structure connection usually has a block diagonal structure:
$\Delta = diag\{\Delta_i\}$.

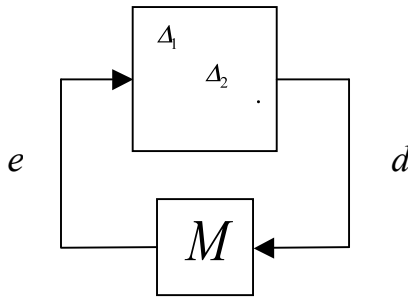

Figure 4.12 Standard $M-\Delta$ configuration with diagonal structure of Δ

The sufficient condition for RS, as defined previously, is:

$\bar{\sigma}(M(i\omega)) < 1,\ \forall\omega$.

Define a scaling matrix as

$$D = diag\{d_i I_i\} \tag{4.33}$$

where d_i is a scalar and I_i is an identity matrix, which has the same dimension as the i^{th} uncertainty Δ_i.

Modified $M-\Delta$ structure is shown in the Figure 4.13.

Including scaling matrix D to the $M-\Delta$ structure does not change the overall system, its stability properties remain the same.

Then condition for RS can be written in the form:

if

$$\bar{\sigma}(DMD^{-1}) < 1,\ \forall\omega \tag{4.34}$$

then closed-loop system is robustly stable.

Less conservative condition for RS can be obtained by minimizing at each frequency the scaled singular value:

$$\min_{D(j\omega)\in\boldsymbol{D}} \bar{\sigma}(D(j\omega)M(j\omega)D^{-1}(j\omega)) < 1,\ \forall\omega \tag{4.35}$$

where D is a set of block-diagonal matrices compatible with Δ:

$$\bar{\sigma}(DMD^{-1}) = \bar{\sigma}(M) \tag{4.36}$$

The Structured Singular Value (SSV) , μ, was first suggested by Doyle in 1982 as a way of analyzing systems with uncertainties. The SSV is defined as follows

$$\mu_{\Delta}(M) \equiv \frac{1}{\min\{\bar{\sigma}(\Delta) : \Delta \in \boldsymbol{\Delta}, \det(1 - M\Delta) = 0\}} \tag{4.37}$$

If there is no $\Delta \in \boldsymbol{\Delta}$ that makes $(1 - M\Delta)$ singular, $\mu_{\Delta}(M)$ is defined as zero.

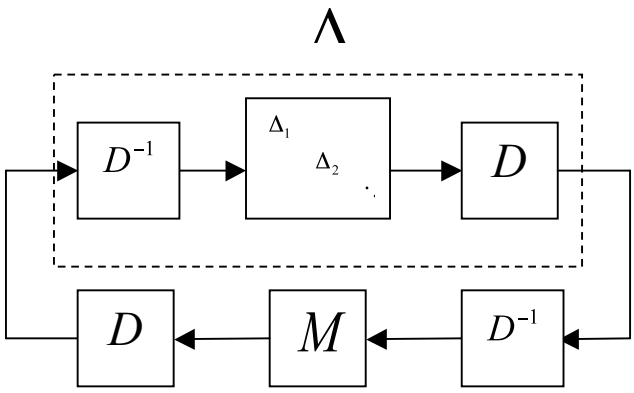

Figure 4.13 Modified $M - \Delta$ Structure

SSV is a function, which provides a generalization of the largest singular value $\bar{\sigma}$. It should be noted, that $\mu_{\Delta}(M)$ depends on both M and structure of Δ.

Computation of a SSV is very difficult procedure; therefore, upper and lower bounds on μ are used:

$$\rho(M) \le \mu_{\Delta}(M) \le \bar{\sigma}(M) \tag{4.38}$$

Still, the gap between spectral radius ρ and largest singular value $\bar{\sigma}$ may be arbitrary large, that is not acceptable. For this reason, it is necessary to define the bounds by scaling in a way that will not affect $\mu_{\Delta}(M)$ but will affect ρ and $\bar{\sigma}$. In particular, the bounds maybe tightened in a following way:

Define two subsets in $\mathbb{C}^{n\times n}$:

$$\boldsymbol{U} = \{U \in \boldsymbol{\Delta} : UU^{*} = I_n\} \tag{4.39}$$

$$\boldsymbol{D} = \left\{ \begin{array}{c} diag[D_1,\ldots,D_s,d_1 I_{m1},\ldots,d_{F-1} I_{mF-1}, I_{mF}]: \\ D_i \in \mathbb{C}^{r_i \times r_i}, D_i = D_i^{*} > 0, d_j \in \mathbb{R}, d_j > 0 \end{array} \right\} \tag{4.40}$$

Then the upper and lower bounds from (4.37) can be tightened to

$$\max_{\boldsymbol{U}\in U} \rho(UM) \le \mu_{\Delta}(M) \le \inf_{\boldsymbol{D}\in D} \bar{\sigma}(DMD^{-1}) \tag{4.41}$$

More detailed information about the SSV and its bounds can be found in [48], [52].

4.4.2 Robust Stability Condition

Consider M and Δ are stable linear systems. Then the closed-loop system $M-\Delta$ is stable for all allowed uncertainties with $\bar{\sigma}(\Delta) < 1$ if and only if

$$\mu_{\Delta}(M(j\omega)) < 1, \ \forall \omega \tag{4.42}$$

4.4.3 Robust Performance Condition

Consider a generalized plant P as it is shown by block diagram in the Figure 4.14

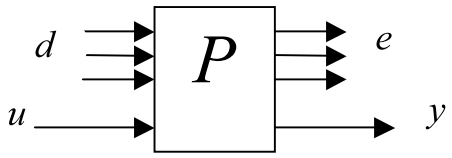

Figure 4.14 Generalized Plant

Let M be the plant after controller has been connected (see Figure 4.15)

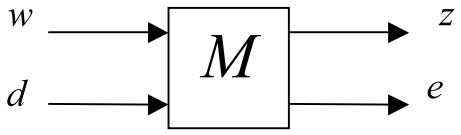

Figure 4.15 Generalized Plant with Controller

Channel $w-z$ is related to uncertainty, channel $d-e$ is related to performance. Both of them should be minimized.

The set of uncertain plants is given as it is shown in the Figure 4.16

Assuming that uncertainties block has a diagonal structure condition for robust performance can be turned into condition for robust stability by adding a fictitious performance block Δ_p (Figure 4.17):

Denote the modified uncertainties block as

$$\tilde{\Delta} = \begin{bmatrix} \Delta_p & 0 \\ 0 & \Delta \end{bmatrix} \tag{4.43}$$

The condition for RP can be written as follows:

$$\mu_{\tilde{\Delta}}(M) < 1, \quad \forall \omega \tag{4.44}$$

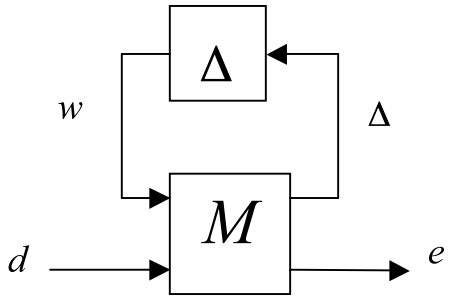

Figure 4.16 Uncertain Plant

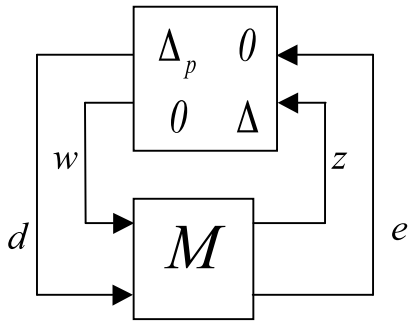

Figure 4.17 Uncertain Plant with Δ_p block

4.5 Robust Controller Design for METU TUAV

The task is to design a pitch and roll displacement autopilots that will bring the airplane to a desired pitch and roll orientations. The control inputs to the system are elevator deflection for a pitch controller, and ailerons deflection for a roll controller.
Design of the robust controller involves the solutions of Algebraic Riccati Equations (ARE) as it had been described in section 4.3. Therefore, design of controllers for METU TUAV is performed using MATLAB Robust Control Toolbox. The toolbox enables to compute a stabilizing H_∞ controller K for a given plant P. For design purposes plant P should be partitioned in terms of the number of the disturbances, the control inputs, errors, and the output measurements provided to the controller. Partitioning of the plant and system interconnection is also performed with MATLAB tools. Next step is to describe the uncertainties and selection of proper weight functions, which would represent the uncertainties and performance characteristics. The command "`hinfsyn`" solves the problem of robust controller synthesis using the procedure given in section 4.3.
Design and simulation of the robust controller for pitch and roll autopilots is performed using the linearized dynamics of the METU TUAV. Simulation through the nonlinear environment is presented in Chapter 5, which gives the comparative analysis of classical and robust controllers' performances.

4.5.1. Choice of Weight Functions for Robust Controller

Consider the the block diagram of a closed-loop system as it is shown in Figure 4.18. It is composed of weight function W_m for multiplicative uncertainty of the actual model, weight function W_p for performance of the controller, W_n for sensor noise, a nominal model G, model error Δ and controller K. It is assumed that the error Δ is

not known, except that it satisfies the condition $\|\Delta\|_\infty < 1$. For H_∞ - synthesis control system from Figure 4.18 can be expressed to a general plant shown in Figure 4.1. Remind that the generalized plant *P* contains what is usually called the plant in a control problem plus all weighting functions. The signal *w* contains all external inputs, including disturbances, sensor noise, and commands, the output *z* is an error signal, *y* is the measured variables, and *u* is the control input. The desired controller *K* satisfies the nominal performance and robust performance.

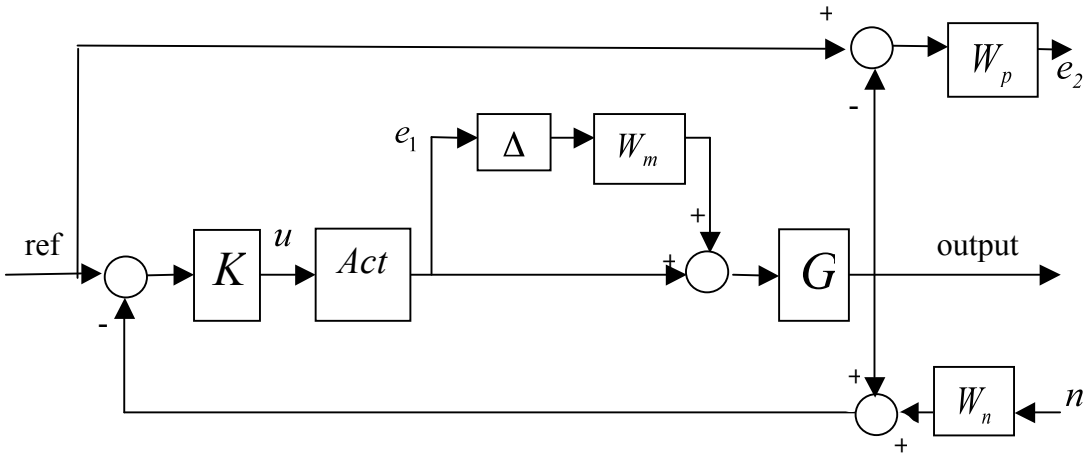

Figure 4.18 Block Diagram of Closed-loop System

First it is necessary to determine weight functions W_m and W_p in order to design the controller *K*. It is known, high suppression ratio to the disturbance is required only in the low-frequency range since only the low-order modes are strongly excited. On the other hand, the error of the nominal system model is small in the low-frequency range, but it can be large in the high-order modes since the high-order modes are

neglected. Weighting transfer function W_m represents the multiplicative uncertainty, it must be chosen such that the effect of the uncertainties of system's parameters will be represented in the best way. For the purposes of this work it is assumed that main source of multiplicative uncertainty is in change of the parameters of the system. It can be found from the Bode plots of the perturbed plants such that the Bode plot of W_m 'covers' the Bode magnitude plots of all the plants with different combinations of uncertainties. Weighting transfer function W_p must be chosen such that the norm $\left\|W_p S\right\|_\infty < 1$, where S is the sensitivity function of the system. Having some knowledge about the frequency characteristics of the Sensitivity function, weighting transfer function W_p is chosen as a low-pass filter.

4.5.2 Robust Controller Design for Pitch Attitude Autopilot

Block diagram of the closed-loop system is shown in Figure 4.18. Plant G represents a transfer function from the system's input (elevator deflection) to the system's output (pitch angle) obtained from the linearized longitudinal dynamics of the METU TUAV:

$$W_{\theta/\delta e} = -\frac{48.7s^2 + 105.3s + 12.5}{s^4 + 5.4919s^3 + 97.428s^2 + 3.5150s + 13.3973} \tag{4.45}$$

Reference input is a pitch input command to the system. System's output is a measured pitch angle.

As it was mentioned above, weighting function W_m reflects system's multiplicative uncertainty. Consider the variation in system's aerodynamics. For longitudinal motion the most important aerodynamic derivatives that effect stability are static longitudinal stability derivative C_{m_α} and pitch-damping derivative C_{m_q}. Therefore, in order to determine a weighting function W_m variations in C_{m_α} and C_{m_q} are considered. 1% and 5% of uncertainty with respect to the nominal value of the

parameter is assumed. (4.11) gives an expression for weighting function that characterizes multiplicative uncertainty. The Bode plot of $\frac{G_p(j\omega)-G(j\omega)}{G(j\omega)}$ is shown in Figure 4.19.

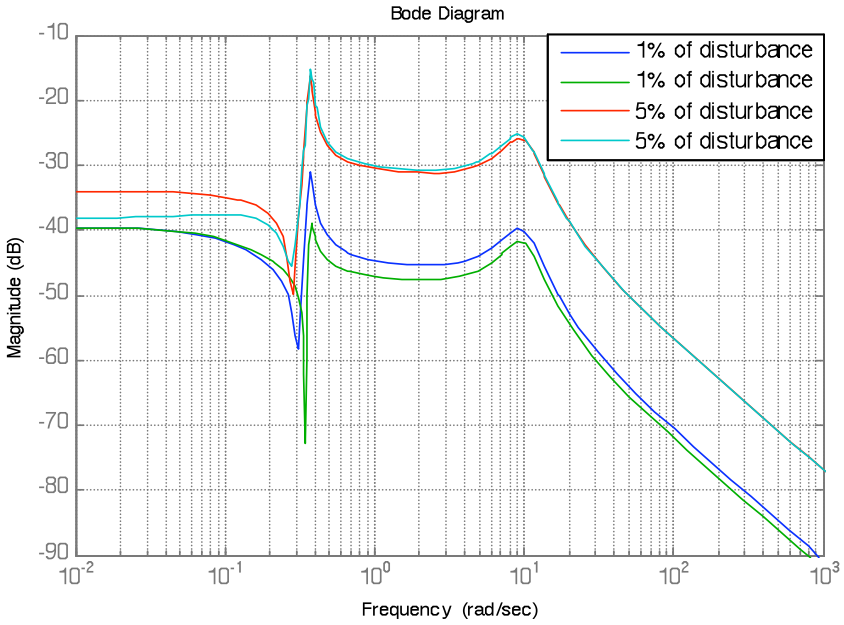

Figure 4.19 Bode Plot of Uncertain Plants

According to this plot, W_m had been chosen as

$$W_m = \frac{0.18s + 0.005}{s + 0.15} \tag{4.46}$$

Its Bode plot is given in Figure 4.20.

W_p is chosen such that it would reflect frequency characteristics of the input signal and satisfies the condition $\left\|W_p S\right\|_\infty < 1$. W_p had been obtained as:

$$W_p = \frac{6}{2.5s + 0.1} \tag{4.47}$$

Its frequency characteristics are shown in a Bode plot in Figure 4.21.

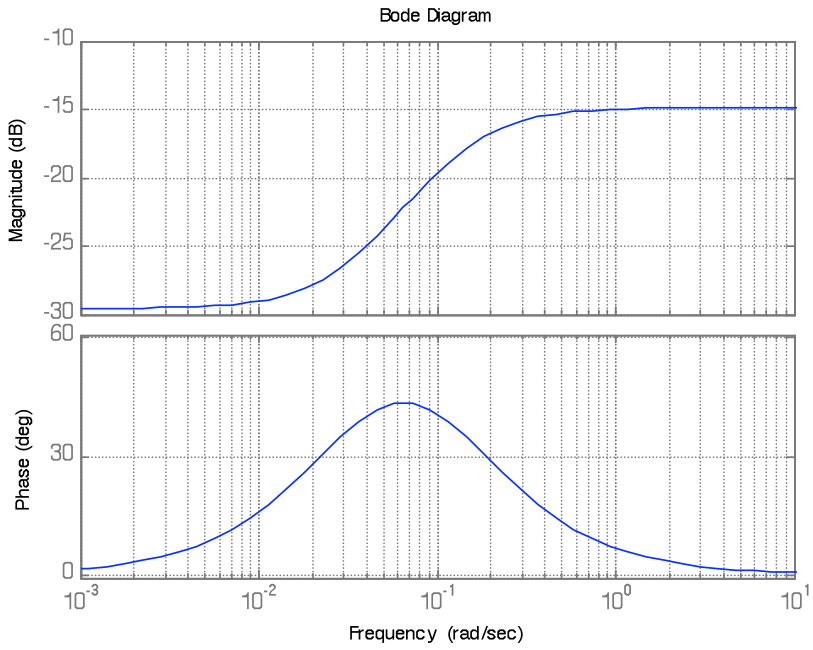

Figure 4.20 Bode Plot of W_m

Weighting function W_n represents effect of the sensor noise on the system's output. Assume 0.1% noise at low frequencies and 1% noise at high frequencies. Transfer function of W_n is obtained as:

$$W_n = 0.01\frac{0.01s+1}{0.001s+1} \tag{4.48}$$

Frequency characteristics of the weighting function W_n are given in Figure 4.22.

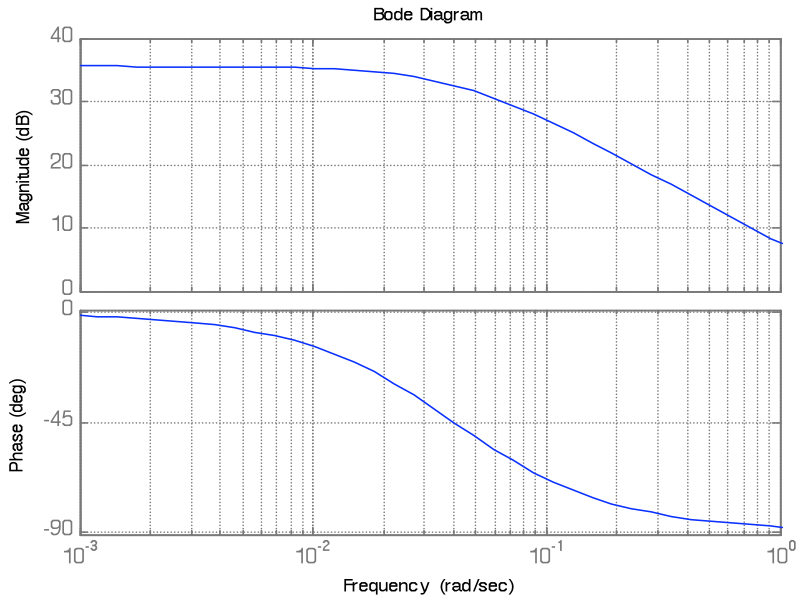

Figure 4.21 Bode plot of W_p

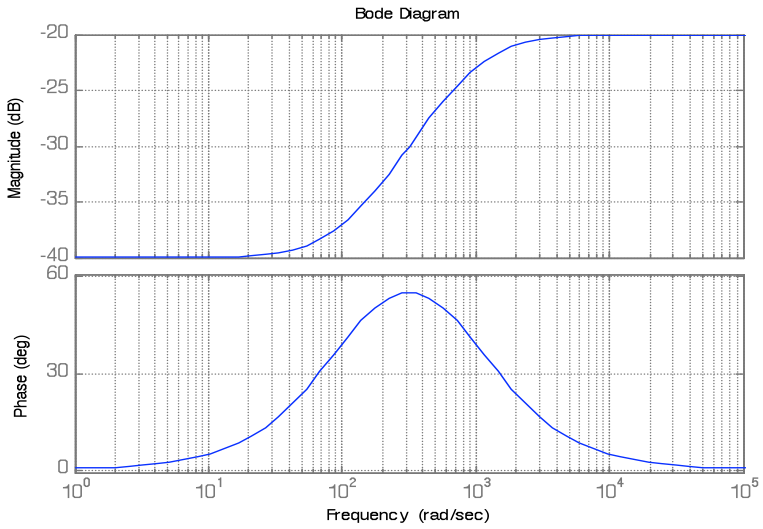

Figure 4.22 Bode Plot of W_n

4.5.2.1 Performance of the Robust Controller for Pitch Attitude Autopilot

Robust controller is designed using MATLAB "hinf" command, which computes the H_∞ controller. As a result the state-space model of the controller is obtained such that the controller has 1 output, 1 input, and 8 states. Pitch angle response of the nominal plant to the 1deg step command input, which is done by a linear simulation, are given below in Figure 4.23. Deflection of the control surface that brings pitch angle to the required value and deflection rate are illustrated in Figures 4.24, 4.25.
Step response characteristics of the closed-loop system with a nominal plant are the following:

- overshoot: 2.89 %
- settling time: < 2.5 sec
- rise time: < 0.5 sec
- steady state error: < 0.4 %

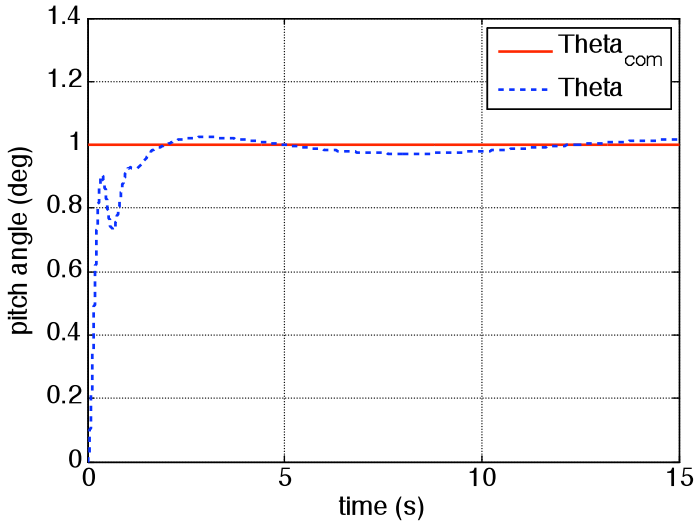

Figure 4.23 Step Input Response of the Nominal Plant: Pitch Angle

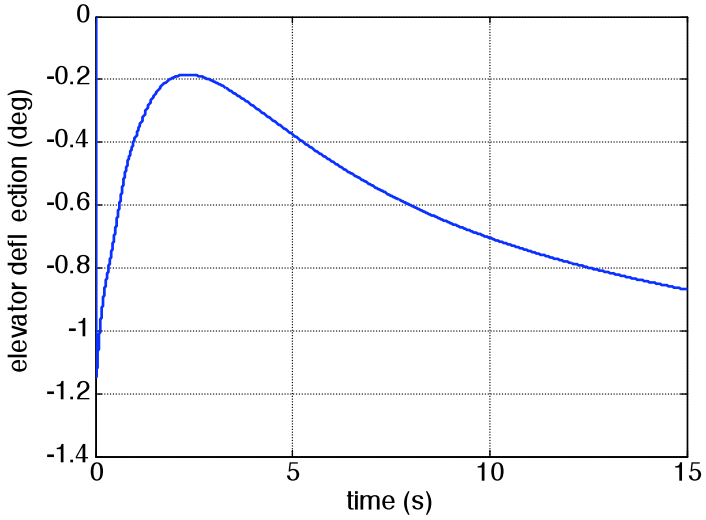

Figure 4.24 Elevator Deflection

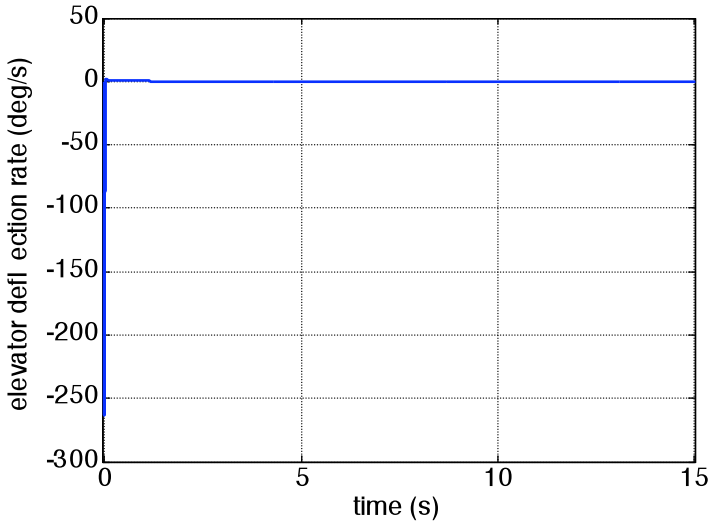

Figure 4.25 Elevator Deflection Rate

4.5.2.2 Robust Performance Analysis

The test for robust performance is performed by "`robustperf`" command in MATLAB, which gives information about the robust performance margin of the uncertain system. If the input system is represented as uncertain state space model ("`uss`" in MATLAB script), then an appropriate frequency grid is automatically generated, and the robust performance analysis is performed on that frequency grid.

The performance of a nominally-stable uncertain system model is measured by the input/output gain, which, in general, degrades (increases) for specific values of its uncertain elements. Moreover, the maximum possible degradation increases as the uncertain elements are allowed to further deviate from their nominal values. A typical tradeoff curve between allowable deviation of uncertain elements from their nominal values and the worst-case system gain is shown in Figure 4.26 (see reference [53]).

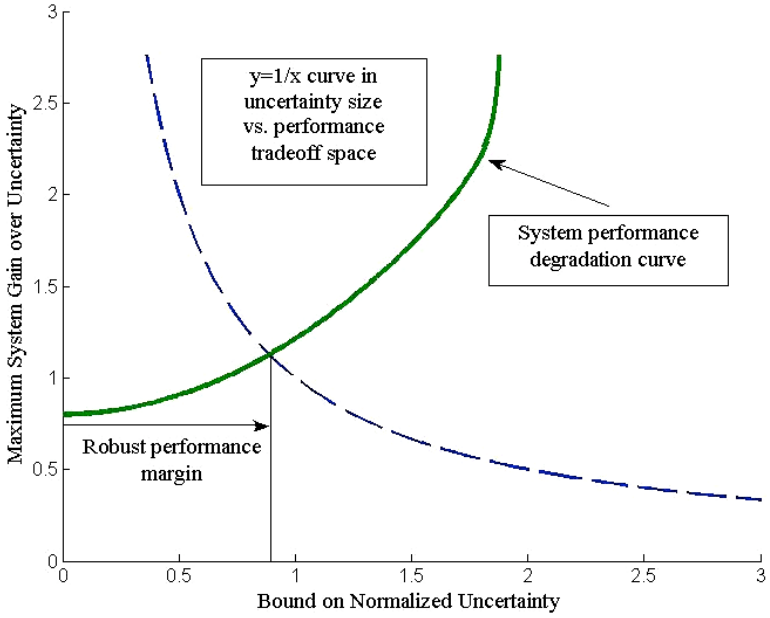

Figure 4.26 Generic Tradeoff Between Uncertainty Level and Performance

Robust performance analysis involves determining where the system performance degradation curve crosses the dashed-line, the y=1/x hyperbola. Robust performance margin, computed by "`robustperf`" command, gives the measure of the level of the input/output gain degradation. The value of robust performance margin greater than 1 implies that the input/output gain (H_∞ norm) of the uncertain system remains less than 1 for all values of the the uncertain systems. A performance robustness margin less than 1 means that certain values of the uncertain elements, within their specified ranges, lead to an input/output gain greater than 1 (see references [53], [54]). "`robustperf`" provides the information about upper (perfmarg.UpperBound) and lower (perfmarg.LowerBound) bounds on performance margin and frequency at which the minimum robust performance margin occurs, associated with upper bound on performance margin; structure of values of uncertain elements associated with perfmarg.UpperBound. Another output arguments of "`robustperf`" command are

"Frequency vector" associated with analysis, cell array (same length as "Frequency vector"), upper and lower bounds from "mussv", structure of compressed data from "mussv". "mussv" is used to compute upper and lower bounds of the Structured Singular Value.

Using the "robustperf" command for the closed-loop system shown in the Figure 4.18, for which plant is represented by the transfer function (4.45), the following results are obtained:

Upper Bound: 0.9434

Lower Bound: 0.9434

Critical Frequency: 0.4921

"perfmargunc" is a structure of values of uncertain elements associated with the hyperbola crossing. By substituting the values into the closed-loop system it can be verified that this collection of values causes the closed-loop system norm to be greater than or equal to the reciprocal of the performance margin upper bound:

perfmargunc = 1.0567

1/(perfmarg.UpperBound) = 1.0600.

Finally, plot of the bounds from "mussv" is illustrated in Figure 4.27.

The peak value is the reciprocal of the performance margin, and the frequency at which the peak occurs is the critical frequency.

4.5.2.3 Robust Performance Analysis: Connection with μ Analysis

Consider the μ-analysis technique, described in the section 4.4. Extract the ($M-\Delta$) decomposition, and call "mussv" command on the appropriate channels of *M*. In order to perform robust performance analysis a fictitious uncertain element must be generated. This fictitious element is often referred to as the "performance block." It should be a complex matrix-valued uncertain element with nominal value of *0*, and norm-bounded by *1*.

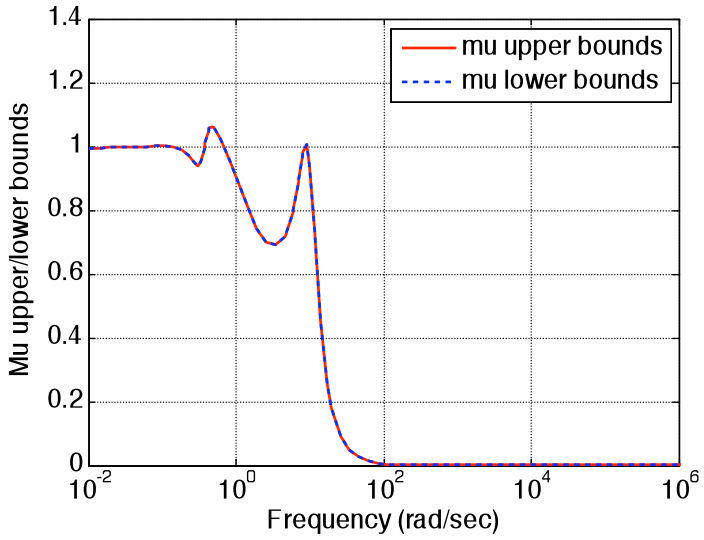

Figure 4.27 μ Bounds for Robust Performance

The block diagram of the uncertain plant with performance block Δ_p is shown in Figure 4.17. In MATLAB Δ_p is created as "`complexm`" object. This element is "wrapped" around the input/output channels of the system under consideration, and then a robust stability analysis is performed. Since the rows of uncertain elements correspond to the columns of M, and vice-versa, the row dimension of the performance block should be the column (input) dimension of closed-loop system. Generating the performance block (denoted as "PerfBlock" in the code) and closing the input/output channels of the closed-loop system with it a modified closed-loop system is created by "`lft`" command. The modified closed-loop system has following characteristics: 13 States, 0 Outputs, 0 Inputs, Continuous System.

It should be noted, that the modified closed-loop system has 0 inputs and 0 outputs (this is expected), but has dependence on the original uncertain elements, as well as the new performance block.

"lftdata" command is used to separate the uncertain system into a certain system M, in feedback with a normalized block diagonal uncertain matrix (call it "NDelta"). The structure of the block-diagonal matrix is described by another output argument ("BlkStruct"), which will be used as the block structure argument to "`mussv`". "`frd`" command is used to compute a frequency response of *M*. The same frequency range as in the "`robustperf`" analysis. "`mussv`" bounds for *M* are generated and their plot is shown in Figure 4.28. It should be noted that the plot is identical to the plot obtained from the "`robustperf`" analysis.

The performance margin is the reciprocal of the structured singular value. Therefore upper bounds from "`mussv`" become lower bounds on the performance margin. Making these conversions the bounds and frequency associated with the upper bound of the performance margin are obtained.

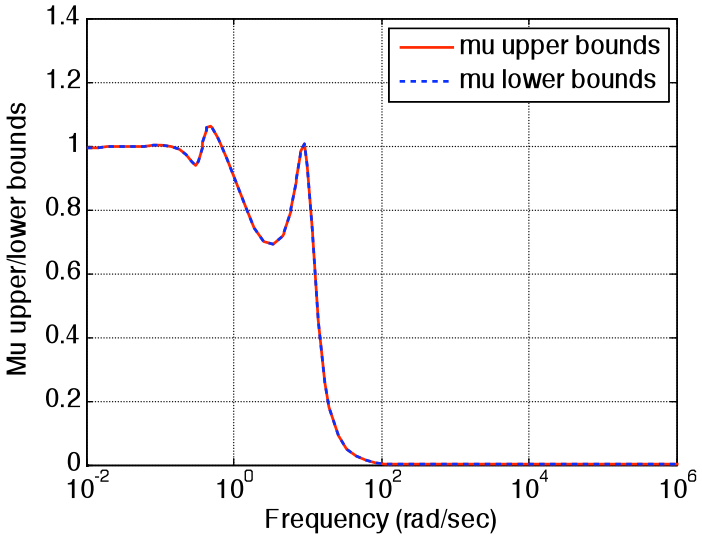

Figure 4.28 μ Bounds for Robust Performance

For comparison compare the lower and upper bounds from "`robustperf`" and "`mussv`" as well as the corresponding critical frequencies are given in Table 4.1.

Table 4.1 Lower and Upper Bounds and Critical Frequency

	"`robustperf`"	"`mussv`"
Lower bound	0.934	0.934
Upper bound	0.934	0.934
Critical frequency	0.4921	0.4921

4.5.3 Robust Controller Design for Roll Autopilot

Consider the block diagram of a feedback control system as it is shown in the Figure 4.18. Plant G represents a transfer function from ailerons deflection to roll angle, which is described by the following expression:

$$W_{\phi/\delta a} = \frac{52.4s^2 + 42.1s + 458.3}{s^4 + 6.544s^3 + 13.36s^2 + 62.69s + 0.5783} \tag{4.49}$$

Reference input to the closed-loop system is a command roll angle. Output of the closed-loop system is the measured value of the roll angle.

Procedure of determining weighting functions required for robust controller design is similar to the procedure described above for the pitch autopilot. In order to derive W_m, consider 1% and 5% of uncertainty of system's parameters that mostly effect airplane stability. Airplane effective dihedral C_{l_β} is of the primary importance for lateral airplane stability. Another important aerodynamic derivative is roll-

damping C_{lp}. Recall (4.11) for the expression for weighting function W_m. Magnitude frequency characteristics of $\frac{G_p(j\omega)-G(j\omega)}{G(j\omega)}$ is shown in Figure 4.29.

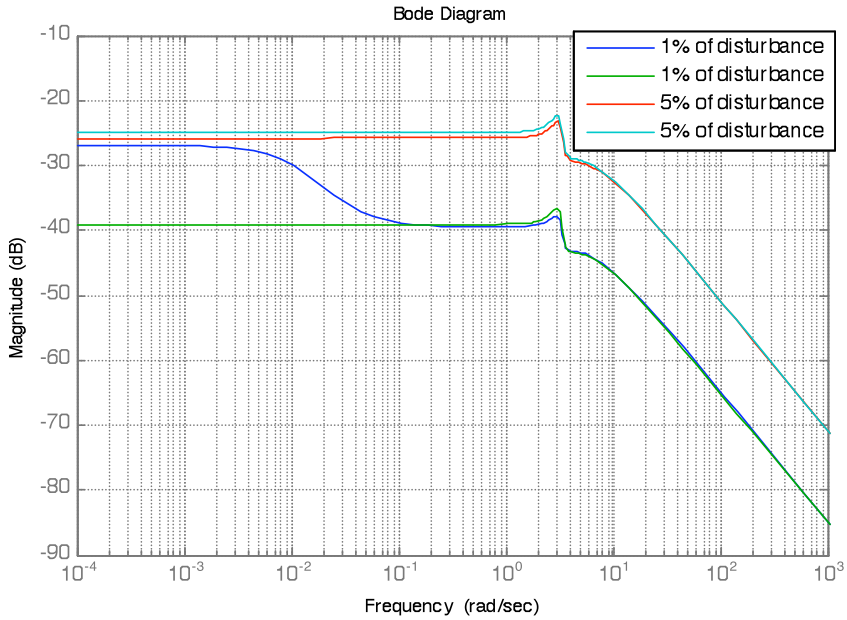

Figure 4.29 Bode Plot of Uncertain Plants

W_m is chosen as given below and its Bode plot is in Figure 4.30 :

$$W_m = \frac{0.6}{s+7} \tag{4.50}$$

Weighting function W_p had been chosen in a similarly to the previous section and is equal to:

$$W_p = \frac{5.8}{2s + 1.1} \tag{4.51}$$

Its frequency characteristics are illustrated in Figure 4.31.

Weighting function W_n is chosen the same as for the pitch controller (see Figure 4.22).

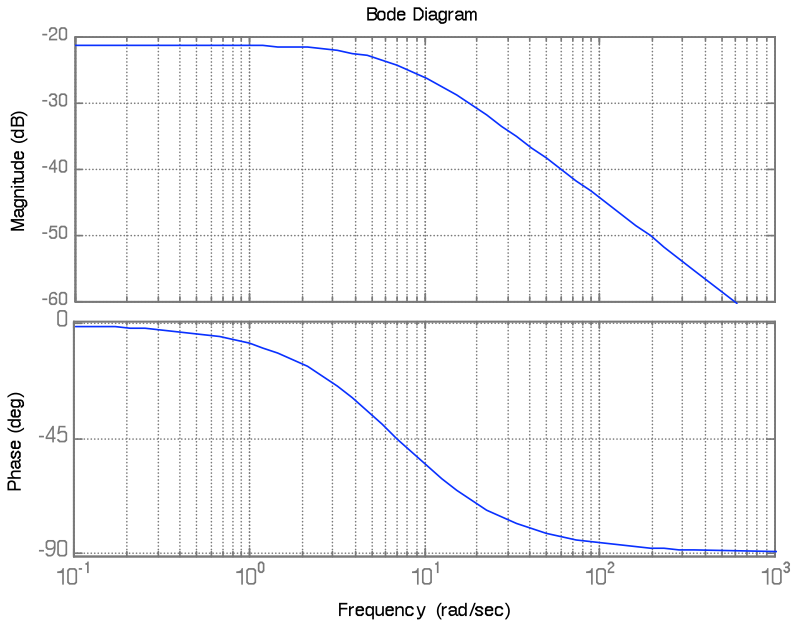

Figure 4.30 Bode Plot of W_m

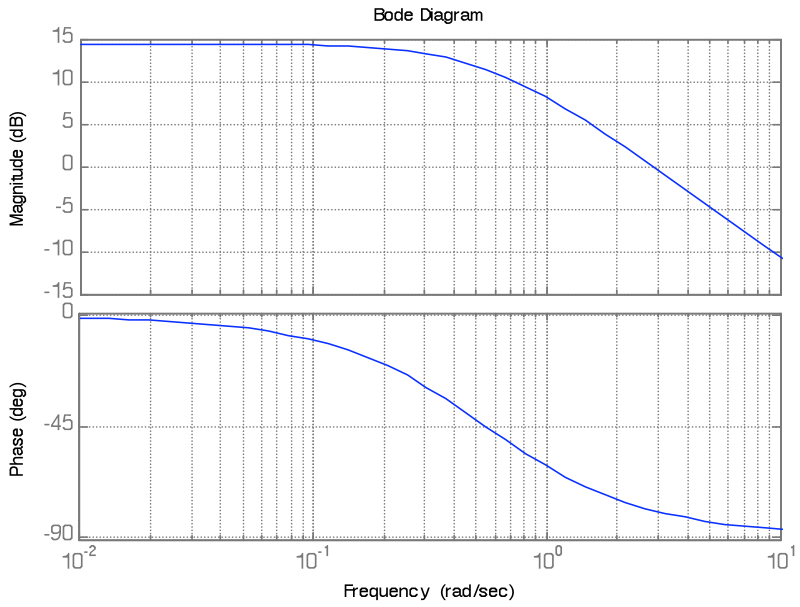

Figure 4.31 Bode Plot of W_p

4.5.3.1 Performance of the Robust Controller for Roll Autopilot

As a result of the design procedure, the controller with 1 output, 1 input, and 8 states is obtained. To estimate performance of the robust controller used for roll autopilot consider response of the nominal plant to a step input of 1 deg, which is represented in Figure 4.32. Simulation is performed for a linear environment. Ailerons deflection, which corresponds to system's response, and deflection rate are shown in Figures 4.33, 4.34.

Step response characteristics of the closed-loop system with a nominal plant are the following:

- overshoot: 2.55%
- settling time: 1.02 sec

- rise time: < 0.5 sec
- steady state error: 0.2%

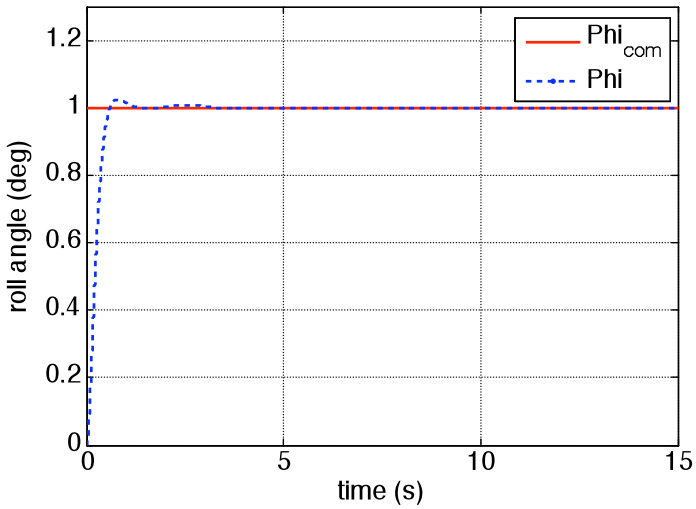

Figure 4.32 Step Input Response of the Nominal Plant: Roll Angle

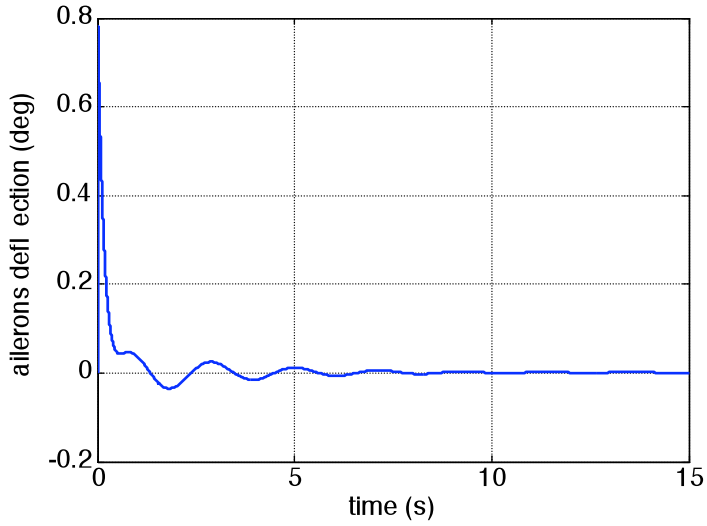

Figure 4.33 Ailerons Deflection

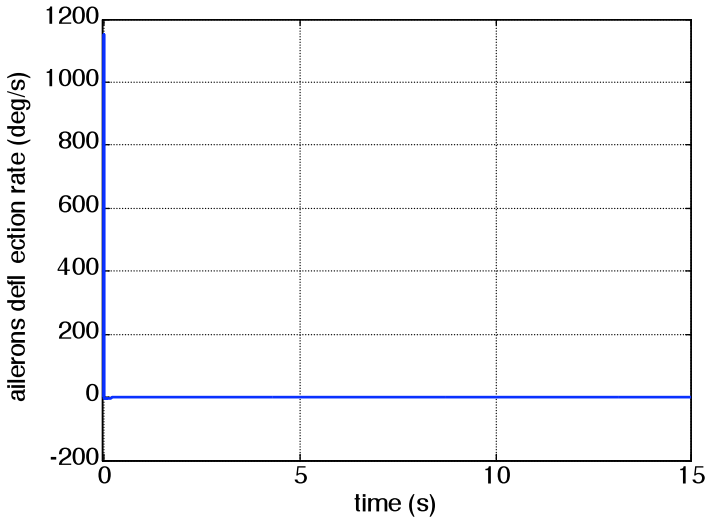

Figure 4.34 Ailerons Deflection Rate

4.5.3.2 Robust Performance Analysis

Robust performance analyses is performed in the same way as it as described in the section 4.5.2.2 for the pitch autopilot.

Applying the "`robustperf`" command for closed-loop system shown in Figure 4.18, where plant is represented by the transfer function (4.49) the following results are obtained:

Upper Bound: 0.9974

Lower Bound: 0.9974

Critical Frequency: 0.5460

perfmargunc = 1.0008

1/perfmarg.UpperBound = 1.0026.

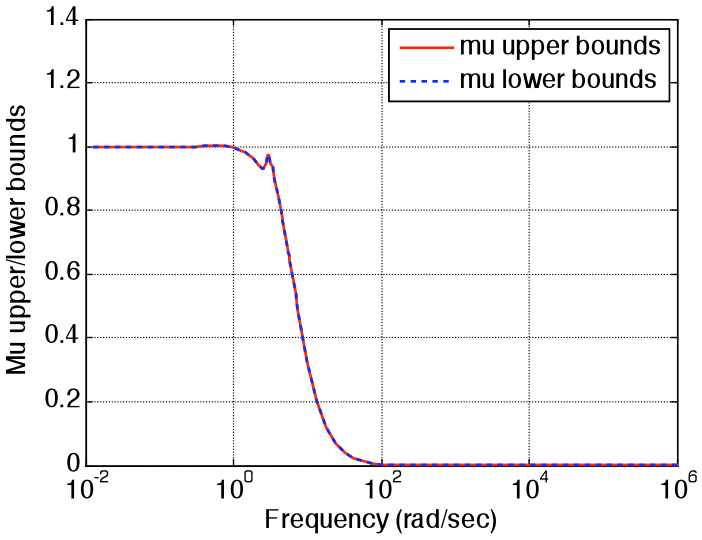

Figure 4.35 μ Bounds for Robust Performance

Figure 4.35 illustrates the plot of the bounds from "mussv". The peak value is the reciprocal of the performance margin, and the frequency at which the peak occurs is the critical frequency.

4.5.3.3 Robust Performance Analysis: Connection with μ Analysis

Using "mussv" algorithm, described in details in section 4.5.2.3, the robust performance is checked and compared to the results obtained in the previous chapter. Modified closed-loop system block has the following characteristics: 13 States, 0 Outputs, 0 Inputs, Continuous System.

Plot of the "mussv" bounds is shown in Figure 3.36, which coincides with the one given in Figure 4.35.

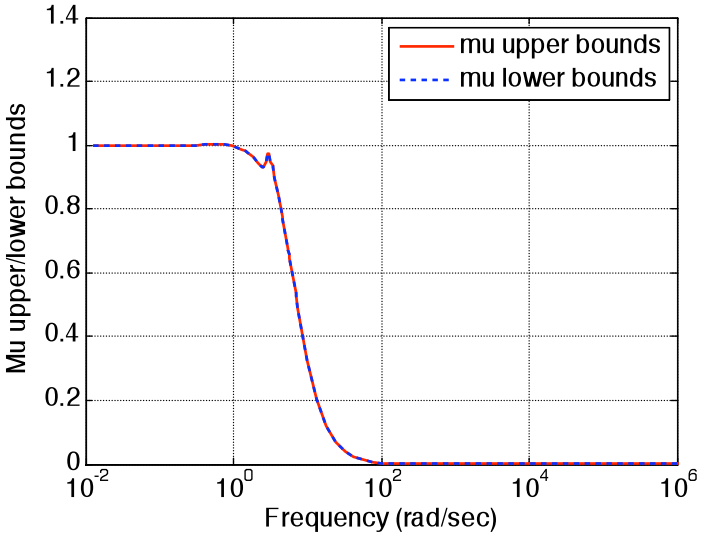

Figure 4.36 μ Bounds for Robust Performance

Table 4.2 Lower and Upper Bounds and Critical Frequency

	"robustperf"	"mussv"
Lower bound	0.9974	0.9974
Upper bound	0.9974	0.9974
Critical frequency	0.5460	0.5460

The lower and upper bounds from "robustperf" and "mussv" as well as the corresponding critical frequencies are given below for comparison in Table 4.2.

4.6 Command Filter Implementation for a Robust Control System

From Figures 4.25 and 4.34 is seen that deflection rate of the control surfaces is too high for realization in the actual physical system. Saturation of the control surfaces and will make controller performance worse. Using a command filter in the control system architecture helps to avoid this problem. Detailed information and structure of the command filter used in simulation is given in section 3.5 of Chapter 3.
The block diagram of the control system with a command filter implementation is shown in Figure 4.37 below. For simulation of the controllers performances linearized models of longitudinal and lateral dynamics are used. Simulation using nonlinear UAV model in comparison to a PID controller performance is presented in Chapter 5.

4.6.1 Robust Pitch Autopilot Performance with a Command Filter Implementation

Consider the block diagram illustrated in Figure 4.37 .

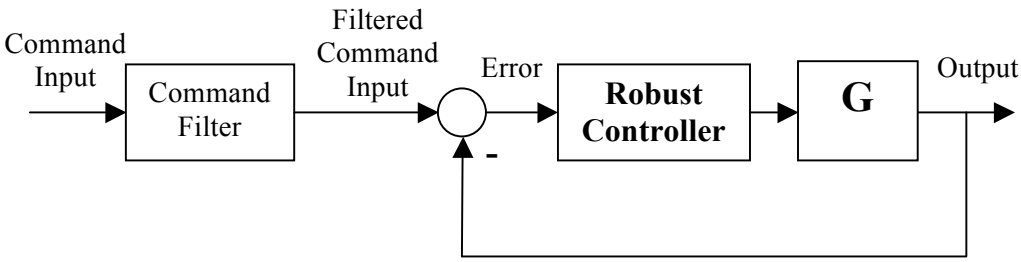

Figure 4.37 Basic Controller Configuration with Command Filter

The plant *G* as in Figure 4.37 represents a transfer function from elevator deflection to pitch angle obtained from the linearized longitudinal dynamics of the METU TUAV. Assume the input to the control system is as it is shown in Figure 4.38. Response of the control system in terms of pitch angle to the given input is shown in Figure 4.39. Elevator deflection and deflection rate are illustrated in Figures 4.40, 4.41.

From the simulation results it is seen that shaping the input command with a command filter sufficiently decreases the rates of actuators making them to correspond to the physical performance capabilities.

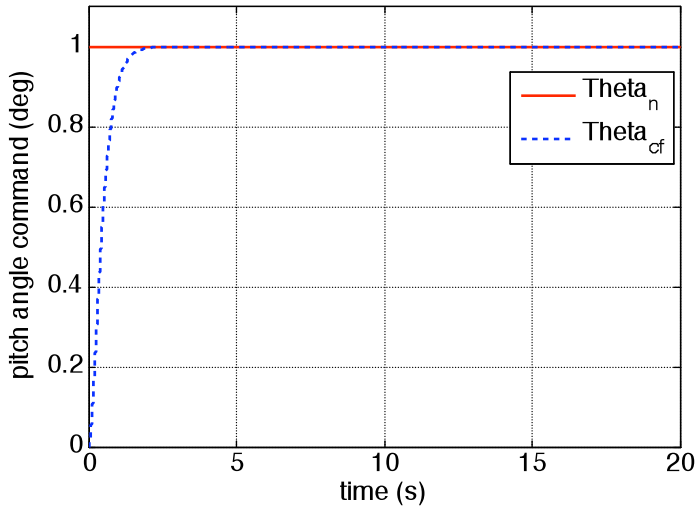

Figure 4.38 Pitch Angle Command

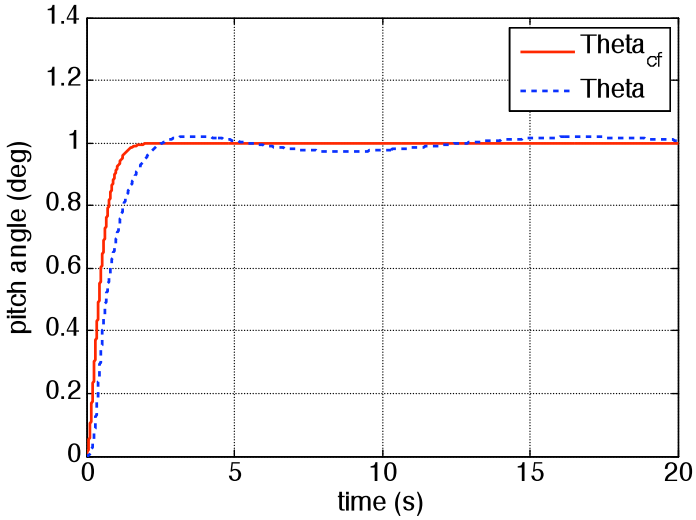

Figure 4.39 System Response to a Pitch Angle Command

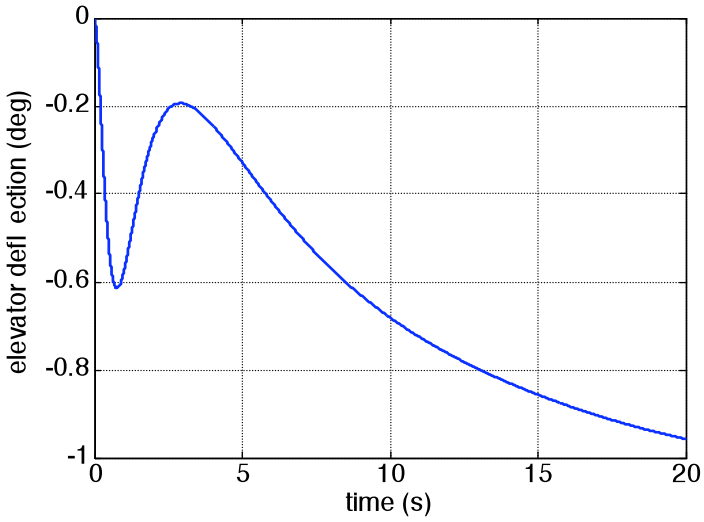

Figure 4.40 Elevator Deflection

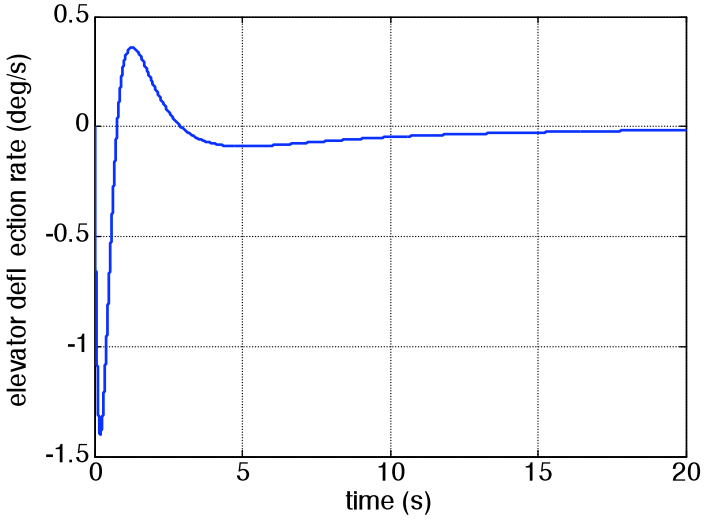

Figure 4.41 Elevator Deflection Rate

4.6.2 Robust Roll Autopilot Performance with a Command Filter Implementation

For the roll autopilot he plant *G* in Figure 4.18 consistes of the transfer function from ailerons deflection to roll angle obtained from the linearized lateral dynamics of the METU TUAV. Consider the following command input to the closed-loop system as it is shown in Figure 4.42. Figures 4.43, 4.44 and 4.45 give the roll angle response, ailerons deflection and rate of ailerons deflection, respectively.

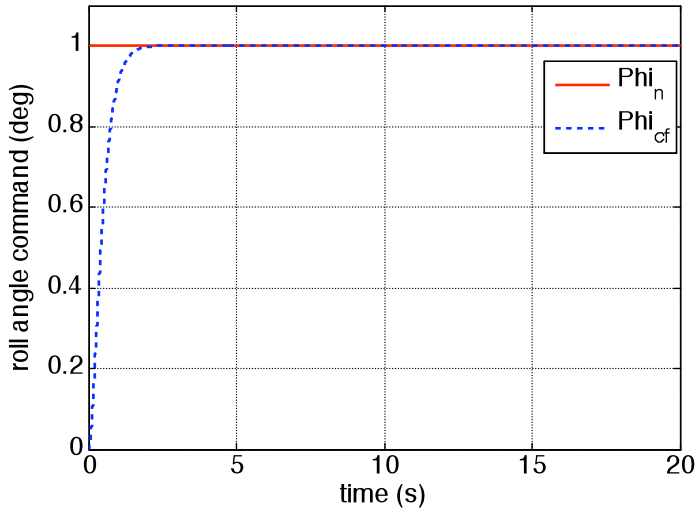

Figure 4.42 Roll Angle Command

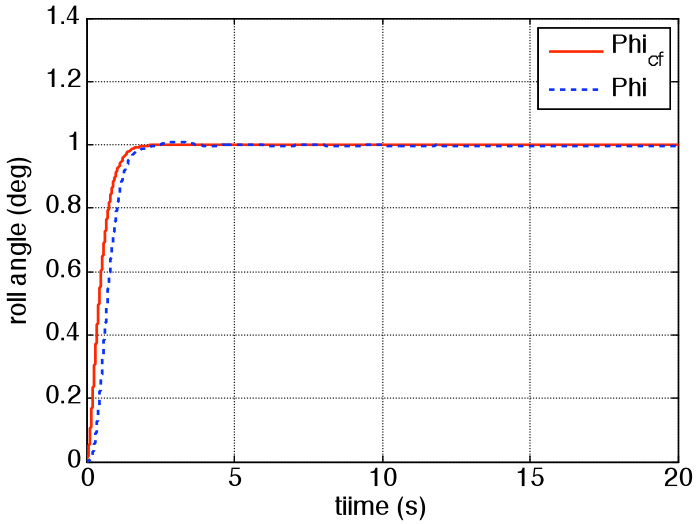

Figure 4.43 System Response to a Roll Command

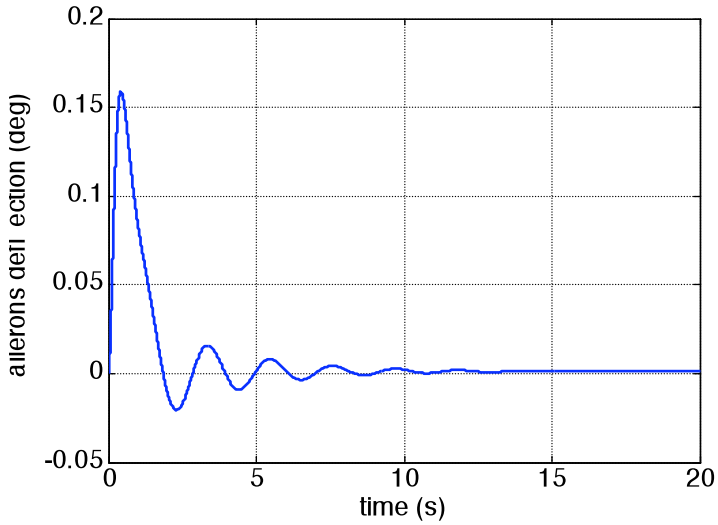

Figure 4.44 Ailerons Deflection

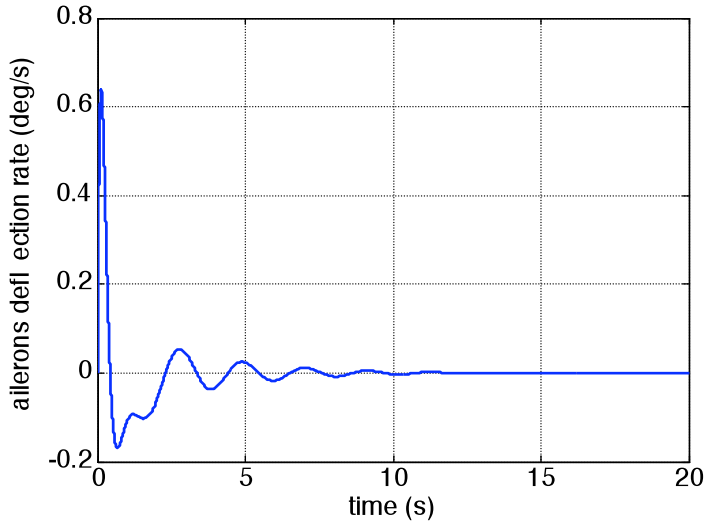

Figure 4.45 Ailerons Deflection Rate

Simulation results give similar conclusions, as made for the pitch autopilot: implementing a command filter to the control system improves its performance in terms of actuators behaviour, mainly by decreasing their rates.

CHAPTER 5

COMPARISON OF PID AND ROBUST CONTROLLERS

This chapter includes comparison of the controller designed using classical control theory, and the controller designed by methods of robust control theory. Comparison analysis of controllers' performances is performed by nonlinear simulation.

5.1 Performance Issues for the Nominal Model

In this section controllers' performances are compared through the nonlinear simulation for a unit step input command. Simulation is performed using a nominal model of the UAV, i.e. no parameter uncertainties is assumed to be present in a system's model.

5.1.1 Pitch Autopilot

Consider the response of the classical and robust controllers designed for a pitch autopilot to a unit a step pitch angle command, which is represented by a pitch angle response given in Figure 5.1 below.

Numerical values of performance characteristics of the PID and robust controllers are listed in Table 5.1.

Change in elevator position and deflection rate for PID and robust controller for a step pitch command is illustrated in Figures 5.2 and 5.3 respectively.

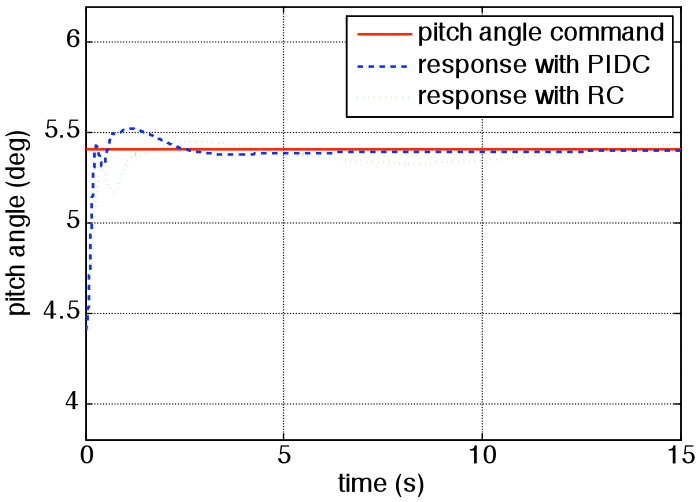

Figure 5.1 Pitch Angle Response to a Unit Step Input

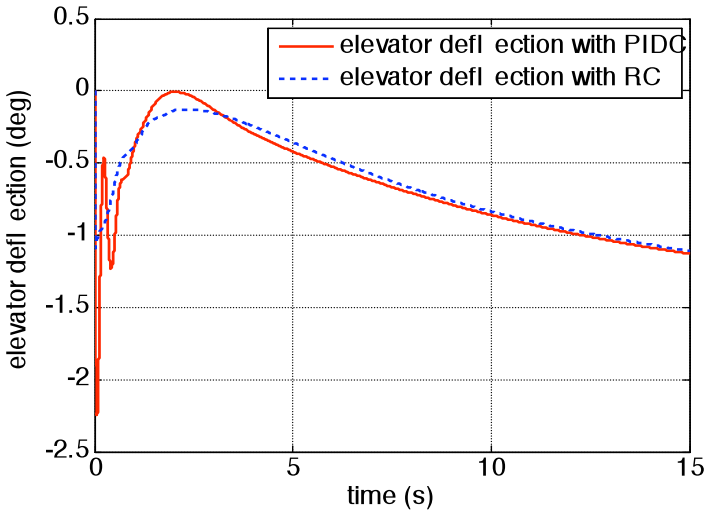

Figure 5.2 Elevator Deflection for a Unit Step Input

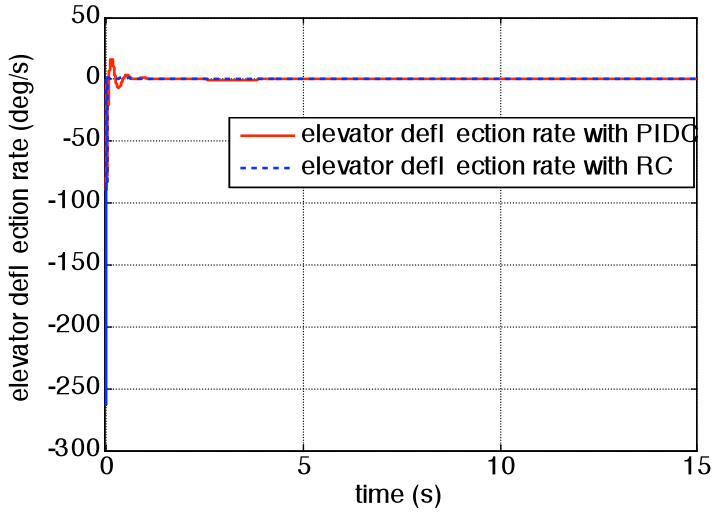

Figure 5.3 Elevator Deflection Rate for a Unit Step Input

Table 5.1 Performance Comparison of Controllers for Pitch Autopilot

Characteristic	Required	Result with CCT	Result with RCT
Overshoot	< 10 %	10 %	6 %
Settling time, s	< 3	< 2	< 3
Rise time, s	< 1	< 0.3	< 0.5
Steady state error	< 3 %	< 0.4 %	< 1%

5.1.2 Roll Autopilot

Consider response of the classical and robust controllers for roll autopilot to a unit step roll angle command in terms of roll angle, ailerons deflection and ailerons deflection rate, given in Figures 5.4 – 5.6, respectively.

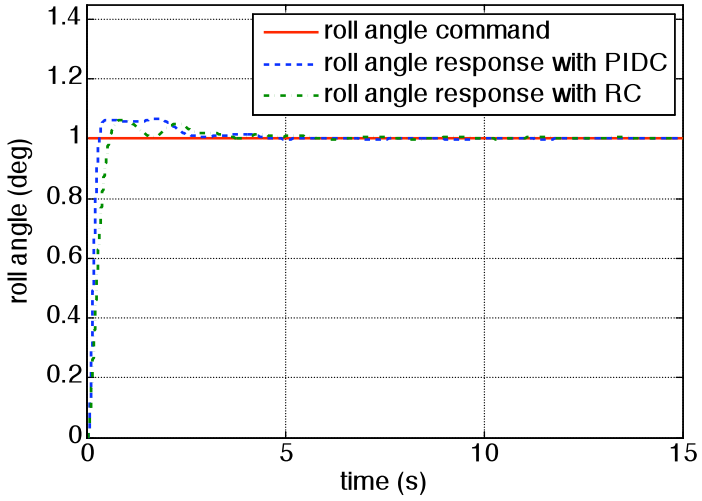

Figure 5.4 Roll Angle Response to a Unit Step Input

Numerical values of performance characteristics of the PID and robust controllers are listed in Table 5.2. Figure 5.4 shows that characteristics of the roll angle response for the robust and PID controllers are satisfactory for the design requirements. However, the actuators rate is high for the robust controller at initial moment of the input (see Figures 5.6), which contradicts the performance capabilities of the physical system. This problem is solved by implementing a command filter to the control system.

Table 5.2 Performance Comparison of Controllers for Roll Autopilot

Characteristic	Required	Result with CCT	Result with RCT
Overshoot	< 10 %	6.4 %	6.8 %
Settling time, s	< 3	<2.5	3
Rise time, s	< 1	< 0.3	< 0.5
Steady state error	< 3 %	0	0.6 %

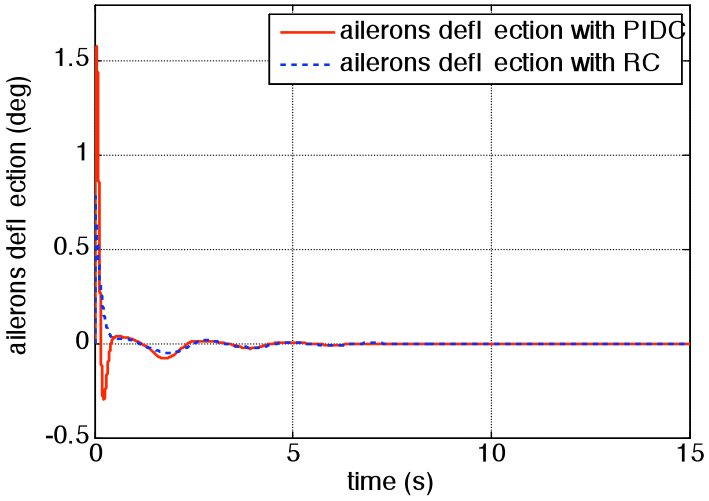

Figure 5.5 Ailerons Deflection for a Unit Step Input

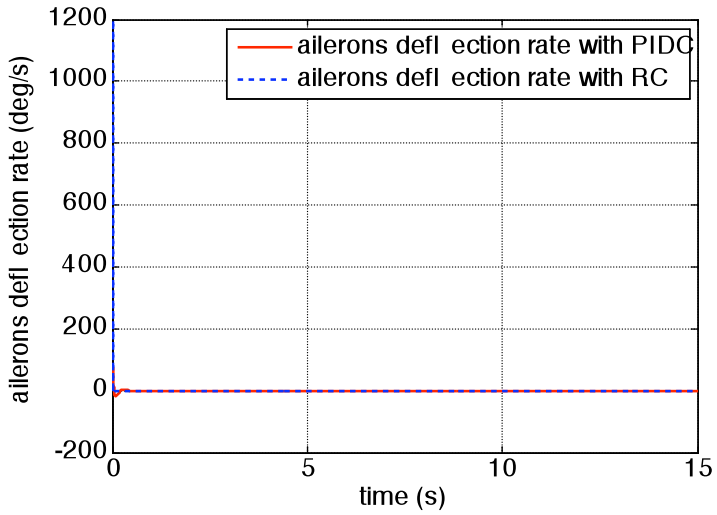

Figure 5.6 Ailerons Deflection Rate for a Unit Step Input

5.2 Performance Issues for the Nominal Model with a Command Filter Implementation

This chapter gives the simulation results of the PID and robust controllers for a nonlinear model of the METU TUAV using a command filter implemented to the control systems.

5.2.1 Pitch Autopilot

Response to the filtered command input for the PID and the robust controllers designed for a pitch autopilot in terms of pitch angle, elevator position and elevator deflection rate is shown in Figures 5.7 – 5.9.

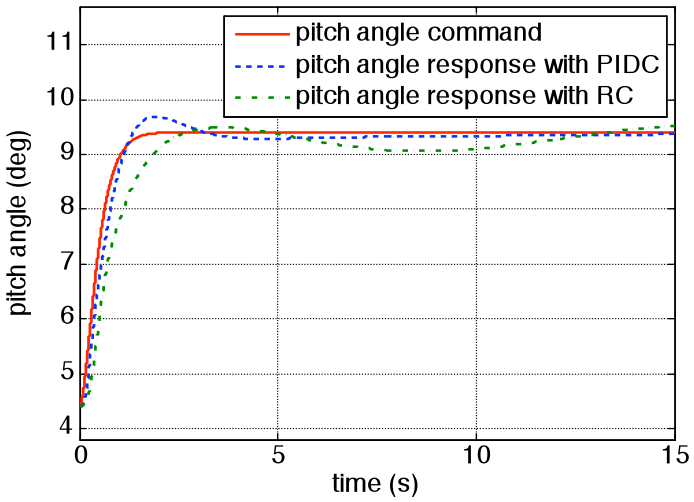

Figure 5.7 Pitch Angle Response

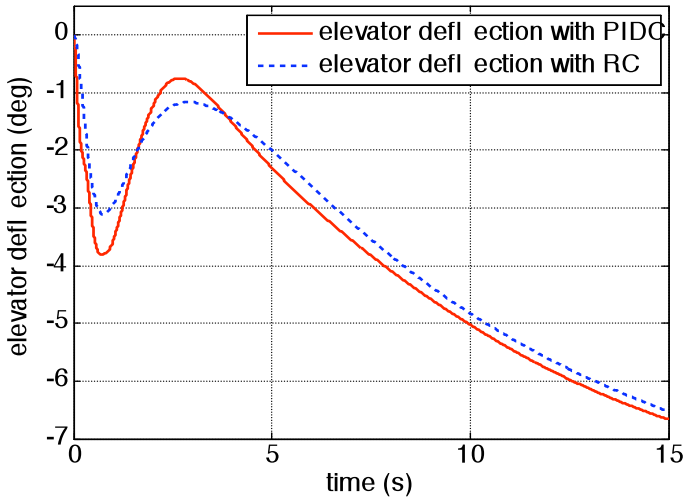

Figure 5.8 Elevator Deflection for the Command Pitch Angle

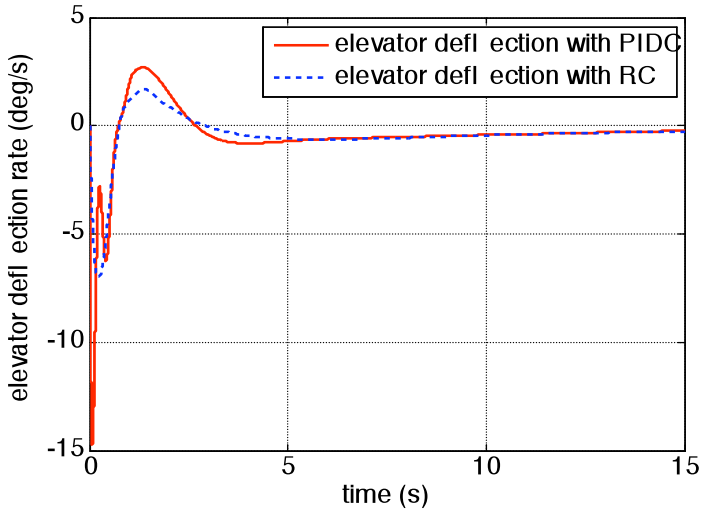

Figure 5.9 Elevator Deflection Rate for the Command Pitch Angle

5.2.1 Roll Autopilot

Consider response to the filtered command of the PID and robust controllers designed for the roll autopilot. Figures 5.10 – 5.12 illustrate change in roll angle, ailerons position and rate of change, respectively.

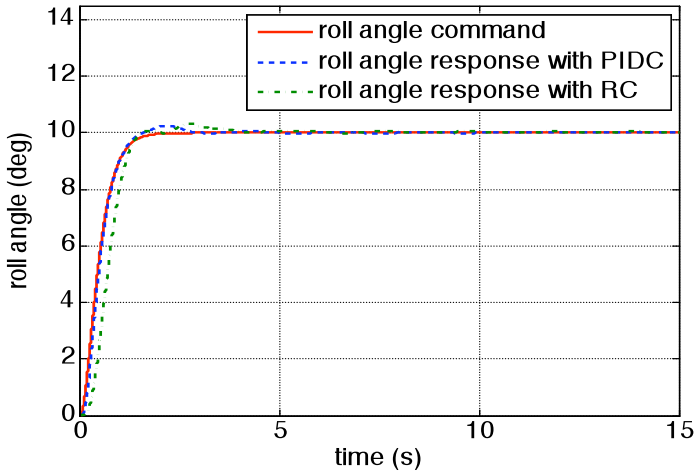

Figure 5.10 Roll Angle Response

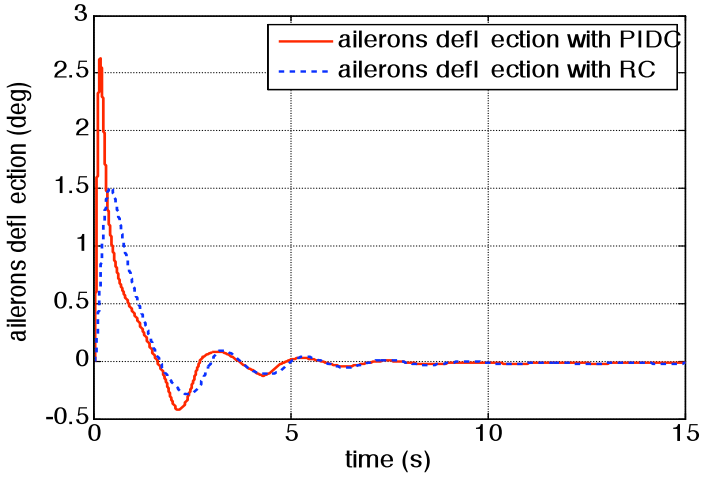

Figure 5.11 Ailerons Deflection for the Command Roll Angle

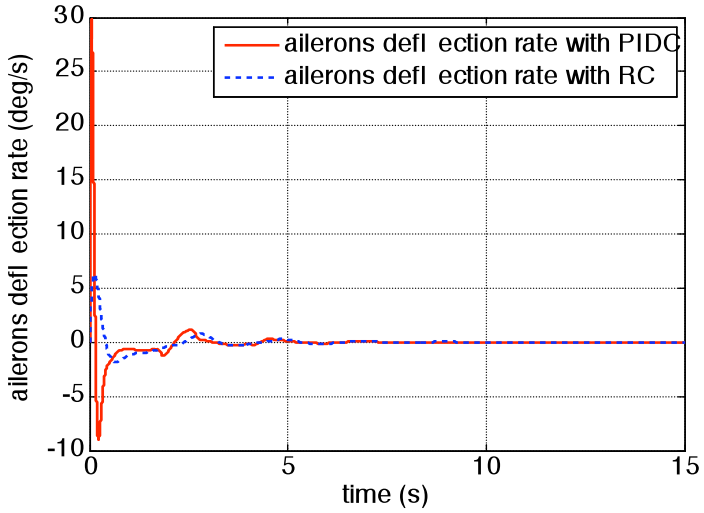

Figure 5.12 Ailerons Deflection Rate for the Command Roll Angle

5.3 Performance Comparison of PID and Robust Controllers for Uncertain Plant

Consider the nonlinear model of the METU TUAV, which has uncertainties due to variation in aerodynamic derivatives. As it have been mentioned in the previous chapters, the most important aerodynamic derivatives that effect stability of the vehicle are static longitudinal stability derivative C_{m_α} and pitch-damping derivative C_{m_q} (for longitudinal dynamics), airplane effective dihedral C_{l_β} and roll-damping C_{lp} (for the lateral dynamics). Simulation is performed assuming 5% of uncertainty with respect to the nominal value of the parameter. Simulations are performed for pitch and roll angle inputs as they are shown in the Figures 5.13 and 5.16 for pitch and roll autopilots, respectively. The results of simulations are illustrated in the figures below.

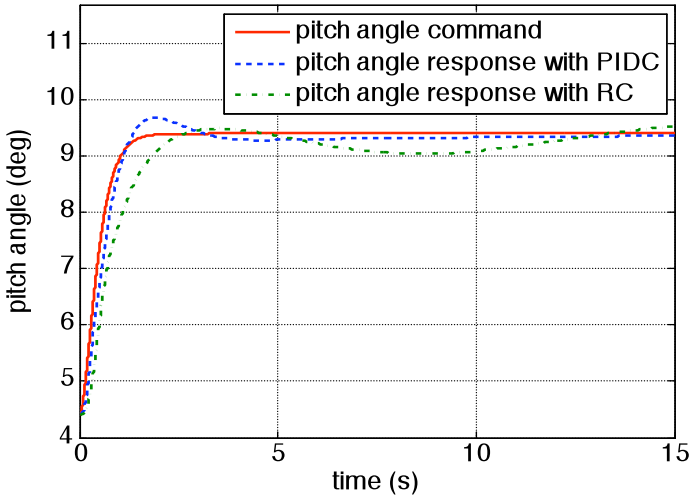

Figure 5.13 Pitch Angle Step Response of Uncertain Model

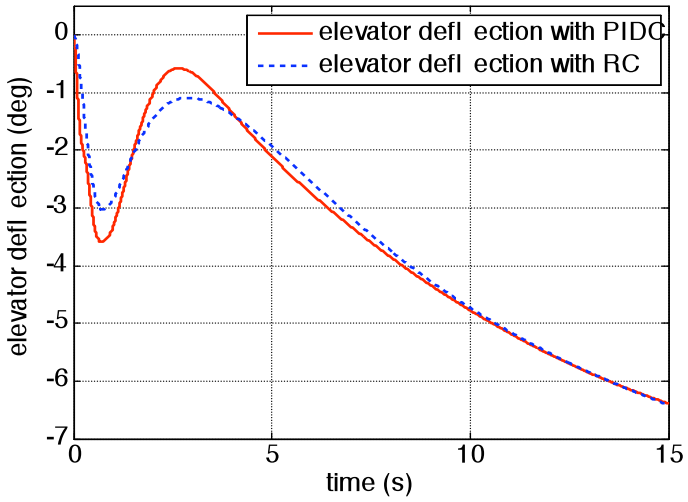

Figure 5.14 Elevator Deflection of Uncertain Model

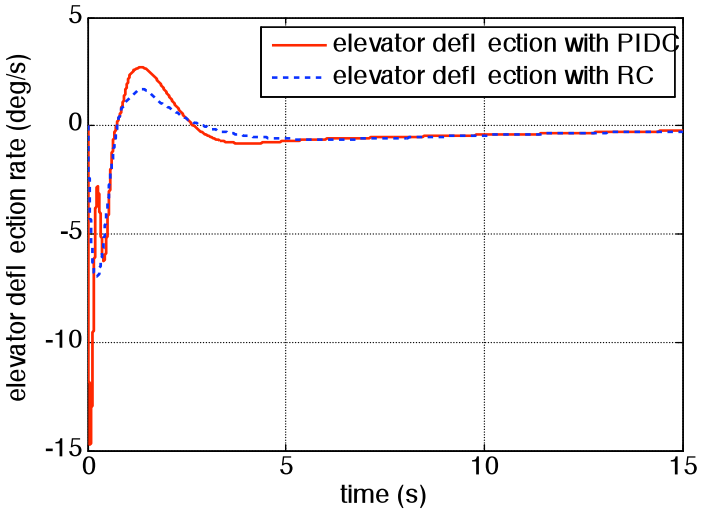

Figure 5.15 Elevator Deflection Rate of Uncertain Model

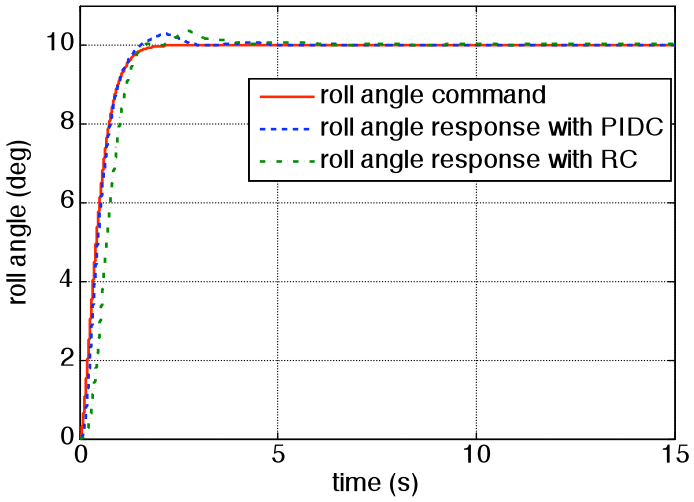

Figure 5.16 Roll Angle Step Response of Uncertain Model

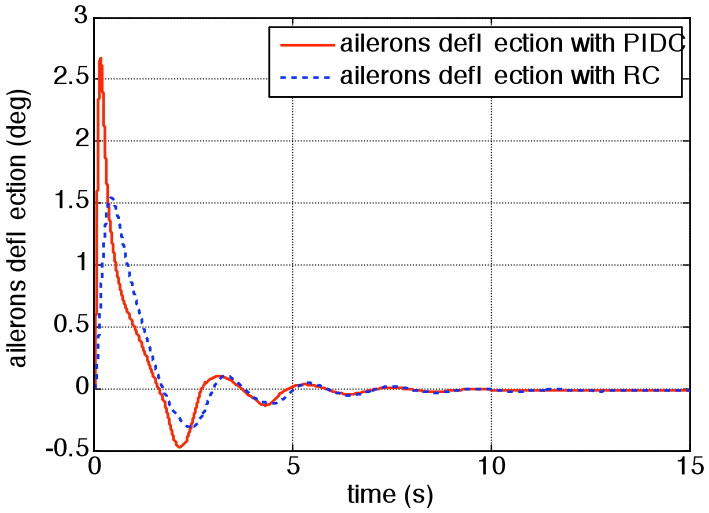

Figure 5.17 Ailerons Deflection of Uncertain Model

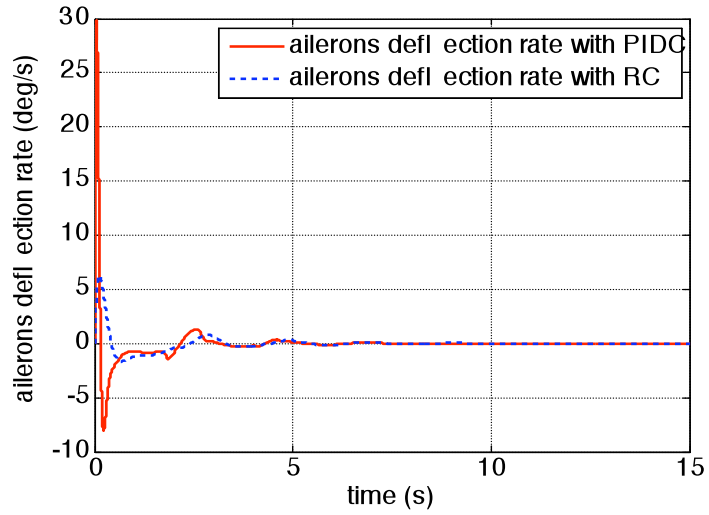

Figure 5.18 Ailerons Deflection Rate of Uncertain Model

Simulations results illustrate, that both PID and robust controllers, designed for pitch and roll autopilots, perform equally well at tracking the input signal for the nominal plant, and for the plant, which has the uncertainties in aerodynamic parameters. Such results are expected from the robust controller, which takes into account model uncertainties in design algorithm. However, it is seen that the PID controller is also able to handle with system uncertainties.

5.4 Performance Comparison of PID and Robust Controllers with a Sensor Noise Presence

Consider the case when there is a noise, present in the system. Assume, that the sensors are the sources of the noise (sensor noise). The simulation for comparison of the classical and robust controllers is performed for the nonlinear nominal model.

5.4.1. Pitch Autopilot

In order to compare performances of the PID and the robust controllers, designed for a pitch attitude autopilot, consider responses of the PID and the robust control systems. Simulation includes responses of the classical and robust control systems to the input, which is shaped by the command filter as it is given in the Figure. Assume presence of the sensor noise with a frequency of 100 Hz and standart deviation of 0.5% of the output nominal value.

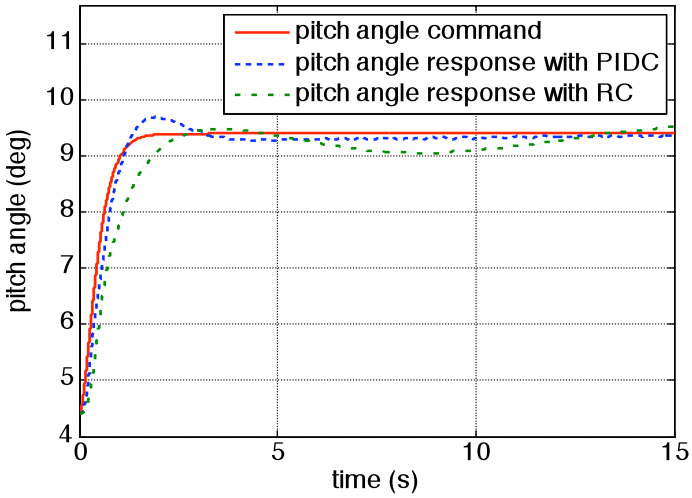

Figure 5.19 Pitch Angle Response

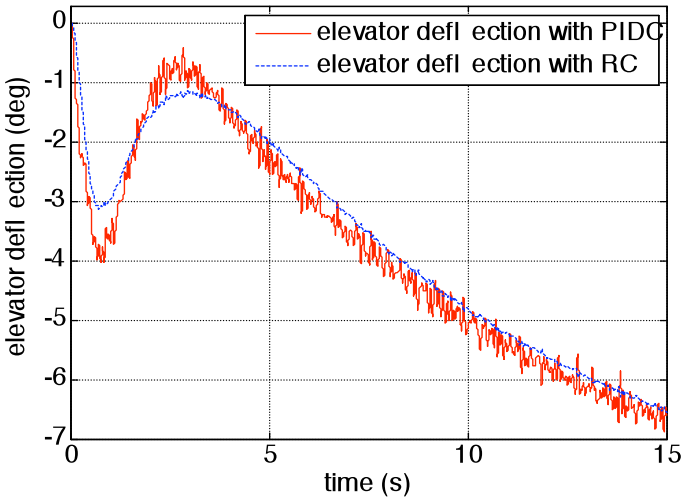

Figure 5.20 Elevator Deflection Response

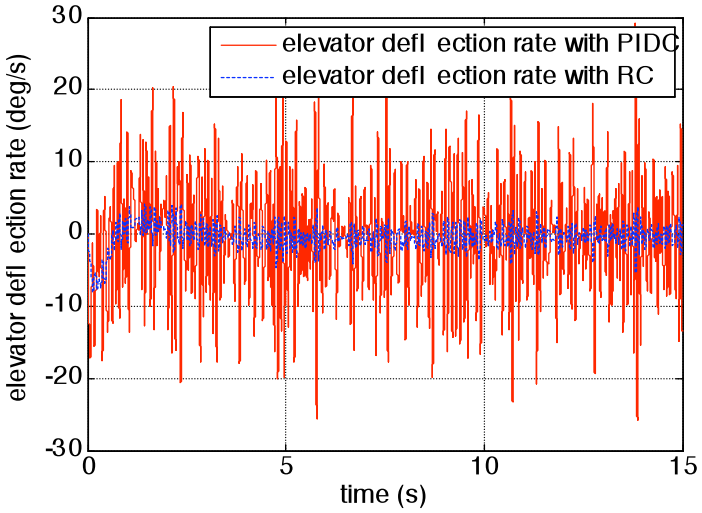

Figure 5.21 Elevator Deflection Rate Response

Simulation results show that both PID and robust controllers show good performance in tracking the input command. However, the PID controller is more sensitive to the noise than the robust controller, it considers noise as a reference input and tries to follow it. This is clearly seen from the position of the control surface, and its rate. Minimization of the actuator's efforts as well as taking sensor noise into account by H_∞ algorithm is performed systematically during the design of the controller.

5.4.2. Roll Autopilot

As for the pitch autopilot, consider responses of the control systems, which use PID and robust controllers, to the input command shown in the Figure 3.19. Simulation is performed for the presence of sensor noise with a frequency of 100 Hz and standart deviation of 0.5% of the output nominal value.

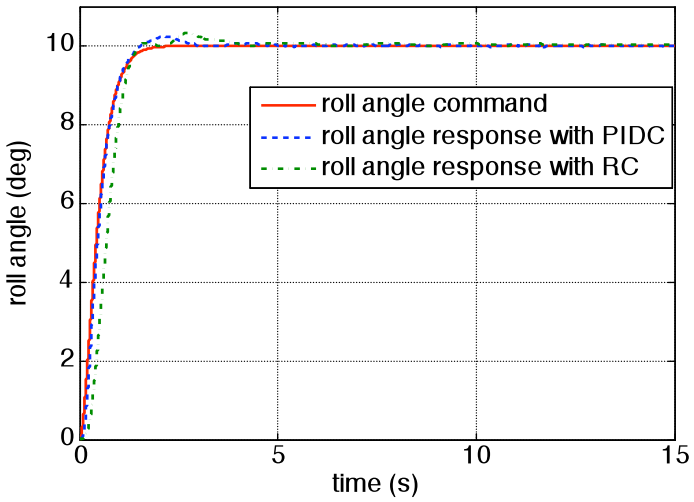

Figure 5.22 Roll Angle Response

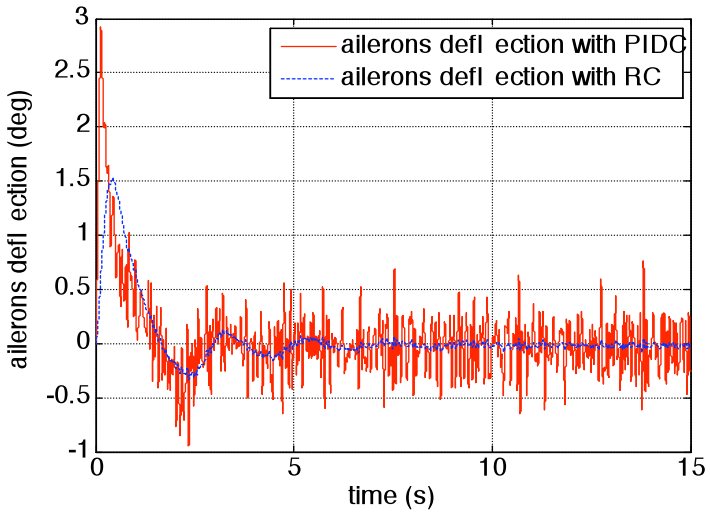

Figure 5.23 Ailerons Deflection Response

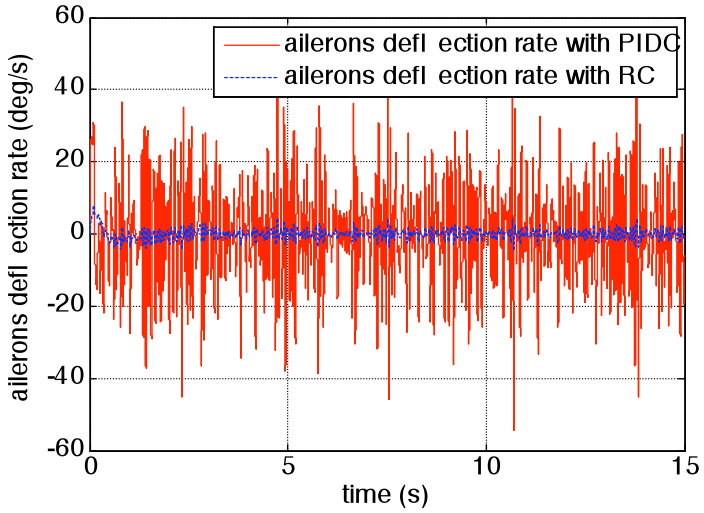

Figure 5.24 Ailerons Deflection Rate Response

According to the obtained results, which are shown in the figures above, robust controller shows satisfactory performance in terms of roll angle response, ailerons position and ailerons deflection rate. PID controller illustrates good input tracking, however it is more sensitive to the sensor noise than the robust controller, which is reflected in actuator's behaviour: ailerons deflection and its rate for the PID controller exceeds the corresponding values for the robust controller.

CHAPTER 6

CONCLUSION

As a result of this work, the pitch and roll autopilots are designed for the METU TUAV. Two different techniques are used for the autopilots design. PID controller is developed by methods of the classical control theory and robust controller is developed by the H_∞ design technique. Performances of both types of controllers for the pitch and roll autopilots are compared by simulations.

Nonlinear 6 DOF dynamic model of the UAV is developed by means of MATLAB/Simulink. The UAV model includes aerodynamics, propulsion, mass-inertia and environment models, and can be modified in terms of aerodynamic and geometric properties of the vehicle. Linearization of the nonlinear model around the specified trim condition is performed using the MATLAB Control Design Toolbox. Characteristics of the UAV dynamics, referred to its longitudinal and lateral dynamics, are established from the linear model and the open-loop response simulations are performed.

Purposes of the pitch and roll autopilots are to follow the input commands. The reason of designing controllers by different control algorithms is to compare which type of the controller would provide better performance when the plant (actual physical model) differs from the nominal model used for controller design. These differences may occur as a result of linearizing the nonlinear dynamics of the UAV; inaccurate aerodynamic model, which does not reflect the aerodynamic properties of the UAV truly; neglecting presence of the sensor noise during the design of the controller. Designing a PID controller, it is impossible to take into account the

uncertainties, which are present in the model parameters. The H_∞ design technique, which is used for the robust controller design, consideres the uncertainties of the model's parameters and the disturbances, which act upon the system. Two approaches are used to establish robust performance of the robust closed-loop system. The "`robuststab`" function gives the answer to the basic robustness question: "is the closed-loop system stable or not?". μ analysis is the mathematical tool used to find the robust stability and robust performence margins. The "`mussv`" function is used directly to compute the structured singular value μ, as a function of frequency.

Simulation results provide comparison of the controllers performances. Simulations are performed for the nominal model, for model that includes uncertainties due to variation in aerodynamic derivatives, and for the case when sensor noise is taken into account. It should be noted, that when sensor noise is present response of the controller designed by H_∞ technique is better than response of the control system with a PID controller. The most efficient way to decrease sensitivity of the PID controller to the noise is decreasing the derivative time T_d. However, this effects the response of the system by increasing overshoot and settling time. Therefore, a trade-off decision should be made between system's performance and its noise rejection capabilities. Implementation of the command filter to the control systems has a positive effect on their performances.

The following suggestions can be made for future work:

- implementation of the model into the open source code Flight Gear for a real-time simulation
- verification of the dynamic model by the flight tests of the METU TUAV

REFERENCES

[1]. Barak J. Carlson, *"Past UAV Program Failures and Implications for Current UAV Programs"*, Maxwell Air Force Base, Maxwell Air Force Base, AL: Air Command and Staff College; Air University Rep. No.037/2001-04.

[2]. Zak Sarris, *"Survey of UAV Applications in Civil Markets"*, Technical University of Crete, 2001

[3]. Koldaev A., Sokut S., *"Russia: Military Conservatism in Relation to Industry UAV Initiatives"*, UAV Systems, The Global Perspectives 2006/2007, p.100 – 104.

[4]. *"UAV Control Systems Hunger for Compute Density"*, COTS Journal, January 2006.

[5]. Roskam, Jan, *"Airplane Design"*, Roskam Aviation and Engineering Corp., 1985.

[6]. Kargın, Volkan, *"Design of an Autonomous Landing Control Algorithm for a Fixed Wing UAV"*, Master Thesis, Ankara : METU, 2007.

[7]. *"Caratteristiche Aerodinamiche Modello SCAUT"*, Politecnico di Torino, 2001.

[8]. Andrievsky B.R., A.L. Fradkov, *"Combined Adaptive Controller for UAV Guidance"*, Proc. European Control Conference ECC 2003, University of Cambridge, UK.

[9]. Fu Xu, Zhou Zhaoying, Xiong Wei, *"MEMS-Based Low-Cost Flight Control System for Small UAVs"*, Tsinghua Science and Technology, vol.13, #5, 2008.

[10]. V.Kargin, I.Yavrucuk*,"Autolanding Strategies for a Fixed wing UAV Under adverse Atmospheric Conditions"*, American Institute of Aeronautics and Astronautics, Guidance, Navigation and Control Conference, Honolulu, HI, USA, August 2008.

[11]. S. Kurnaz, O. Cetin, O. Kaynak, "*Fuzzy Logic Based Approach to Design of Flight Control and Navigation Tasks for Autonomous Unmanned Aerial Vehicles"*, Journal of Intelligent and Robotic Systems, 2008.

[12]. M. Sadraey, R. Colgren, *"Robust Nonlinear Controller Design for a Complete UAV Mission"*, AIAA Guidance, Navigation, and Control Conference and Exhibit, Keystone, Colorado, Aug. 21-24, 2006.

[13]. Etkin, Bernard, *"Dynamics of Atmospheric Flight"*, New York, Wiley 1972.

[14]. Peter H. Zipfel, *"Modeling and simulation of aerospace vehicle dynamics"*, AIAA, 2007.

[15]. Jan Roskam, *"Airplane Flight Dynamics and Automatic Flight Controls"*, Lawrence, DARcorporation, 1995.

[16]. Limbach Flugmotoren website, *"http://www.limflug.de/"*, as accurate of 15 July, 2009.

[17]. U.S. Standard Atmosphere, 1976, U.S. Government Printing Office, Washington, D.C., 1976.

[18]. A. Aslanyan, "*Automatic Control Flight Control Systems of Vehicles"*, Kiev, 1984.

[19]. Kotwani, K., Sane, S. K., Arya H. and Sudhakar, K., *"Performance Mapping of Mini Aerial Vehicle Propellers"*, Indian Institute of Technology, Bombay, India, 2004.

[20]. National Imagery and Mapping Agency, Technical Report 8350.2, Third Edition, Department of Defence World Geodetic System, 1984.

[21]. Hitay Özbay, **"***Introduction to feedback control theory"***,** CRC Press, 2000.

[22]. Charles L. Phillips, Royce D. Harbor, *"Feedback control systems"***,** Prentice Hall, 1991.

[23]. Ogata, Katsuhiko, *"Modern Control Engineering"***,** Prentice Hall, 2002.

[24]. Peter H. Zipfel*, "Modeling and Simulation of Aerospace Vehicle Dynamics"*, AIAA, 2007.

[25]. Sellers, David, *"An Overview of Proportional plus Integral plus Derivative Control and Suggestions for Its Successful Application and Implementation",* Retrieved on 2007-05-05.

[26]. Kok Kiong Tan, Wang Qing-Guo, Hang Chang Chieh, *"Advances in PID Control"*, Springer, 1999.

[27]. Antonio Visioli, *"Practical PID Control"*, Springer, 2006.

[28]. Morari, Manfred, *"Robust Process Control"*, Prentice Hall, 1989.

[29]. *"Avionics Fundamentals"*, Jeppesen and United Airlines, 2006.

[30]. Aidan O'Dwyer, *"Handbook of PI and PID Controller Tuning Rules"*, Imperial College Press, London, 2003.

[31]. Guillermo J. Silva, Aniruddha Datta, S.P. Bhattacharyya, *"PID Controllers for Time-Delay Systems"*, Birkhauser, Boston, 2005.

[32]. Cheng-Ching Yu, *"Autotuning of PID Controllers: A Relay Feedback Approach"*, Springer, 2006.

[33]. Mickle, M. C ., Zhu, J. J., *"Simulation Results for Missile Autopilot Design Based on Extended Mean Assignment"*, System Theory, Proceedings of the Twenty-Eight Southern Symposium, 1996.

[34]. George Ellis, *"Observers in Control Systems: A Practical Guide"*, Academic Press, 2002.

[35]. Richard C. Dorf, Robert H. Bishop, *"Modern Control System"*, Pearson Prentice Hall, 2005.

[36]. Karl J. Astrom, Tore Hagglund, *"Advanced PID Control"*, ISA-The Instrumentation, Systems, and Automation Society, 2006.

[37]. Karl J. Astrom, Tore Hagglund, *"Automatic Tuning of PID Controllers"*, Instrument Society of America, 1988.

[38]. G. Zames, *"Feedback and Optimal Sensitivity: Model Reference Transformations, Multiplicative Seminorms, and Approximate Inverses", IEEE Trans. Automat. Contr.*, vol. AC-26, 1981.

[39]. G. Zames and B.A. Francis, *"Feedback, Minimax Sensitivity, and Optimal Robustness"*, *IEEE Transactions on Automatic Control*, AC-28:585–600, 1983.

[40]. Athans, M., *"The Role and Use of the Stochastic Linear-Quadratic-Gaussian Problem in Control System Design"*, *IEEE Transactions on Automatic Control* AC-16, 1971.

[41]. Safanov, M.G., *"Stability and Robustness of Multivariable Feedback Systems"*, M.I.T. Press, Cambridge, 1980.

[42]. Grimble, M.J. and Johnson, M.A., *"Optimal Control and Stochastic Estimation: Theory and Application"*, Vols 1 and 2, John Wiley & Sons, Chichester, UK, 1988

[43]. B. A. Francis, *"A Course in H-infinity Control Theory"*, Lecture Notes in Control and Information Sciences, vol. 88, 1987.

[44]. B. A. Francis and J. C. Doyle, *"Linear control theory with an H-infinity optimality criterion"*, SIAM J. Control Opt., vol. 25, 1987.

[45]. J. C. Doyle, K. Glover, P.P Khargonekar, B. A. Francis, *"State-space Solutions to Standard H_2 and H_∞ Control Problems"*, AC-34:831–847, 1989.

[46]. D.C. MacFarlane, K. Glover, *"A Loop Shaping Design Procedure Using H_∞-synthesis"*, AC-37:759–769, 1992.

[47]. K. Zhou, J.C. Doyle, *"Essentials of Robust Control"*, Prentice Hall, 1998.

[48]. K. Zhou, J.C. Doyle, K. Glover, *"Robust and Optimal Control"*, Prentice Hall, 1996.

[49]. D.-W. Gu, P.Hr. Petkov, M.M. Konstantinov, *"Robust Control Design with MATLAB"*, 2005.

[50]. J. C. Doyle, B. Francis, A. Tannenbaum, *"Feedback Control Theory"*, Macmillan Publishing Co., 1990

[51]. S. Ariki, *"A New System Invariant and an Algebraic Proof of the Standard* H_∞ *Problem"*, Conference Proceeding, 35th Conference on Decision and Control, 1996

[52]. Alok Sinha, *"Linear Systems : Optimal and Robust Control"*, Boca Raton, FL: CRC Press, 2007.

[53]. The MathWorks website, *"http://www.mathworks.com"*, as accurate of July 28, 2009.

[54]. *"Robust Control Toolbox for Use with MATLAB"*, User's Guide, The MathWorks, Inc., 2001.

[55]. William S. Levine, *"The Control Handbook"*, CRC Press, IEEE Press, 1996.

APPENDIX A

AERODYNAMIC COEFFICIENTS AND DERIVATIVES

This section contains values of the aerodynamic coefficients and derivatives, which are used for the aerodynamic model of the UAV. These data were obtained by the wind tunel tests for the SCAUT UAV at the Politecnico di Torino, Italy. METU TUAV is very similar to SCAUT UAV by geometrical and mass-inertia properties. Therefore, these data are assumed to be suitable for the purposes of the thesis.

$C_{L\dot{\alpha}}$ = 1.46

C_{Lq} = 3.9

$C_{L\delta e}$ = 0.4275

$C_{D\dot{\alpha}}$ = 0

C_{Dq} = 0

$C_{D\delta e}$ = 0.0741

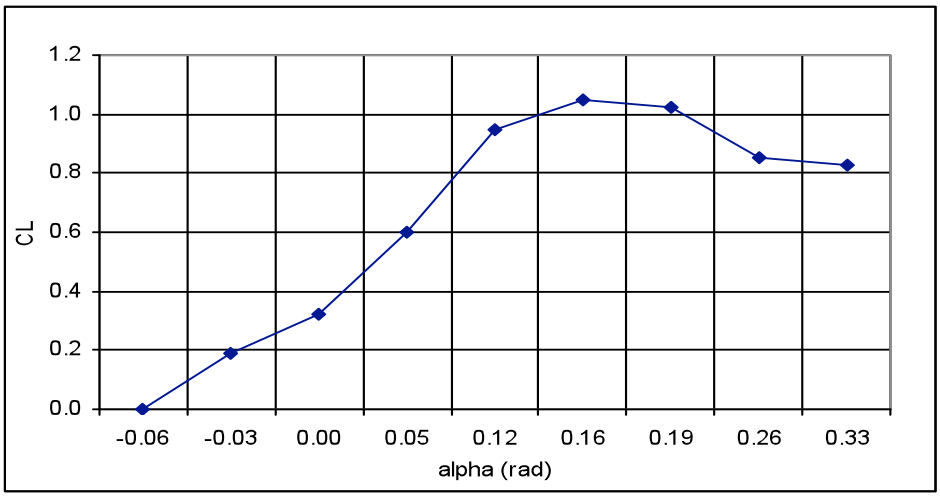

Figure A-1. C_L vs. α

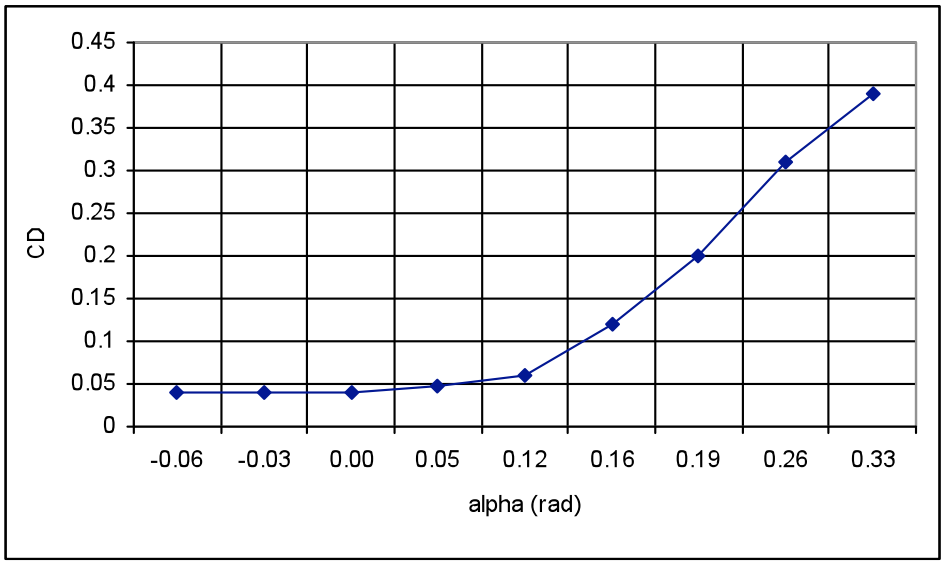

Figure A-2. C_D vs. α

$C_{m\dot{\alpha}}$ = -5.2

C_{mq} = -13.3

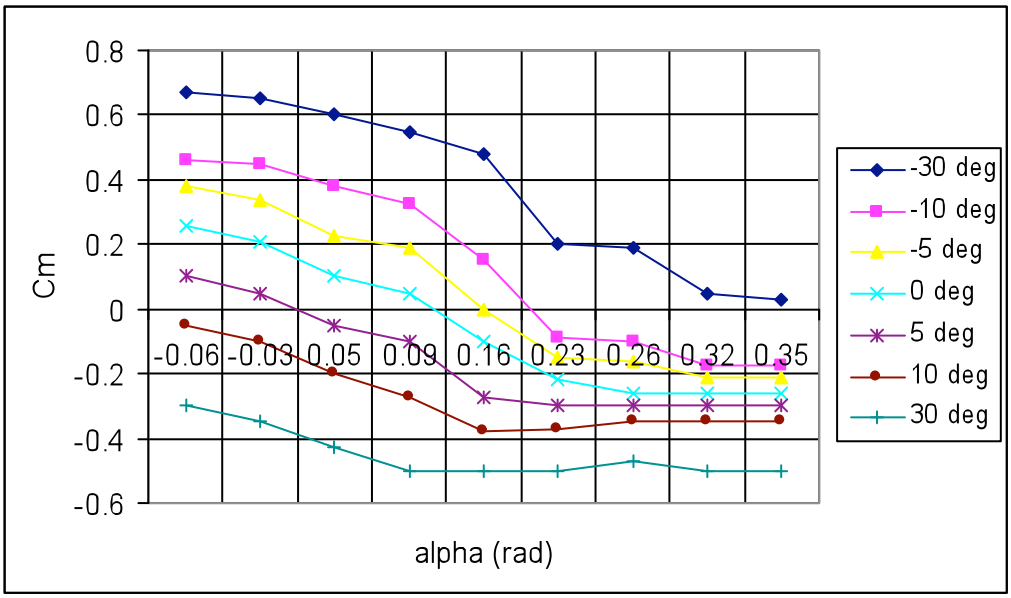

Figure A-3. C_m vs. α for Different Elevator Positions

C_{Yp} = -0.03

C_{Yr} = 0.13

$C_{Y\delta a}$ = 0.019

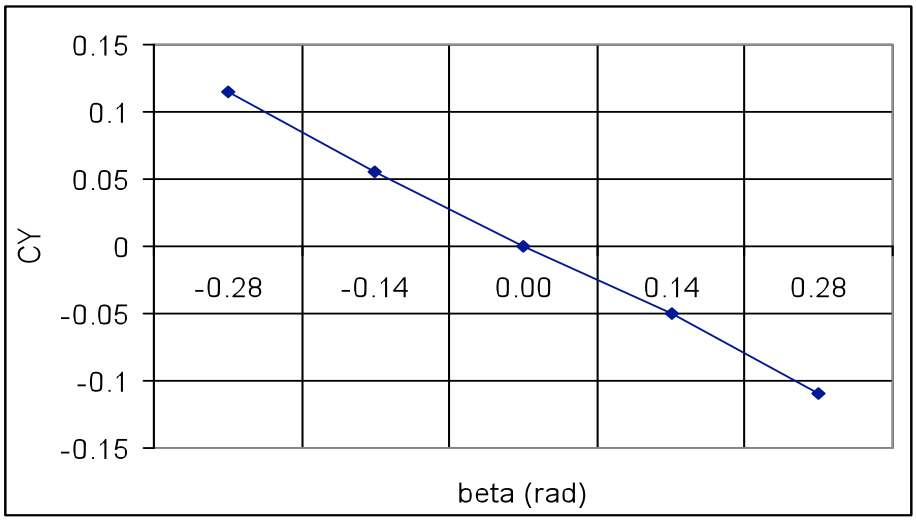

Figure A-4. C_Y vs. β

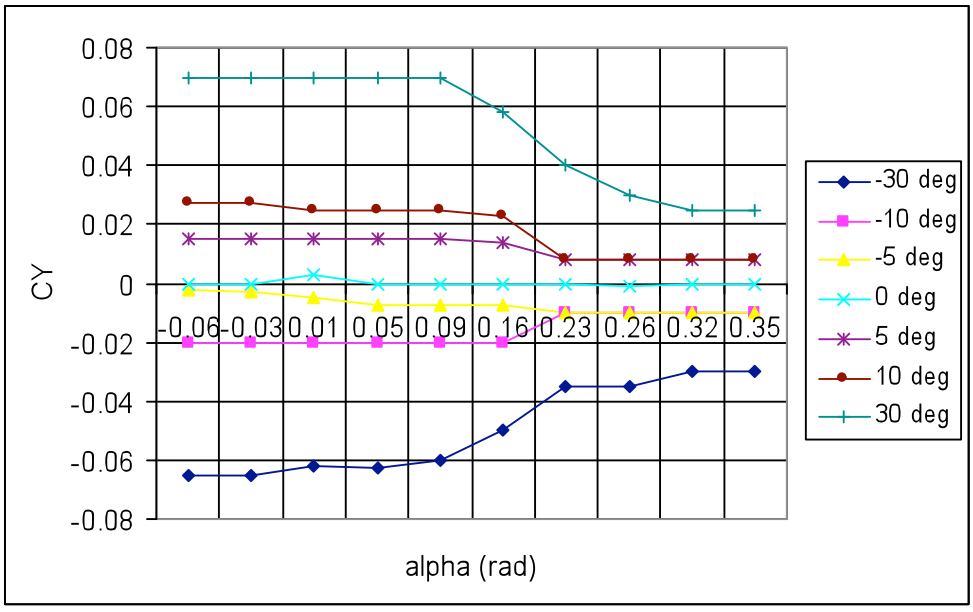

Figure A-5. C_Y vs. α for Different Rudder Positions

C_{l_p} = -0.87

C_{l_r} = 0.13

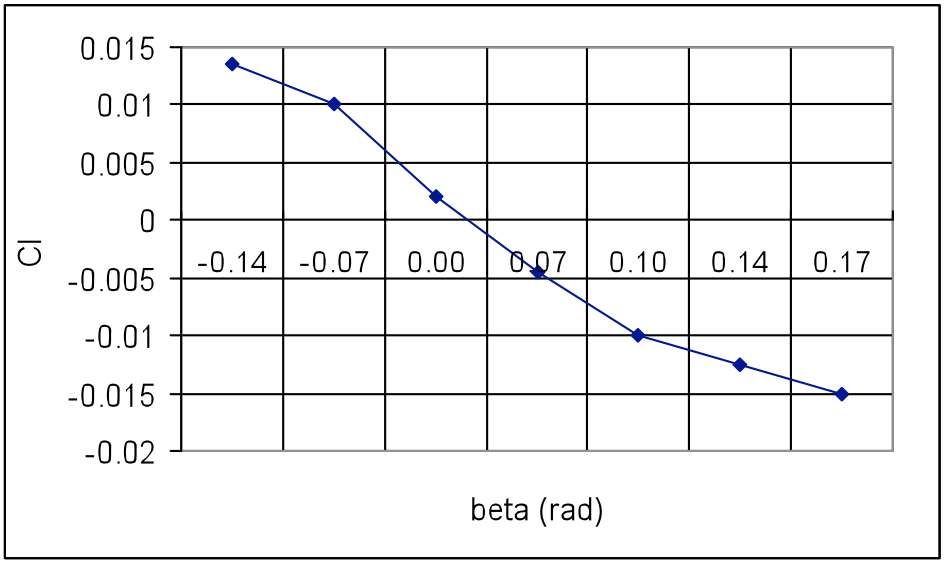

Figure A-6. C_l vs. β

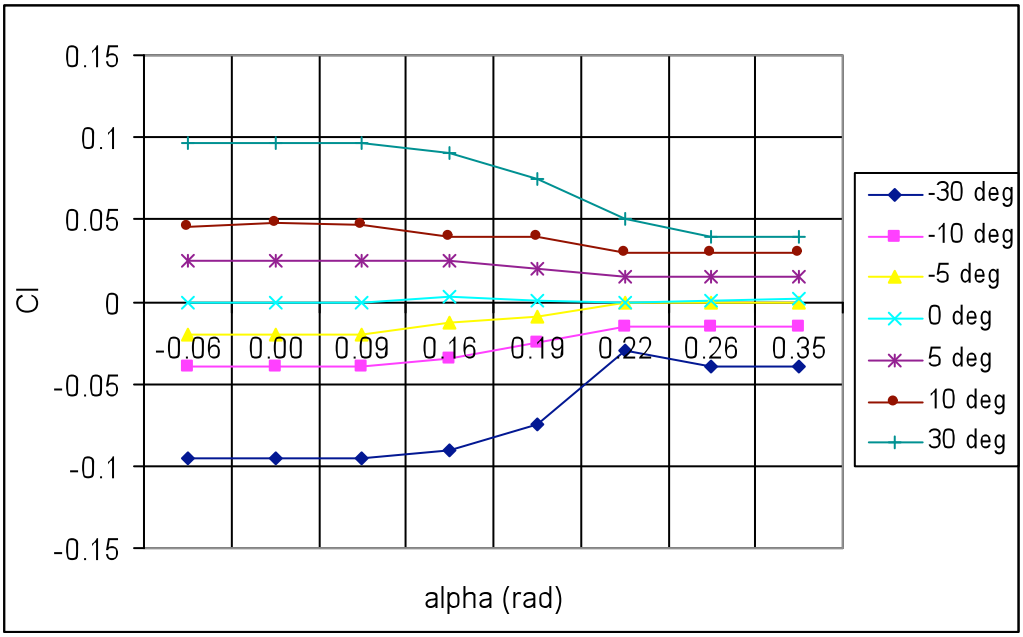

Figure A-7. C_l vs. α for Different Ailerons Positions

C_{np} = -0.03

C_{nr} = -0.099

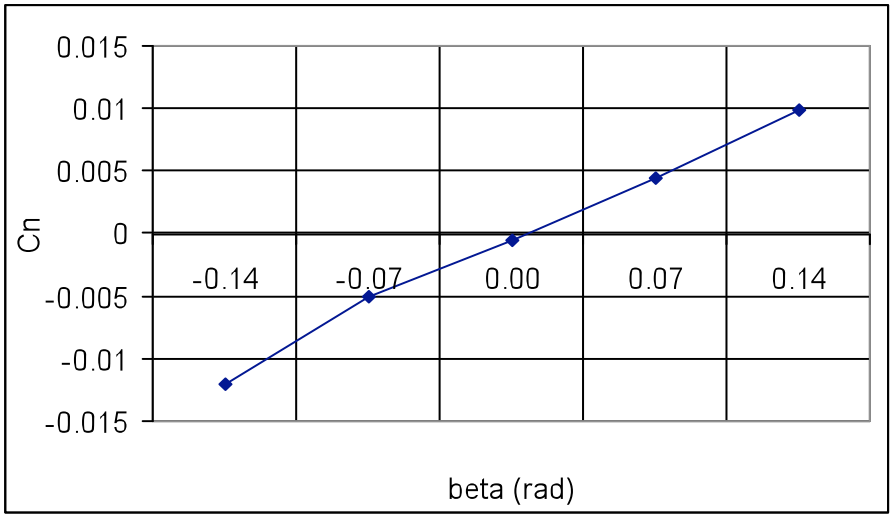

Figure A-8. C_n vs. β

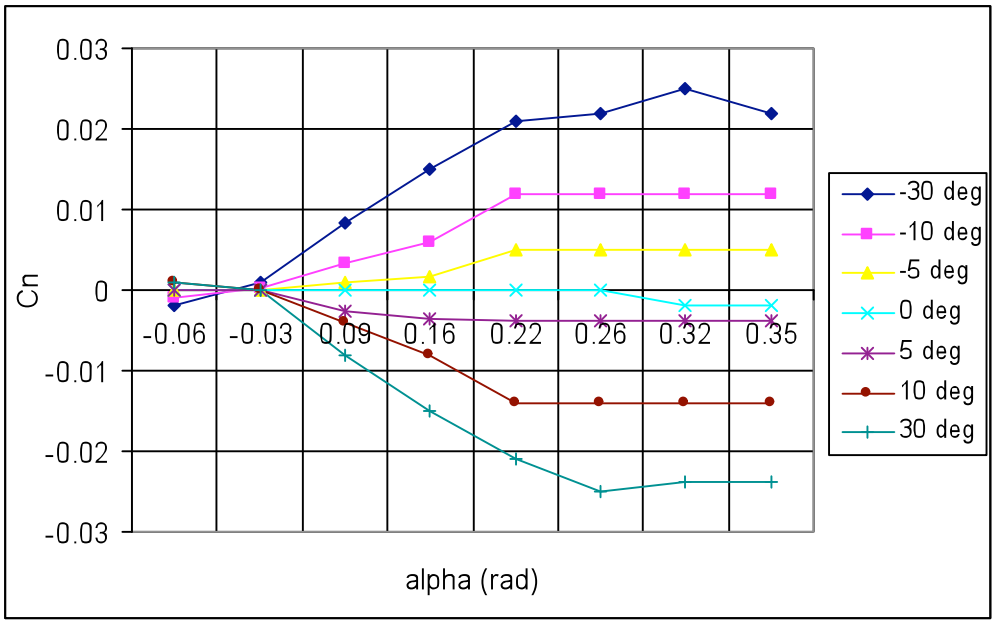

Figure A-9. C_n vs. α for Different Ailerons Positions

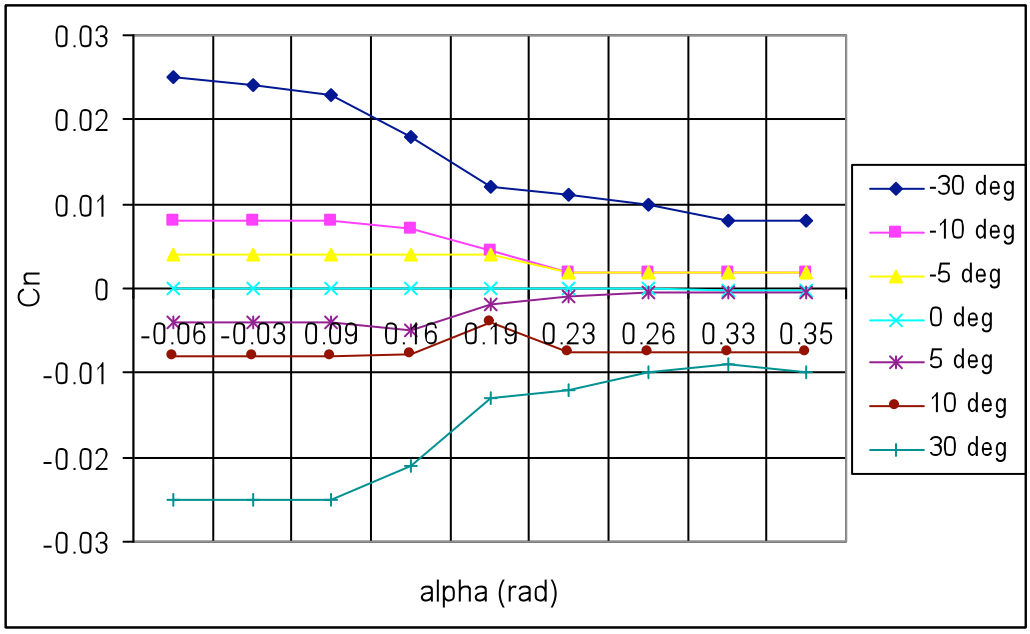

Figure A-10. C_n vs. α for Different Rudder Positions

APPENDIX B

LINEARIZATION OF EQUATIONS OF MOTION

Linearization of the equations of motion is performed using the small disturbance theory.

The scalar force and moment equations of motion in the airplane body-fixed axis system:

$$m(\dot{u} - rv + qw) = -mg\sin\theta + X \tag{B-1.a}$$

$$m(\dot{v} + ru - pw) = mg\cos\theta\sin\phi + Y \tag{B-1.b}$$

$$m(\dot{w} - qu + pv) = mg\cos\varphi\cos\theta + Z \tag{B-1.c}$$

$$I_{xx}\dot{p} - I_{xz}\dot{r} - I_{xz}pq + (I_{zz} - I_{yy})qr = L \tag{B-2.a}$$

$$I_{yy}\dot{q} + (I_{xx} - I_{zz})pr + I_{xz}(p^2 - r^2) = M \tag{B-2.b}$$

$$I_{zz}\dot{r} - I_{xz}\dot{p} + (I_{yy} - I_{xx})pq + I_{xz}qr = N \tag{B-2.c}$$

Kinematic equations:

$$p = \dot{\varphi} - \dot{\psi}\sin\theta \tag{B-3.a}$$

$$q = \dot{\theta}\cos\phi + \dot{\psi}\cos\theta\sin\phi \tag{B-3.b}$$

$$r = \dot{\psi}\cos\theta\cos\phi - \dot{\theta}\sin\phi \tag{B-3.c}$$

Assume the small perturbations on the states, forces and moments. The steady-state values are denoted by subscript *e* (for equilibrium) and changes from them by the prefix Δ.

Motion variables:

$$
\begin{aligned}
u &= u_e + \Delta u \qquad & p &= p_e + \Delta p \qquad & \psi &= \psi_e + \Delta\psi \\
v &= v_e + \Delta v \qquad & q &= q_e + \Delta q \qquad & \theta &= \theta_e + \Delta\theta \\
w &= w_e + \Delta w \qquad & r &= r_e + \Delta r \qquad & \varphi &= \varphi_e + \Delta\varphi
\end{aligned}
\tag{B-4}
$$

Forces:

$$
\begin{aligned}
X &= X_e + \Delta X \\
Y &= Y_e + \Delta Y \\
Z &= Z_e + \Delta Z
\end{aligned}
\tag{B-5}
$$

Moments:

$$
\begin{aligned}
L &= L_e + \Delta L \\
M &= M_e + \Delta M \\
N &= N_e + \Delta N
\end{aligned}
\tag{B-6}
$$

Carrying out these perturbation substitutions into the general airplane equations of motion (1.1) and (1.2) result in:

$$
\begin{aligned}
&m[\Delta\dot{u} + (q_e + \Delta q)(w_e + \Delta w) - (r_e + \Delta r)(v_e + \Delta v)] = \\
&-mg\sin(\theta_e + \Delta\theta) + X_e + \Delta X
\end{aligned}
\tag{B-7.a}
$$

$$
\begin{aligned}
&m[\Delta\dot{v} + (r_e + \Delta r)(u_e + \Delta u) - (p_e + \Delta p)(w_e + \Delta w)] = \\
&mg\cos(\theta_e + \Delta\theta)\sin(\varphi_e + \Delta\varphi) + Y_e + \Delta Y
\end{aligned}
\tag{B-7.b}
$$

$$
\begin{aligned}
&m[\Delta\dot{w} + (p_e + \Delta p)(v_e + \Delta v) - (q_e + \Delta q)(u_e + \Delta u)] = \\
&mg\cos(\theta_e + \Delta\theta)\cos(\varphi_e + \Delta\varphi) + Z_e + \Delta Z
\end{aligned}
\tag{B-7.c}
$$

$$
I_{xx}\Delta\dot{p} - I_{xz}\Delta\dot{r} - I_{xz}(p_e + \Delta p)(q_e + \Delta q) + (I_{zz} - I_{yy})(q_e + \Delta q)(r_e + \Delta r) = L_e + \Delta L
\tag{B-8.a}
$$

$$
I_{yy}\Delta\dot{q} + (I_{xx} - I_{zz})(p_e + \Delta p)(r_e + \Delta r) + I_{xz}[(p_e + \Delta p)^2 - (r_e + \Delta r)^2] = M_e + \Delta M
\tag{B-8.b}
$$

$$
I_{zz}\Delta\dot{r} - I_{xz}\Delta\dot{p} + (I_{yy} - I_{xx})(p_e + \Delta p)(q_e + \Delta q) + I_{xz}(q_e + \Delta q)(r_e + \Delta r) = N_e + \Delta N
\tag{B-8.c}
$$

Following approximations are applied:

$$\cos\Delta\theta = \cos\Delta\varphi \approx 1,\ \ \sin\Delta\theta = \Delta\theta,\ \sin\Delta\varphi = \Delta\varphi;$$

$$\sin(\theta_e + \Delta\theta) \approx \sin\theta_e + \Delta\theta\cos\theta_e$$

$$\sin(\varphi_e + \Delta\varphi)\cos(\theta_e + \Delta\theta) \approx$$
$$\sin\varphi_e\cos\theta_e - \Delta\theta\sin\varphi_e\sin\theta_e + \Delta\varphi\cos\varphi_e\cos\theta_e - \Delta\varphi\Delta\theta\cos\varphi_e\sin\theta_e$$

$$\cos(\varphi_e + \Delta\varphi)\cos(\theta_e + \Delta\theta) \approx$$
$$\cos\varphi_e\cos\theta_e - \Delta\theta\cos\varphi_e\sin\theta_e - \Delta\varphi\sin\varphi_e\cos\theta_e + \Delta\varphi\Delta\theta\sin\varphi_e\sin\theta_e$$

Force and moment equations can be written in the following form:

$$\underline{m(-v_e r_r + w_e q_e)} + m(\Delta\dot{u} - v_e\Delta r - r_e\Delta v + w_e\Delta q + q_e\Delta w) + \underline{\underline{m(-\Delta v\Delta r + \Delta w\Delta q)}} =$$
$$\underline{-mg\sin\theta_e + X_e} - mg\Delta\theta\cos\theta_e + \Delta X$$

(B-9.a)

$$\underline{m(u_e r_e - w_e p_e)} + m(\Delta\dot{v} + u_e\Delta r + r_e\Delta u - w_e\Delta p - p_e\Delta w) + \underline{\underline{m(\Delta u\Delta r - \Delta w\Delta p)}} =$$
$$\underline{mg\sin\varphi_e\cos\theta_e + Y_e} - mg\Delta\theta\sin\varphi_e\sin\theta_e + mg\Delta\varphi\cos\varphi_e\cos\theta_e + \Delta Y -$$
$$\underline{\underline{mg\Delta\varphi\Delta\varphi\cos\varphi_e\sin\theta_e}}$$

(B-9.b)

$$\underline{m(-u_e q_e + v_e p_e)} + m(\Delta\dot{w} - u_e\Delta q - q_e\Delta u + v_e\Delta p + p_e\Delta v) + \underline{\underline{m(-\Delta u\Delta q + \Delta v\Delta p)}} =$$
$$\underline{mg\cos\varphi_e\cos\theta_e + Z_e} - mg\Delta\theta\cos\varphi_e\sin\theta_e - mg\Delta\varphi\sin\varphi_e\cos\theta_e + \Delta Z +$$
$$\underline{\underline{mg\Delta\varphi\Delta\varphi\sin\varphi_e\sin\theta_e}}$$

(B-9.c)

$$\underline{-I_{xz}p_e q_e + (I_{zz} - I_{yy})r_e q_e} + I_{xx}\Delta\dot{p} - I_{xz}\Delta\dot{r} - I_{xz}(p_e\Delta q + q_e\Delta p) +$$
$$(I_{zz} - I_{yy})(r_e\Delta q + q_e\Delta r) \underline{\underline{- I_{xz}\Delta p\Delta q + (I_{zz} - I_{yy})\Delta r\Delta q}} = \underline{L_e} + \Delta L \qquad \text{(B-10.a)}$$

$$\underline{(I_{xx} - I_{zz})p_e r_e + I_{xz}(p_e^2 - r_e^2)} + I_{yy}\Delta\dot{q} + (I_{xx} - I_{zz})(p_e\Delta r + r_e\Delta p) +$$
$$I_{xz}(2p_e\Delta p - 2r_e\Delta r) + \underline{\underline{(I_{xx} - I_{zz})\Delta p\Delta r + I_{xz}(\Delta p^2 - \Delta r^2)}} = \underline{M_e} + \Delta M \qquad \text{(B-10.b)}$$

$$\underline{(I_{yy}-I_{xx})p_e q_e + I_{xz}q_e r_e} + I_{zz}\Delta\dot{r} - I_{xz}\Delta\dot{p} + (I_{yy}-I_{xx})(p_e\Delta q + q_e\Delta p) + I_{xz}(q_e\Delta r + r_e\Delta q) + \underline{\underline{(I_{yy}-I_{xx})\Delta p\Delta q + I_{xz}\Delta q\Delta r}} = \underline{N_e} + \Delta N \quad \text{(B-10.c)}$$

The thin underlined terms in the equations above represent the general steady-state equations of motion and assuming that they are inherently satisfied they can be eliminated from without loss of generality. The double underlined terms are referred to non-linear terms, which are assumed to be negligible compared with the linear terms, therefore can be eliminated from the equations. The result is the following equations:

$$m(\Delta\dot{u} - v_e\Delta r - r_e\Delta v + w_e\Delta q + q_e\Delta w) = -mg\Delta\theta\cos\theta_e + \Delta X \quad \text{(B-11.a)}$$

$$m(\Delta\dot{v} + u_e\Delta r + r_e\Delta u - w_e\Delta p - p_e\Delta w) = -mg\Delta\theta\sin\varphi_e\sin\theta_e + mg\Delta\varphi\cos\varphi_e\cos\theta_e + \Delta Y \quad \text{(B-11.b)}$$

$$m(\Delta\dot{w} - u_e\Delta q - q_e\Delta u + v_e\Delta p + p_e\Delta v) = -mg\Delta\theta\cos\varphi_e\sin\theta_e + -mg\Delta\varphi\sin\varphi_e\cos\theta_e + \Delta Z \quad \text{(B-11.c)}$$

$$I_{xx}\Delta\dot{p} - I_{xz}\Delta\dot{r} - I_{xz}(p_e\Delta q + q_e\Delta p) + (I_{zz}-I_{yy})(r_e\Delta q + q_e\Delta r) = \Delta L \quad \text{(B-12.a)}$$

$$I_{yy}\Delta\dot{q} + (I_{xx}-I_{zz})(p_e\Delta r + r_e\Delta p) + I_{xz}(2p_e\Delta p - 2r_e\Delta r) = \Delta M \quad \text{(B-12.b)}$$

$$I_{zz}\Delta\dot{r} - I_{xz}\Delta\dot{p} + (I_{yy}-I_{xx})(p_e\Delta q + q_e\Delta p) + I_{xz}(q_e\Delta r + r_e\Delta q) = \Delta N \quad \text{(B-12.c)}$$

Obtained equations represent coupled linearized equations of motion of an airplane. Forces and moments are represented in terms of the stability derivatives. For example, force in x-axis in terms of stability derivatives can be written as follows:

$$\Delta X = \frac{\partial X}{\partial u}\Delta u + \frac{\partial X}{\partial w}\Delta w + \frac{\partial X}{\partial \delta_e}\Delta\delta_e + \frac{\partial X}{\partial \delta_T}\Delta\delta_T,$$

where $X_u = \frac{\partial X}{\partial u}$, $X_w = \frac{\partial X}{\partial w}$, $X_{\delta_e} = \frac{\partial X}{\partial \delta_e}$, $X_{\delta_T} = \frac{\partial X}{\partial \delta_T}$

Equations of motion can be uncoupled and airplane longitudinal and lateral dynamics under certain assumptions. States that are referred to the longitudinal dynamics are $\lfloor \Delta u, \Delta w, q, \Delta\theta \rfloor$, the input is elevator deflection $\lfloor \Delta\delta_e \rfloor$. States, referred to the lateral airplane's dynamics are: $\lfloor v, p, r, \Delta\phi \rfloor$, inputs are ailerons and rudder deflections: $\lfloor \Delta\delta_a, \Delta\delta_r \rfloor$. In these notations it is assumed that equilibrium values for angular rates and body y-velocity are equal to zero, therefore:

$p = \Delta p, q = \Delta q, r = \Delta r, v = \Delta v$.

State and input matrices for the longitudinal dynamics are:

$$A_{long} = \begin{bmatrix} \frac{X_u}{m} & \frac{X_w}{m} & 0 & -g\cos\theta_e \\ \frac{Z_u}{m - Z_{\dot{w}}} & \frac{Z_w}{m - Z_{\dot{w}}} & \frac{Z_q + mu_0}{m - Z_{\dot{w}}} & -\frac{mg\sin\theta_e}{m - Z_{\dot{w}}} \\ \frac{1}{I_y}\left[M_u + \frac{M_{\dot{w}} Z_u}{m - Z_{\dot{w}}}\right] & \frac{1}{I_y}\left[M_w + \frac{M_{\dot{w}} Z_u}{m - Z_{\dot{w}}}\right] & \frac{1}{I_y}\left[M_q + \frac{M_{\dot{w}}(Z_q + mu_0)}{m - Z_{\dot{w}}}\right] & -\frac{M_{\dot{\alpha}} mg\sin\theta_e}{I_y(m - Z_{\dot{w}})} \\ 0 & 0 & 1 & 0 \end{bmatrix}$$

$$B_{long} = \begin{bmatrix} \frac{X_{\delta e}}{m} \\ \frac{Z_{\delta e}}{m - Z_{\dot{w}}} \\ \frac{1}{I_y}\left[M_{\delta e} + \frac{M_{\dot{w}} Z_{\delta e}}{m - Z_{\dot{w}}}\right] \\ 0 \end{bmatrix}$$

State and input matrices that describe lateral dynamics are the following:

$$A_{lat} = \begin{bmatrix} \frac{Y_v}{m} & \frac{Y_p}{m} & \frac{Y_r}{m} - u_0 & g\cos\theta_0 \\ \frac{Y_v}{J_x} + J_{zx} N_v & \frac{Y_p}{J_x} + J_{zx} N_p & \frac{Y_r}{J_x} + J_{zx} N_r & 0 \\ J_{zx} L_v + \frac{N_v}{J_z} & J_{zx} L_p + \frac{N_p}{J_z} & J_{zx} L_r + \frac{N_r}{J_z} & 0 \\ 0 & 1 & \tan\theta_0 & 0 \end{bmatrix}$$

$$B_{lat} = \begin{bmatrix} \frac{Y_{\delta_a}}{m} & \frac{Y_{\delta_r}}{m} \\ \frac{L_{\delta_a}}{J_x} + J_{zx} N_{\delta_a} & \frac{L_{\delta_r}}{J_x} + J_{zx} N_{\delta_r} \\ J_{zx} L_{\delta_a} + \frac{N_{\delta_a}}{J_z} & J_{zx} L_{\delta r} + \frac{N_{\delta_r}}{J_z} \\ 0 & 0 \end{bmatrix}$$

where $J_x = (I_x I_z - I_{zx}^2)/I_z$

$$J_z = (I_x I_z - I_{zx}^2)/I_x$$

$$J_{zx} = I_{zx}/(I_x I_z - I_{zx}^2) .$$